NAA-SR-9626
COPY
126 PAGES



# ANALYSIS OF THE RESPONSE OF THE SNAP 8 NUCLEAR SYSTEM DURING STARTUP OF THE POWER CONVERSION SYSTEM

(Title Unclassified)

*AEC Research and Development Report*



ATOMICS INTERNATIONAL
A DIVISION OF NORTH AMERICAN AVIATION, INC.

## DISCLAIMER

## LEGAL NOTICE



Printed in USA Price $2.45 Available from the

U. S. Atomic Energy Commission
Technical Information Extension,
P. O. Box 1001
Oak Ridge, Tennessee.

Please direct to the same address inquiries covering the procurement of other classified AEC reports.

NAA-SR-9626
SNAP REACTOR,
SNAP PROGRAM
M-3679 (34th Ed.)

# ANALYSIS OF THE RESPONSE OF THE SNAP 8 NUCLEAR SYSTEM DURING STARTUP OF THE POWER CONVERSION SYSTEM

(Title Unclassified)

By

C.J. CODE, JR.



ATOMICS INTERNATIONAL

A DIVISION OF NORTH AMERICAN AVIATION, INC.
P.O. BOX 309 CANOGA PARK, CALIFORNIA

CONTRACT: AT(11-1)-GEN-8
ISSUED: JUNE 8, 1964

# DISTRIBUTION

## SYSTEMS FOR NUCLEAR AUXILIARY POWER (SNAP)-REACTOR SNAP PROGRAM M-3679 (34th Ed.)

| | No of Copies |
|---|---|
| Aerojet-General Corporation (NASA) | 1 |
| Aerojet-General Nucleonics | 1 |
| Aeronautical Systems Division | 2 |
| Aerospace Corporation | 1 |
| Aerospace Test Wing (AFSC) | 1 |
| Air Force Weapons Laboratory | 2 |
| AiResearch Manufacturing Company, Phoenix | 1 |
| Army Ballistic Research Laboratories | 1 |
| Army Materials Research Agency | 1 |
| Army Missile Command | 1 |
| Army Nuclear Defense Laboratory | 1 |
| ARO, Inc. | 1 |
| Air University Library | 1 |
| Argonne National Laboratory | 1 |
| Army Combat Developments Command | 1 |
| Astropower, Inc. | 1 |
| Avco Corporation | 1 |
| Battelle Memorial Institute | 1 |
| Bendix Corporation (AF) | 1 |
| Brookhaven National Laboratory | 1 |
| Bureau of Naval Weapons | 2 |
| Bureau of Ships | 2 |
| Bureau of Yards and Docks | 1 |
| California Patent Group | 1 |
| Central Intelligence Agency | 1 |
| Chicago Patent Group | 1 |
| Defense Atomic Support Agency, Sandia | 1 |
| Department of the Army | 1 |
| Director of Defense Research and Engineering (OAP) | 1 |
| Edgerton, Germeshausen and Grier, Inc., Goleta | 1 |
| Foreign Technology Division (AFSC) | 1 |
| General Atomic Division | 1 |
| General Dynamics/Astronautics (AF) | 1 |
| General Dynamics/Fort Worth | 1 |
| General Electric Company, Cincinnati | 1 |
| General Electric Company (FPD) | 2 |
| General Electric Company (MSVD) | 1 |
| General Electric Company, Richland | 2 |
| General Electric Company, San Jose | 1 |
| General Electric Company, San Jose (AF) | 1 |
| General Technologies Corporation | 1 |
| Institute for Defense Analysis | 1 |
| Ion Physics Corporation | 1 |
| Jet Propulsion Laboratory | 2 |
| Johns Hopkins University (APL) | 1 |
| Lockheed-Georgia Company | 1 |
| Lockheed Missiles and Space Company | 1 |
| Los Alamos Scientific Laboratory | 1 |
| Martin-Marietta Corporation, Denver | 1 |
| Monsanto Dayton Laboratory | 1 |
| NASA Ames Research Center | 1 |
| NASA Goddard Space Flight Center | 2 |
| NASA Langley Research Center | 1 |
| NASA Lewis Research Center | 4 |
| NASA Manned Spacecraft Center | 1 |
| NASA Marshall Space Flight Center | 1 |
| NASA Scientific and Technical Information Facility | 3 |
| National Aeronautics and Space Administration, Washington | 1 |
| NASA Western Operations Office | 1 |
| Naval Air Development Center | 1 |
| Naval Ordnance Laboratory | 2 |
| Naval Postgraduate School | 1 |
| Naval Radiological Defense Laboratory | 1 |
| Naval Research Laboratory | 2 |
| Naval Underwater Ordnance Station | 1 |
| Navy Marine Engineering Laboratory | 1 |
| New York Operations Office | 1 |
| New York Operations Office, Canel Project Office | 1 |
| North American Aviation, Inc., Downey | 1 |
| Nuclear Metals, Inc. | 1 |
| Office of Naval Research | 2 |
| Office of the Assistant General Counsel for Patents (AEC) | 1 |
| Office of the Chief of Engineers | 1 |
| Office of the Chief of Naval Operations | 3 |
| Office of the Chief of Naval Operations (OP-03EG) | 2 |
| Office of the Chief of Transportation | 1 |
| Phillips Petroleum Company (NRTS) | 4 |
| Pratt and Whitney Aircraft Division | 1 |
| Pratt and Whitney Aircraft Division (NASA) | 1 |
| Rand Corporation | 1 |
| Republic Aviation Corporation | 1 |
| Sandia Corporation | 1 |
| School of Aerospace Medicine | 1 |
| Union Carbide Corporation (ORNL) | 8 |
| USAF Headquarters | 1 |
| University of California, Livermore | 1 |
| Westinghouse Electric Corporation (NASA) | 1 |
| Division of Technical Information Extension | 40 |
| AI Library (Includes 2 copies to CPAO, 2 copies to AEC, Washington, 2 copies to COO) | 109 |

## CONTENTS

## CONTENTS



## TABLES



## FIGURES

## FIGURES

## FIGURES

## FIGURES

## FIGURES

## FIGURES

## ACKNOWLEDGMENT

The author wishes to express his appreciation for the advice and assistance of many Atomics International and Aerojet-General Corporation personnel. In particular, the excellent work of Luther N. Wimberly of AI in programming and in operation of the analog computer is greatly appreciated.

## ABSTRACT

In order to determine the response of the SNAP 8 nuclear system to power conversion system startup, these systems were simulated on a combination of three general purpose analog computers. Parameter studies were made to determine the permissible range of system parameters and startup conditions. A set of design levels for system startup parameters was selected.

Detailed results of the parameter studies are presented. The analog simulation is described and discussed, including the analytical model and analog circuits used. The overall optimization of system parameters results in a well-controlled response of the SNAP 8 system to power conversion system startup.

BLANK

# I. INTRODUCTION

## A. PURPOSE OF STUDY

Since the startup of the SNAP 8 Power Conversion System (PCS) involves large changes in nuclear system (NS) coolant flow and power level, considerable transients in fuel and coolant temperatures can be expected. Limitations must be placed on the magnitudes and rates of changes of these temperatures in order to avoid physical damage to the NS or PCS. The maxima of nuclear system power and outlet coolant temperature must also be kept below the scram levels of the ground test safety system.

An analog model of the system was developed to study the PCS startup transients and to determine what range of system parameters, startup conditions, and startup methods would meet the prescribed limitations. This study was based on the SNAP 8 flight reference design. However, constraints imposed by ground test requirements were also considered.

The SNAP 8 reactor, control system, NaK-Hg heat exchanger (boiler), and associated piping were simulated on a combination of two PACE 231-R and one PACE 1631 analog computers. Parameter studies were made to determine a permissible range of system parameters and startup conditions, and a set of design parameters was chosen.

Detailed results of the most recent phase of the parameter studies are presented here, as well as partial results of earlier phases. The earlier phases involved primarily development of the analog model. These phases also included some study of the effects of various parameters, progressively approaching the choice of design parameters. Several different system concepts were involved in the early phases as well as various procedures for starting up the power conversion system.

## B. DESCRIPTION OF THE SYSTEM

### 1. General

SNAP 8 is a nuclear power system designed to produce approximately 35 kw of electric power for use in spacecraft. The system, which is being developed jointly by NASA and the AEC, employs a nuclear system (being developed by Atomics International under contract to the AEC) as the heat source for a mercury Rankine cycle power conversion system (being developed by Aerojet-General Corporation under contract to NASA).

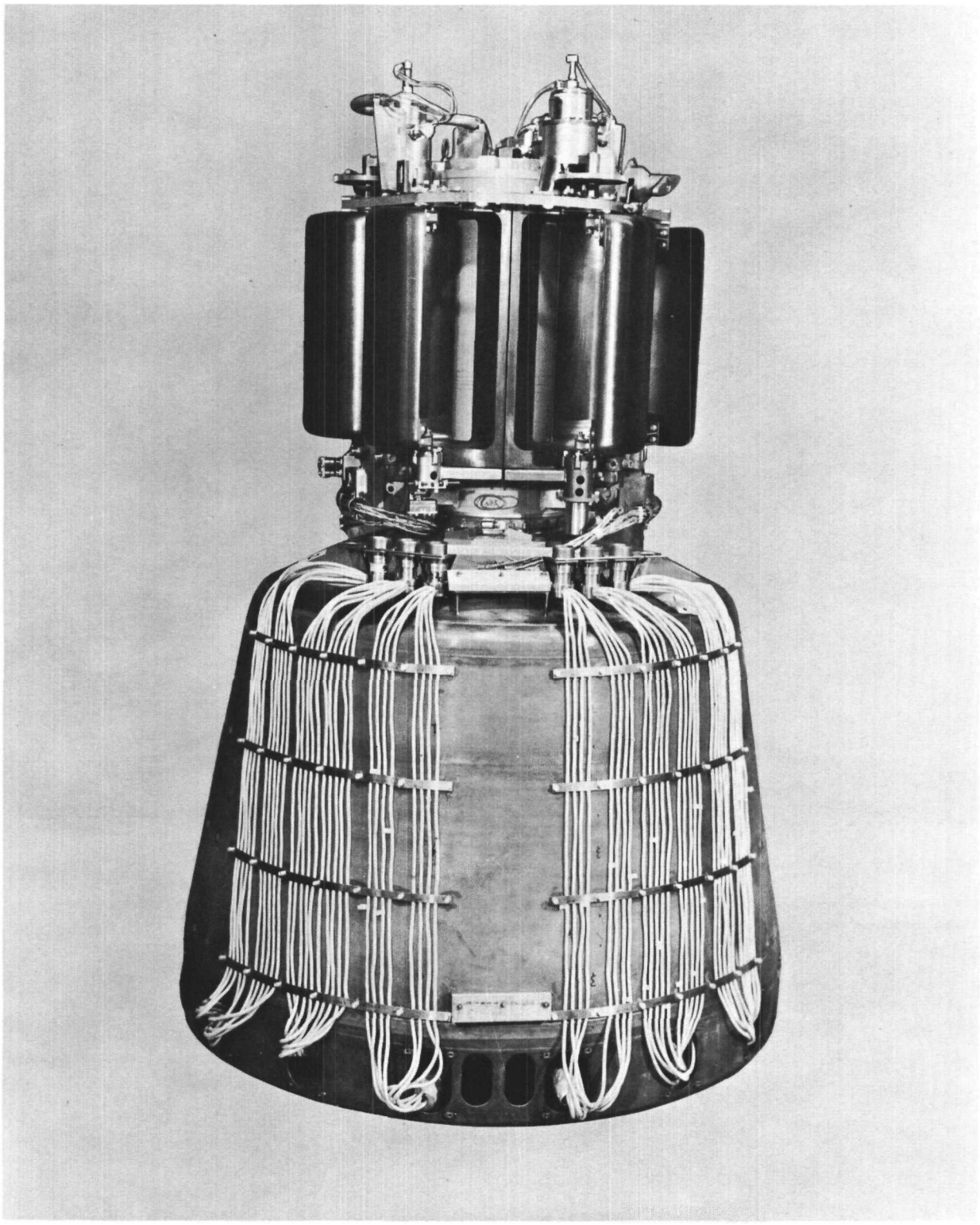

7-22-63 7568-1217-A

Figure 1. SNAP 8 Nuclear System

2. Nuclear System

The SNAP 8 nuclear system (Figure 1) includes a moderated, beryllium reflected reactor containing highly enriched uranium. The core contains 211 fuel elements, each 0.56 in. OD and approximately 17 in. long. Each fuel element consists of a fuel-moderator rod composed of a hydrided zirconium-uranium alloy. The fuel rods are provided with a ceramic-lined Hastelloy-N cladding. The ceramic coating is applied to the inside surface of the cladding to minimize loss of the hydrogen moderator by diffusion through the cladding.

The fuel elements are held in place by upper and lower grid plates, each containing 211 holes for the fuel element end-pins and 372 coolant flow holes. The primary coolant, flowing through the reactor core, is NaK-78 eutectic. This coolant enters a plenum at the bottom of the core vessel, goes through a flow-shaping baffle plate, through the lower grid plate, past the fuel elements, through the upper grid plate into another plenum, and then out of the core vessel.

The core vessel is essentially a right circular cylinder of stainless steel, 9.2 in. ID by 26.2 in. long, with a hemispherical upper plenum and a dished lower plenum. The vessel is surrounded radially by an annulus of beryllium approximately 3 in. thick and 18.5 in. long, which forms the external radial reflector. Figure 2 shows the layout of the reactor components.

The SNAP 8 nuclear system is designed to transfer 600 thermal kw to the NaK coolant. It may be operated at any constant power level desired from approximately 10 to 100% of rated power. The reactor is designed for a nominal core outlet NaK coolant temperature of 1300°F and a nominal core inlet NaK temperature of 1100°F.

3. Control System

The radial neutron reflector contains six movable semicylindrical sections or drums as shown in Figure 2. Nuclear system control is accomplished by rotation of these drums toward or away from the core to increase or decrease the fraction of leakage neutrons reflected back to the core.

Three of the six reflector drums are designated as startup drums and will be rotated to the "full-in" position by springs. The remaining three drums are called control drums, and will be rotated toward or away from the core by geared-down stepper motors.

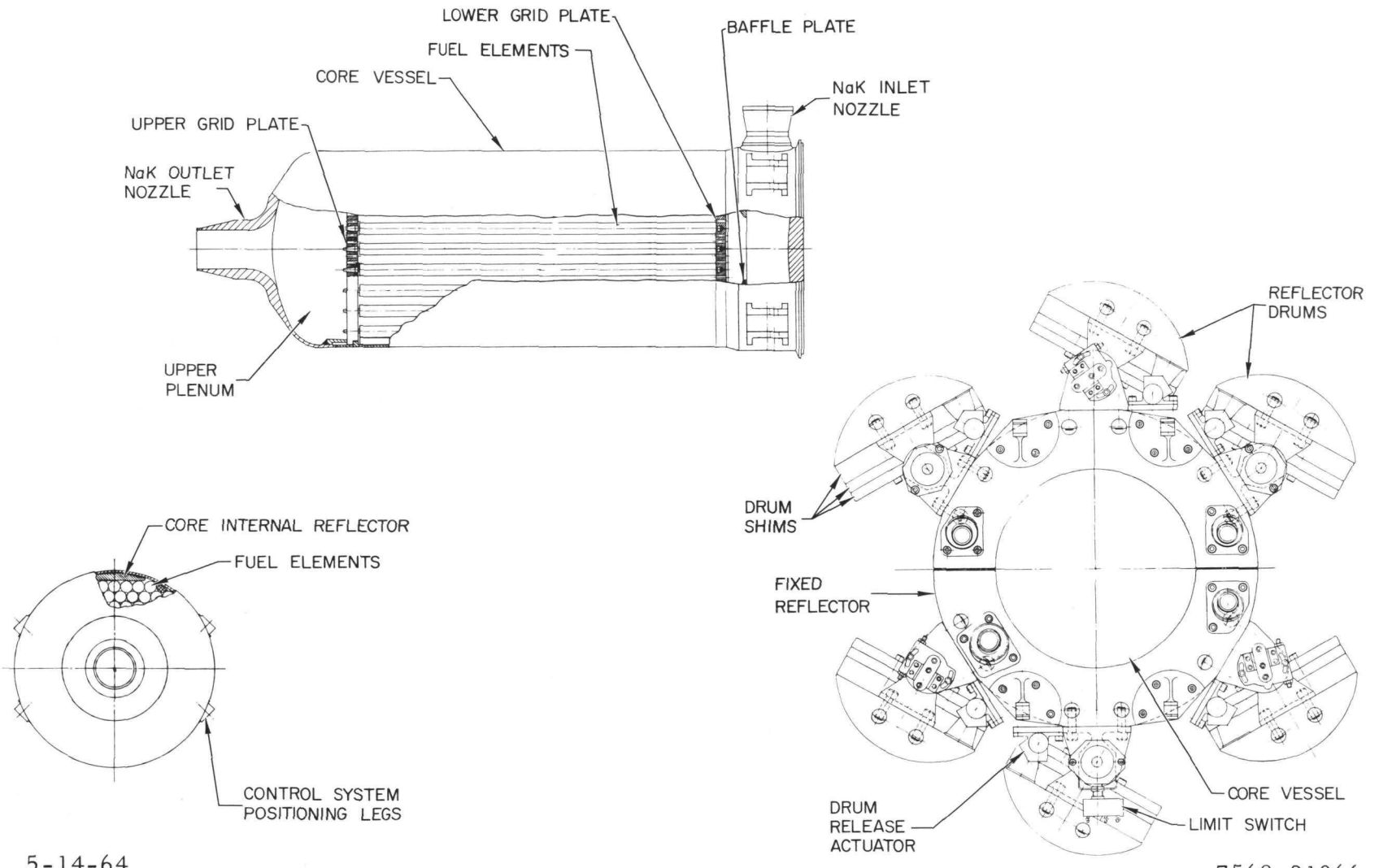


Figure 2. Cross Section of Reactor and Control System

Control of the SNAP 8 nuclear system is based on its outlet coolant temperature. This temperature is maintained at approximately 1300°F by an on-off digital acting control system having a deadband extending from 1270 ± 10°F to 1330 ± 10°F. When the outlet NaK temperature is within the deadband, the controller does not change the position of the control drums.

There are two distinct phases involved in startup of SNAP 8. First is nuclear startup, which brings the reactor from subcritical to critical and brings the nuclear system outlet coolant temperature, as measured by the temperature sensor, to the rated level of 1300°F. Throughout most of the nuclear startup, the control system will be operating in the startup mode, wherein all drum rotation is toward the core. Prior to power conversion system startup, the control system will change from the startup mode to the long-term control mode. In long-term control, the control drum rotation may be either toward or away from the core as follows. Whenever the measured outlet coolant temperature ($T_{cm}$) goes outside the control deadband, the control system steps the control drums 0.52 ± 0.10 degrees in such a direction as to return $T_{cm}$ to within the deadband. If a single control drum step is not sufficient, the control system continues to provide steps at discrete time intervals until $T_{cm}$ remains within the deadband.

4. Power Conversion System

The SNAP 8 Power Conversion System includes the intermediate (NaK-Hg) heat exchanger (or boiler), the turbine and alternator, the auxiliary startup heat exchanger, the parasitic load, and the necessary pumps and piping (see Figure 3). Heat generated by the nuclear system is transferred from the primary NaK to mercury through a shell-tube counterflow heat exchanger. Mercury vaporized in the heat exchanger drives a turbine which, in turn, drives an alternator to provide electrical power to the payload. A condenser is provided between the mercury loop and the heat rejection NaK loop.

The auxiliary startup heat exchanger (AHX) provides a controllable load to increase nuclear system power prior to and during PCS startup. The AHX transfers heat from the primary NaK loop to the heat rejection NaK loop. The parasitic load takes the electrical power not used by the payload and dissipates it as heat in the primary NaK line near the NS inlet.

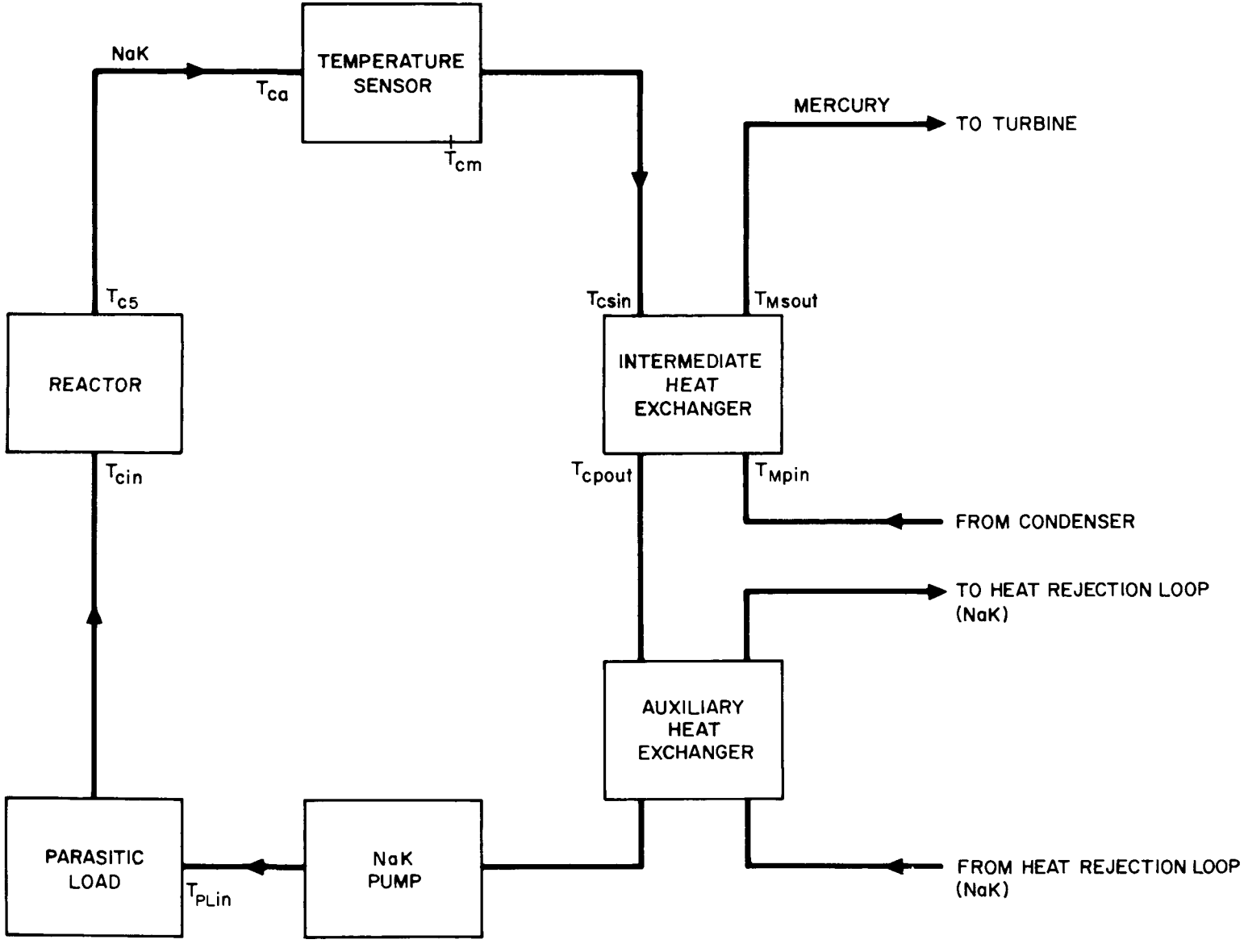


Figure 3. Nuclear System, Primary Coolant Loop, and Heat Exchanger Schematic

Since the effect of the PCS on the nuclear system is felt primarily through the NaK coolant, the main concern of this study, in addition to the reactor and control system, is with the NaK-Hg heat exchanger. Of secondary concern are the parasitic load and the auxiliary heat exchanger.

## C. STARTUP PROCEDURES

### 1. Initial Conditions

Just before the startup of the power conversion system, nuclear startup having been completed, the nuclear system will have reached the following conditions. The measured outlet coolant temperature will be somewhere within the deadband, presently assumed to be 1270 to 1330°F. Nuclear system NaK flow will be somewhat less than rated flow, and the power will be considerably less than rated power (the recommended values of initial flow and power are determined in this study). Mercury flow will be zero, and NS inlet NaK temperature will be determined by the above flow, power, and outlet temperature conditions. The control system will be in the long-term control mode, with an interval between successive steps as determined by this study and other transient conditions. Control step size will be determined by the control drum differential reactivity worths and the control drum position. The startup drums will be in the full-in position. The control drum position will be dependent on such parameters as initial excess reactivity, temperature and power defects, xenon and samarium buildup, and samarium prepoison burnout.

### 2. Final Conditions

At the end of PCS startup, the nuclear system will be at reference power and NaK flow. The measured outlet NaK temperature will be within the deadband, and the inlet NaK temperature will be about 180°F lower than the outlet, depending on the above power and flow conditions and the power being dissipated through the parasitic load resistor. Mercury flow will be at the rated level, the control system will remain in the long-term control phase, and the control drums will be within 3° of their position at the beginning of PCS startup.

### 3. Startup Sequence

The PCS startup sequence is presently conceived to be generally as listed below. The timing of the individual steps of the sequence is determined in this study.

a) At time t = 0, the mercury flow is injected in such a way as to rise linearly from zero to the injection level.

b) During this period of mercury flow increase, the turbine-alternator assembly begins rotating, increasing the power to the primary loop NaK pump. This brings the NaK flow up from its initial value to rated flow.

c) When the mercury flow reaches the injection level, the parasitic load resistor begins to feed all excess electrical power from the turbine-alternator assembly into the NS inlet NaK line as heat.

d) After the mercury flow has been at the injection level for a specified time, it begins a linear rise to rated flow.

e) About 10 min after the mercury flow reaches the rated level, the nuclear system reaches steady-state conditions.

## D. ANALYTICAL MODEL

The analog computer model developed to study the PCS startup transient consists of the following:

1) Six delayed-neutron group reactor kinetics with variable temperature coefficients of reactivity for the fuel and grid plates;

2) Five axial node plus entrance fuel node "backward difference" core heat transfer model;

3) A three-section, shifting-interface model for the NaK-Hg heat exchanger;

4) Cascaded simple lags with flow-dependent time constants for coolant transport delay; and

5) A flexible model of the control system providing variations of step size, stepping interval, and deadband temperature settings.

During the course of the PCS startup study, it was found that simulation of the NaK-Hg heat exchanger is very critical. Various attempts at simplified single node simulations all yielded nonconservative results, especially in determining rates of change of temperature.

The method of simulating coolant transport delays and the method of computing rates of change of temperature were also found to be quite important. In core heat transfer, the entrance fuel node model was developed to avoid the anomalies inherent in a linear gradient or "central difference" model.

## E. SUMMARY OF RESULTS

The results of this study compared very favorably on trends and optimum parameter values with a similar study made by Aerojet-General Corporation (AGC). The analytical model used by AGC was similar to the one used here for the NaK-Hg heat exchanger, but differed considerably in simulation of the coolant transport delays, the reactor core, and the control system. Tables 1 and 2 show the parameters that were studied, the range studied, the permissible range and design level chosen where applicable, or the expected value where no design choice was made.

Figures 4, 5, and 6 are reproductions of the analog computer traces for three representative cases among the hundreds of cases analyzed. Figure 4 shows the results of a PCS startup simulation using the recommended design levels for all variables studied. Among the variables to which the simulation was most sensitive were the initial NS coolant flow ($w_{c0}$), the initial power ($P_0$), and the time to increase mercury flow from zero to the injection level ($t_{1M}$). Figure 5 shows the results of excessively low values of $w_{c0}$ and $P_0$. Figure 6 shows the consequences of $t_{1M}$ being far too short, although most other variables were near the recommended design levels.

Initial conditions for the parameters shown on the analog traces are given in Table 3. A list of the nomenclature used throughout this report is given in Appendix F.

TABLE 1

PARAMETER RANGES AND DESIGN CHOICES

| Parameter | Range Studied | Permissible Range | Design Choice | Units |
|---|---|---|---|---|
| $t_{1M}$ = time of mercury flow increase from zero to the injection level | 0 to 90 | $\geq 75$ | 90 | sec |
| $t_c$ = time of increase of NaK flow | 9 to 100 | $\geq 25$ | 30 | sec |
| $w_{c0}/w_{cr}$ = ratio of initial to reference NaK flow | 10 to 80 | $\geq 35$ | 50 | % |
| $P_0$ = initial core thermal power | 9 to 160 | 40 to 120 | 50 | kwt |
| $\Theta_{core,0}$ = initial difference between core inlet and core outlet NaK temperatures | 12 to 400 | 40 to 150 | 50 | °F |
| $T_{\Delta R}$ = interval between successive control drum steps in the same direction | 60 to 360 | $\geq 180$ | 240 | sec |
| $t_{2M}$ = time of mercury flow increase from injection to reference level | 100 to 750 | $\geq 300$ | 500 | sec |

TABLE 2

PARAMETER RANGES AND EXPECTED VALUES

| Parameter | Range Studied | Expected Value | Units |
|---|---|---|---|
| $\Delta R$ = control drum step size | 1 to 5 | 3.8 | cents |
| $w_{MI}/w_{Mr}$ = ratio of mercury flow rate at end of injection phase to reference flow rate | 20 to 50 | 40 | % |
| $\tau_c$ = delay before increase of NaK flow | 0 to 42 | 40 | sec |
| $T_{c50}$ = initial value of core outlet coolant temperature | 1270 to 1330 | 1300 | °F |
| $\alpha_f$ = fuel temperature coefficient of reactivity | -0.05 to -0.15 | -0.05 | ¢/°F |
| $\alpha_{\ell g}$ = lower grid plate temperature coefficient of reactivity | -0.02 to -0.10 | -0.04 | ¢/°F |
| $\alpha_{ug}$ = upper grid plate temperature coefficient of reactivity | -0.03 to -0.10 | -0.06 | ¢/°F |
| $\tau_M$ = delay before increase of mercury flow from injection level | 85 to 350 | 190 | sec |

TABLE 3

INITIAL CONDITIONS FOR ANALOG TRACES
FROM PCS STARTUP SIMULATION

| Variable | Figure 4 | Figure 5 | Figure 6 |
|---|---|---|---|
| $T_{cin}$ | 1249°F | 1249°F | 1224°F |
| $T_{c5}$ | 1300°F | 1300°F | 1300°F |
| $\bar{T}_f$ | 1283°F | 1276°F | 1272°F |
| $w_c/w_{cr}$ | 0.5 | 0.1 | 0.4 |
| $L_s$ | 67.7 ft | 67.7 ft | 67.7 ft |
| $n/n_r$ | 0.126 | 0.025 | 0.152 |
| $w_{ML}$ | 0 | 0 | 0 |

NOTES:

1. For PCS startup, the initial time ($t = 0$) is defined as the beginning of the first increase in mercury flow.
2. Initial values of the following variables are assumed to be zero: $R^{\$}$, $\dot{\bar{T}}_f$, $\dot{T}_{f4}$, $\dot{T}_{cin}$, $\dot{T}_{c1}$, $\dot{T}_{c2}$, $\dot{T}_{c3}$, $\dot{T}_{c4}$, $T_{c5}$.
3. A list of the nomenclature used throughout this report is given in Appendix F.

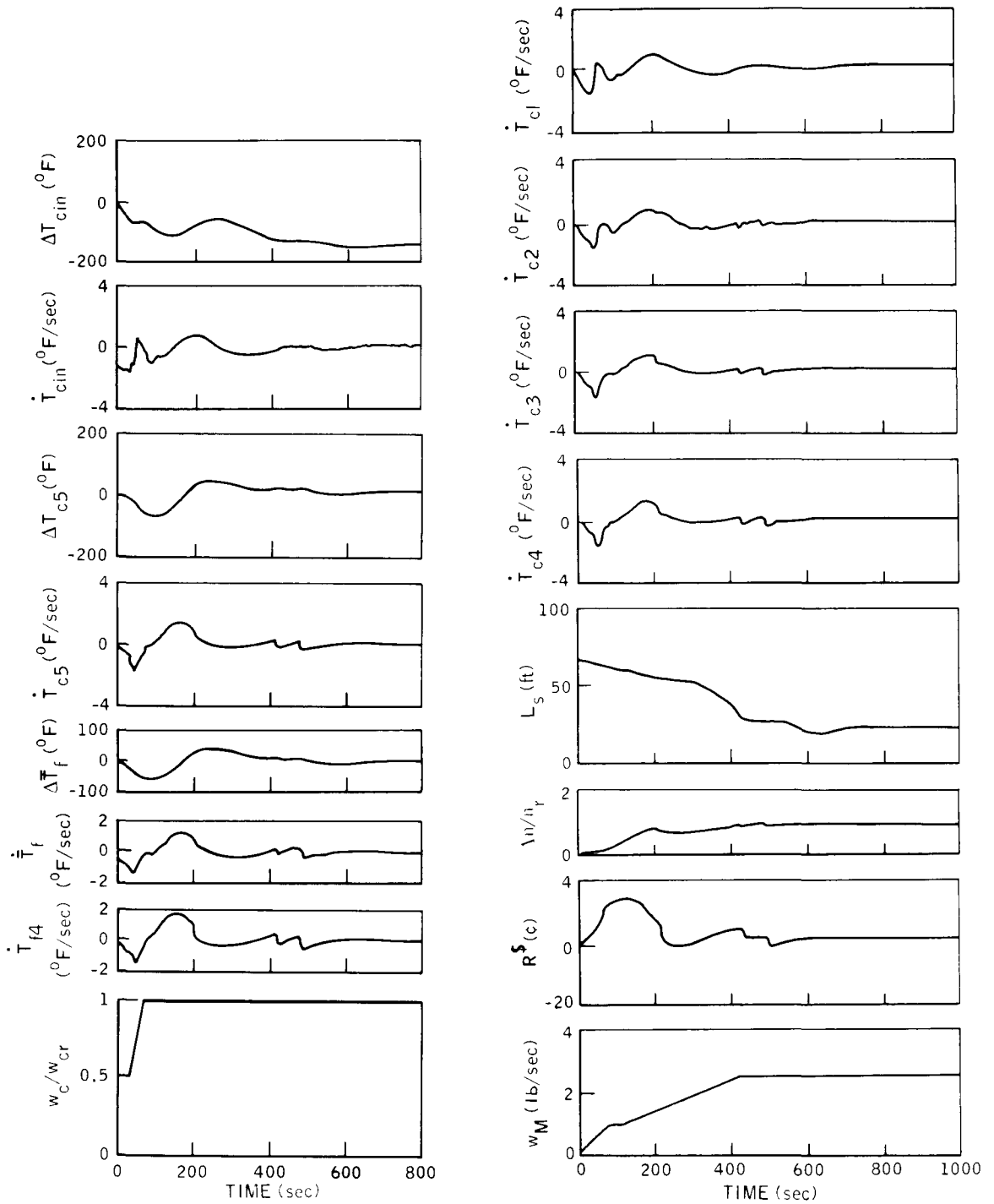


3-30-64 7568-01010-1 3-30-64 7568-01010-2

Figure 4. Analog Computer Traces From Power Conversion System Startup Simulation Based on Recommended Design Levels for all Variables

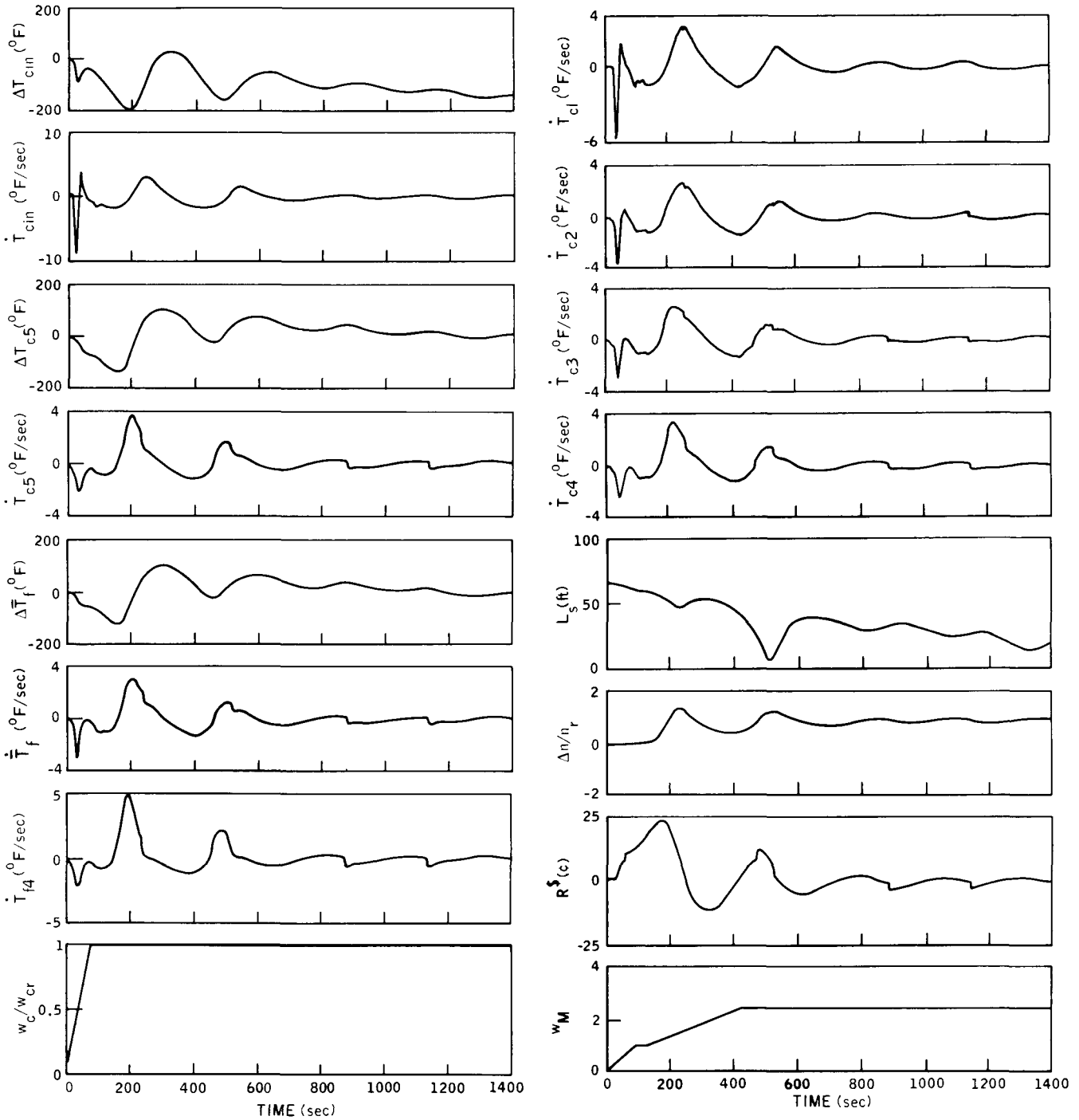


Figure 5. Analog Computer Traces from Power Conversion System Startup Simulation Based on Excessively Low Values of Initial NaK Coolant Flow Rate and Initial Power

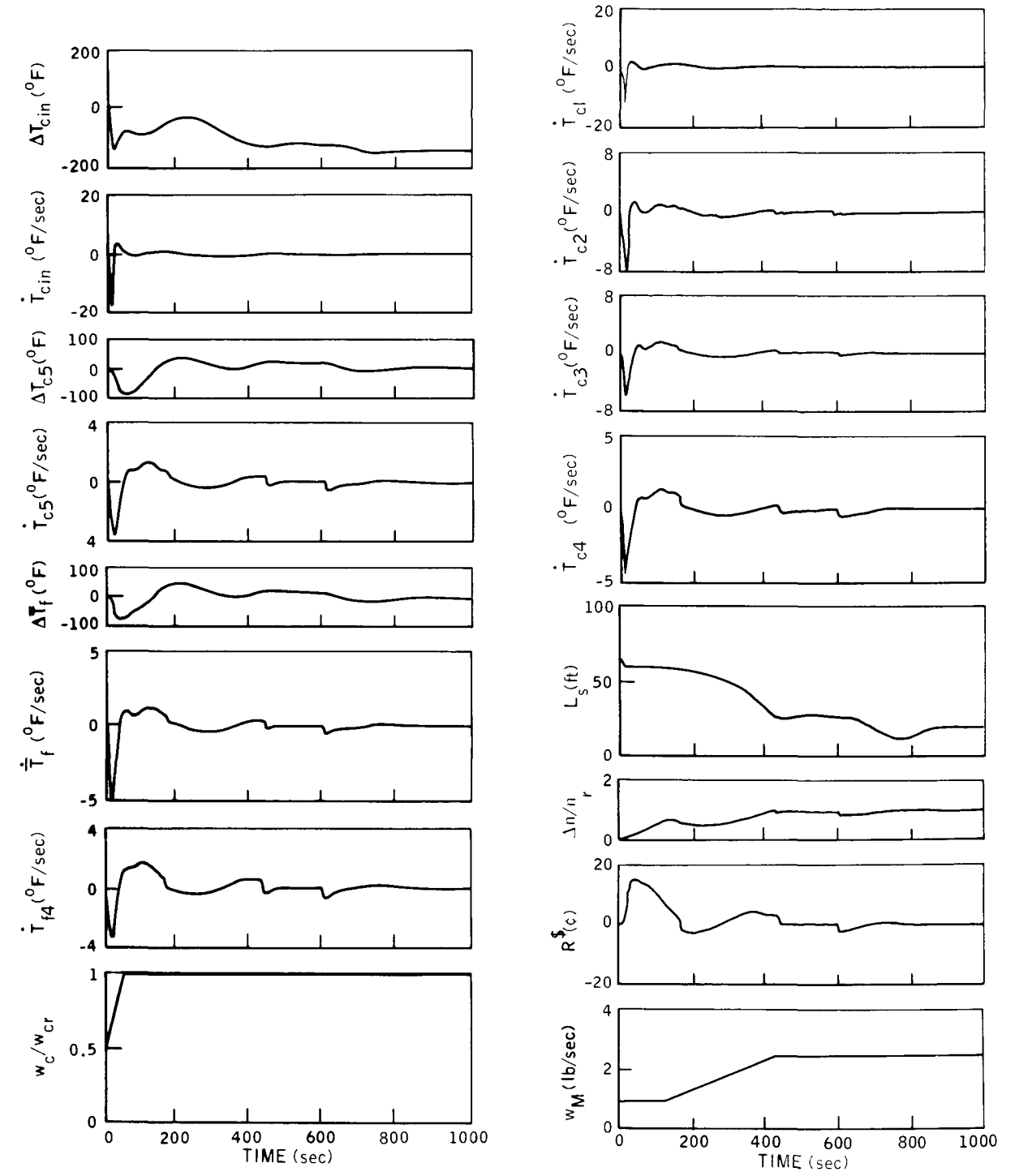


3-30-64 7568-01009-1 3-30-64 7568-01009-2

Figure 6. Analog Computer Traces From Power Conversion System Startup Simulation Based on Excessively Short Time for First Increase in Mercury Flow Level

BLANK

# II. METHOD OF ANALYSIS

## A. MATHEMATICAL MODEL

### 1. General

Analysis of the response of the SNAP 8 nuclear system to power conversion system startup was accomplished by simulating the primary coolant loop (NaK) and portions of the mercury loop on a combination of two PACE 231R and one PACE 1631 analog computers. A thorough simulation of the reactor, controller, intermediate (NaK-Hg) heat exchanger (IHX), and coolant transport delays was used. The effects of the turbine-alternator pump combination, the auxiliary heat exchanger, the parasitic load, the heat rejection loop were programmed in from information furnished by Aerojet-General Corporation.[1] Detailed equations used in the simulation are presented in Appendix A. The analog computer diagrams used in the simulation are presented in Appendix B. Computer potentiometer (pot) settings are also given in Appendix B, and the system constants and reference levels are tabulated in Appendix C.

The optimization of the many parameters involved in this study was done by setting up an initial base case, with parameter values set by preliminary estimates, and varying each parameter individually from the base. As trends in effects were observed, the base case was revised, and parameter variations were limited to those showing strong effects. After repeated optimization resulted in an acceptable set of design conditions, the effect of each parameter was again checked. Finally, a complete set of design conditions could be chosen.

### 2. Reactor Kinetics

The standard reactor kinetics equations[2] were normalized to a reference level and modified to a "delta ($\Delta$) model" wherein changes from initial levels were computed. Six delayed neutron precursor groups were simulated. Changes in reactivity were computed by summing the effects of control drum action and of feedbacks due to changes in temperature of the fuel and grid plates. The temperature coefficients of reactivity for the fuel and grid plates were varied from case to case as part of the parameter study.

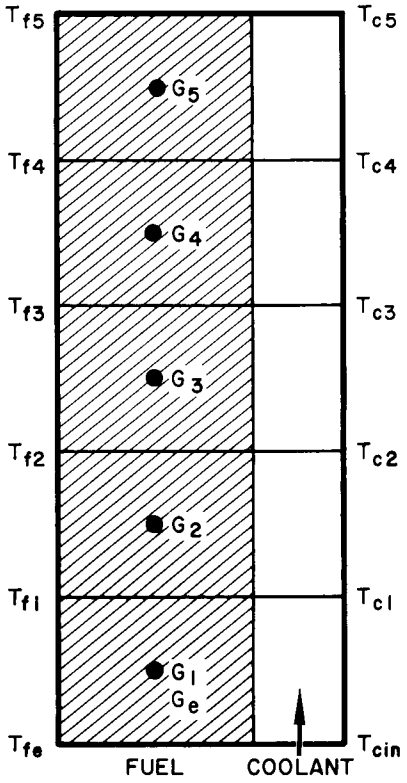


Figure 7. Core Heat Transfer Nodes

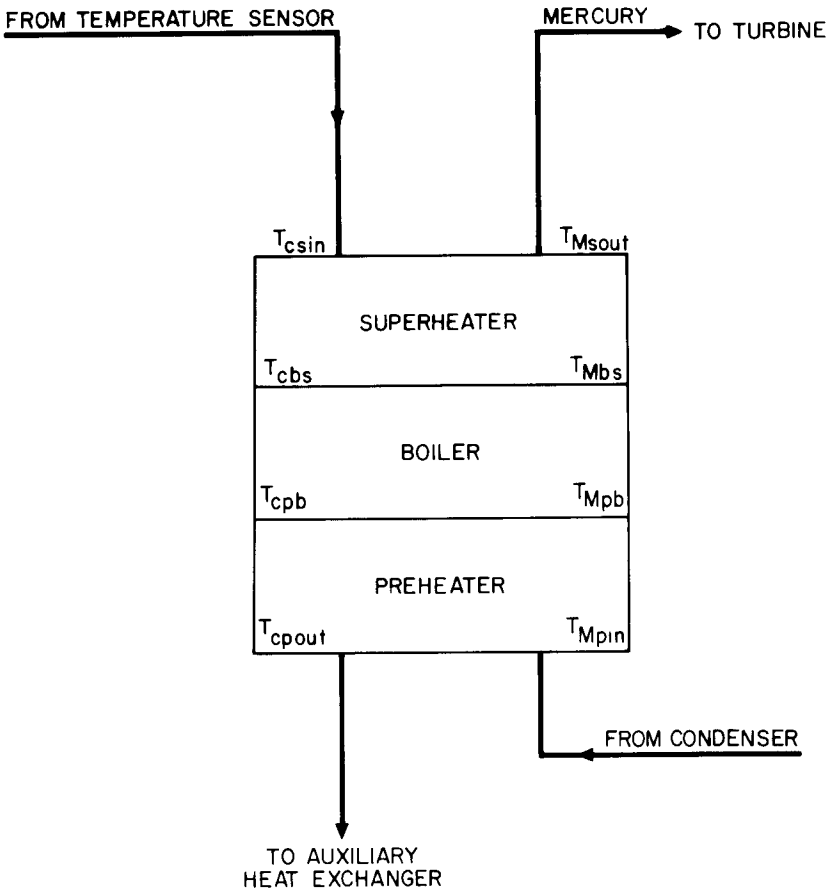


Figure 8. Intermediate Heat Exchanger Schematic

3. Core Heat Transfer

The reactor core heat transfer equations are based on an entrance fuel node model developed by D. G. Mason and R. W. Winson at Atomics International.[3] The model is basically a modified "backward difference" model involving five equally spaced axial fuel and coolant nodes and an entrance fuel node (see Figure 7). This model was developed as a substitute for the few node linear gradient or "central difference" model.

The usual central-difference model gives an anomalous decrease in outlet coolant temperature in response to a rapid increase in inlet coolant temperature. This anomaly is avoided by the entrance fuel node model which uses the entrance node to correct the error in average fuel temperature resulting from the backward-difference technique.

Mason and Winson show that the five node plus entrance fuel node model responds quite accurately to large step changes in power and inlet coolant temperature when compared with a 40-node central-difference model. For a step change in power level, the entrance fuel node model with 5 fuel nodes yields a maximum transient error of 5% and a steady-state error of less than 1.5% in average fuel temperature. The response of the entrance fuel node model to a step change in inlet coolant temperature is practically identical to that of a multi-node central-difference model except that the entrance node model has no anomalous dip in outlet coolant temperature. The core heat transfer equations were also written as a $\Delta$ model. They include heat generation within the fuel, heat transfer from fuel to coolant, and heat transfer by transport of the coolant from one node to the next. The NaK coolant flow rate was programmed as a variable function of time in these equations. The heat generation within each fuel node is dependent on the reactor power level as calculated by the reactor kinetics equations. Core average fuel temperature was computed as a direct average of the temperatures of the five axial fuel nodes and the entrance fuel node.

The temperatures of the lower and upper grid plates are calculated from the core inlet and core outlet coolant temperatures by using effective values for heat conduction area and path length.

4. Intermediate Heat Exchanger (IXH)

The equations for simulation of the intermediate (NaK-Hg) heat exchanger were supplied by AGC.[1] For purposes of this simulation, the heat exchanger was considered to consist of three sections, preheater, boiler, and superheater (Figure 8).

a. Preheater Section

The heat given up by NaK in the preheater section is equal to the heat transferred to the mercury plus the heat stored in the heat exchanger materials. Heat transferred to the mercury is based on a log-mean temperature difference and an overall heat transfer coefficient dependent on mercury flow. The length of the preheater section is dependent on the mercury temperatures and flow rate. The mercury pressure at the interface between the preheater and boiler sections is dependent on the pressure at the boiler outlet, mercury flow rate, and boiler section length. The temperature of the mercury at this interface is a function of the pressure. Mercury flow rate is programmed as a function of time.

b. Boiler Section

The boiler section heat balance is computed by assigning the heat lost by the NaK in the boiler section to boiling the mercury and heating the heat exchanger materials. The log-mean temperature difference and overall heat transfer coefficient for the boiler section were assumed to be constant at the reference level. The length of the boiler section was based on the NaK and mercury temperatures in the section and the NaK flow rate. Mercury pressure in the boiler section was computed from the pressure in the superheater section. The mercury temperature at the interface of the boiler and superheater sections was programmed as the saturation temperature corresponding to the mercury pressure at the interface.

c. Superheater Section

The heat lost by the NaK in the superheater section goes to heat up the heat exchanger materials in this section and to heat the mercury vapor. The heat absorbed by the mercury vapor is computed from the mercury and NaK flow rates, temperatures of NaK and mercury at their respective inlets to this section, the superheater section length, and an overall heat transfer coefficient for the section. The superheater section length is calculated by subtracting the

variable preheater and boiler section lengths from the fixed length of the entire heat exchanger. The overall heat transfer coefficient for the superheater section is assumed to vary as a function of the mercury flow. The mercury pressure in the superheater section is computed from the ideal gas law. It is based on an average mercury temperature for the section and a flow dependent mercury vapor density. The mercury vapor flow rate at the outlet of the heat exchanger is computed from the sonic nozzle relationship between flow, pressure, and temperature at the turbine nozzle.

5. Controller

The simulated controller used in this study provides a step change in reactivity each time the measured core outlet coolant temperature ($T_{cm}$) goes above or below the temperature deadband. If $T_{cm}$ stays out of the deadband, an additional reactivity step is provided after each "stepping interval." The step size ($\Delta R$), interval between successive steps in the same direction ($T_{\Delta R}$), and the temperature deadband limit settings (UDB and LDB) can be varied in this model.

The time constant for the temperature sensor is simulated by a simple lag between the core outlet coolant temperature ($T_{c5}$) and the measured temperature ($T_{cm}$).

$$T_{cm} = \frac{T_{c5}}{1 + \tau_m S}$$

where $\tau_m$ is the sensor time constant. The analog computer diagram for the controller is shown in Appendix A.

6. Transport Delays

The delay times involved in transporting the NaK coolant through the primary coolant loop were simulated in two sections. One section simulated the transport delay time from the core outlet to the intermediate heat exchanger NaK inlet. This delay is designated as $\tau_{TRI}$. The second delay section includes the transport delay times from the intermediate heat exchanger to the auxiliary heat exchanger ($\tau_{TIA}$), from the auxiliary heat exchanger to the parasitic load ($\tau_{TAP}$), and from the parasitic load to the core inlet ($\tau_{TPR}$). This combination was designated $\tau_{TIR}$ and was computed from:

$$\tau_{TIR} = \tau_{TIA} + \tau_{TAP} + \tau_{TPR}$$

Each section of the transport delay was approximated by a series of nine cascaded simple lags, each having 1/9 of the time constant of the section. The approximation used for the transport delay time $\tau_{TRI}$ is:

$$T_{csin} = T_{c5}\left[\frac{1}{1+\left(\frac{\tau_{TRI}}{9}\right)S}\right]^9 \simeq T_{c5}\, e^{-\tau_{TRI}S}$$

where:

$T_{csin}$ = NaK coolant temperature at the NaK inlet to the IHX superheater section.

$T_{c5}$ = core outlet NaK temperature.

Accordingly, the transport delay $\tau_{TIR}$ was approximated by

$$T_{cin} = T_{cpout}\left[\frac{1}{1+\left(\frac{\tau_{TIR}}{9}\right)S}\right]^9 \simeq T_{cpout}\, e^{-\tau_{TIR}S}$$

7. Miscellaneous

For this study, the auxiliary heat exchanger (AHX) was assumed to provide a constant load throughout PCS startup. The magnitude of this load was adjusted to give the desired initial reactor power level when added to expected heat losses from the primary coolant loop. The parasitic load (PL) was assumed to add heat to the NaK coolant in proportion to the rate of mercury vapor flow. Both the heat lost through the AHX and the heat regained from the parasitic load were incorporated in the primary coolant loop as simple changes in coolant temperature. These temperature changes are dependent on NaK flow rate as well as on the amount of heat lost or gained.

The mercury flow rate was programmed into the IHX equations as a series of linear functions of time. These functions were based on calculations of turbine speed buildup and controlled mercury injection rates by AGC.[1] The primary NaK flow rate was also programmed as a series of linear functions of

time based on calculations of turbine, alternator, and pump speeds. Generalized plots of mercury and NaK flow as functions of time are given in Figures 9 and 10. The various delays and time of flow increase ($\tau_c$, $\tau_M$, $t_c$, $t_{1M}$, $t_{2M}$) as shown in Figures 9 and 10 were varied as part of the parameter study.

## B. LIMITATIONS ON SYSTEM VARIABLES

Throughout the PCS startup transient, the rates of change of reactor fuel and NaK coolant temperatures must be controlled. If these rates of change are excessive, damage to the ceramic lining of the fuel cladding could result, leading to excessive leakage of the hydrogen moderator. It is assumed for this study that the rate of change of cladding temperature can be equal to the highest rate of change of either fuel or coolant temperature. The present limit on rate of change of cladding temperature is 150°F/minute.

The nuclear system outlet NaK temperature, after mercury flow reaches 100% of the reference level, ($T_{c5min2}$) must be kept above 1270°F. This minimum temperature is required to avoid suppressed boiling in the NaK-Hg heat exchanger and the resultant carryover of liquid mercury into the turbine.

In addition to the above requirements, safety considerations during testing of SNAP 8 require that the maxima of reactor power and outlet coolant temperature be kept below the safety system scram settings. The present scram settings are 130% of reference power and 1375°F core outlet coolant temperature.

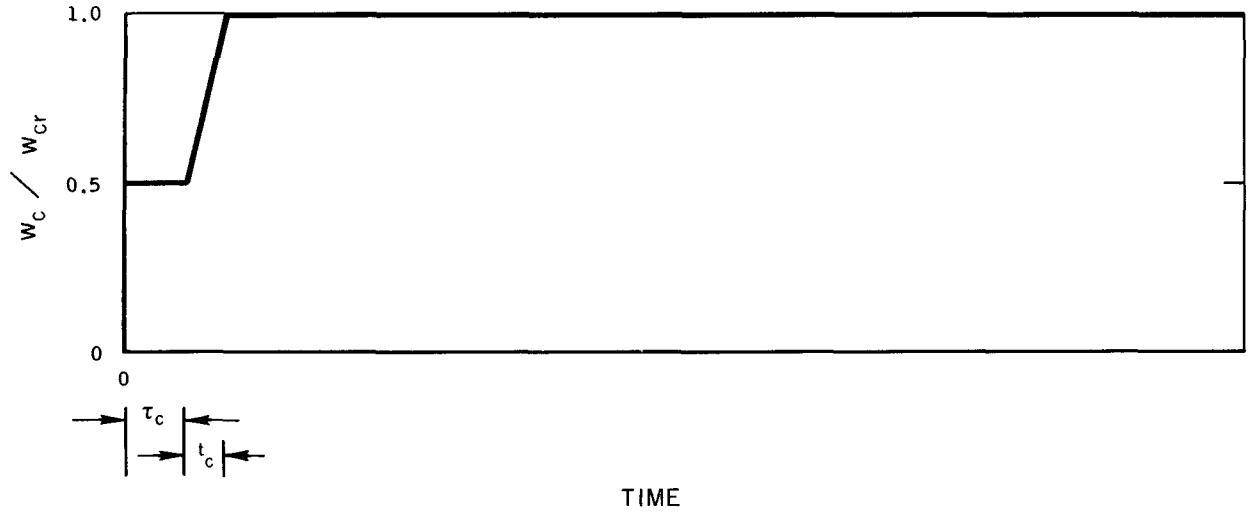


4-1-64 7568-01011

Figure 9. NaK Flow Rate During Simulated Startup of Power Conversion System

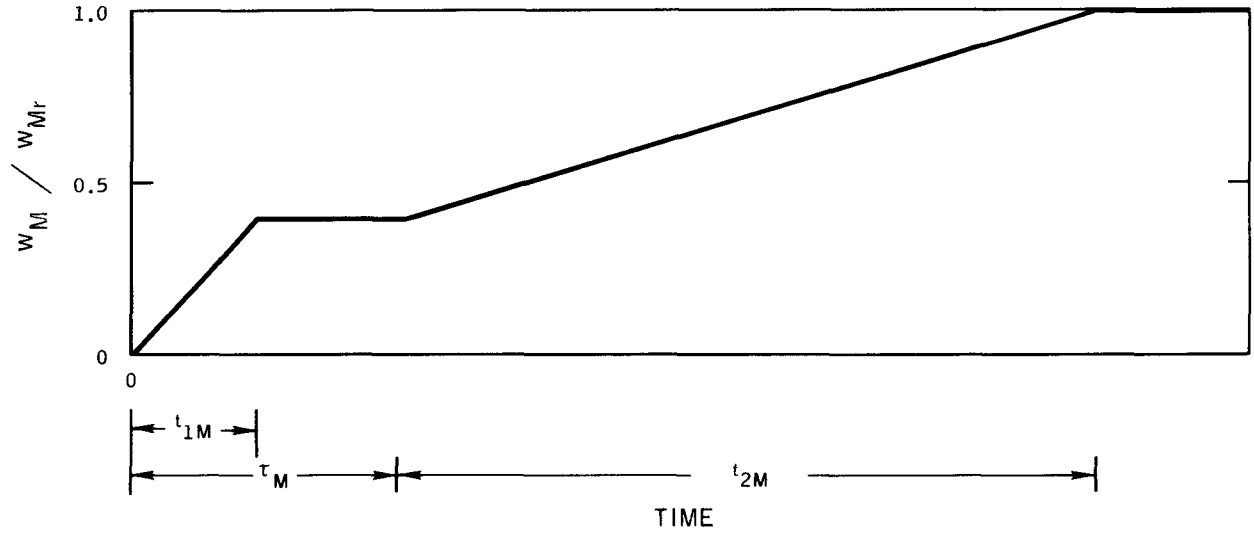


4-1-64 7568-01012

Figure 10. Mercury Flow Rate During Simulated Startup of Power Conversion System

## III. RESULTS

### A. GENERAL

Figures 11 through 71 present "cross plots" of the results of the parameter study of power conversion system startup. The variables chosen for plotting show the effect of parameter changes on meeting the prescribed limitations mentioned previously. It was found that, of the fuel and coolant temperatures at any position in the reactor core, the core inlet coolant temperature ($T_{cin}$) had the greatest rate of change for any transient driven primarily by mercury or NaK flow changes. For transients that also involve comparatively large changes in reactor power, the core outlet coolant temperature ($T_{c5}$) or the fuel temperature in the fourth axial node ($T_{f4}$) showed the highest rate of change.

Two distinct "side effects" must be carefully accounted for during analysis of the results of the PCS startup analog simulation. The first of these is the effect of control drum steps on the magnitudes and rates of change of the output variables. The second is that the final values of temperatures and power are fixed by the rated NaK flow through the reactor and the load imposed by the PCS at full mercury flow. Thus, the lowest values of maximum temperatures and power are restricted, no matter how much a given parameter is changed.

During PCS startup, the control system will be operating in the long-term control mode. When the NaK outlet coolant temperature goes beyond the range of the deadband, the control drum will step in such a direction as to return the outlet temperature to within the deadband. If a single drum step is not sufficient to effect this return, the controller will wait for a specified time interval ($T_{\Delta R}$) and then provide an additional drum step. When comparing a set of analog cases to determine the effect of any parameter other than step interval, one must be certain that the control step sequence is the same for all runs considered. If the step sequence changes, the true effect of the parameter being studied might be masked by the effect of the control steps. For this study, the deadband was assumed to be 1280°F to 1320°F which is the smallest deadband possible with the present nominal settings and tolerances.

Since in this study the final NaK outlet coolant temperature is held between 1280 and 1320°F by the control system, the maximum value of reactor outlet coolant temperature will always be at least 1280°F, regardless of

the rest of the transient. Also, with the reference power level set at 400 kwt, of which about 35 kwt is returned to the primary NaK by the parasitic load, the maximum power level during any run will be at least 365 kwt. To this figure must be added the load imposed by the auxiliary heat exchanger. Thus the effect of some parameter variations may also be obscured because the maxima of the output variables cannot be below the above mentioned levels.

## B. PRIMARY EFFECTS

Several parameters were found to have a stronger effect on the PCS startup transient than the other parameters studied. First among these are the rates of change of mercury and NaK flow, which provide the driving forces of the transient. Also of major importance are the initial NaK flow, initial power level or core temperature difference, and the interval between control drum steps. The range of these parameters which has been studied was given in Table 1.

The initial rate of change of mercury flow has its strongest effect on the rates of change of reactor temperatures. If the time for mercury flow to increase from 0 to 40% of rated flow ($t_{1M}$) is less than 75 seconds, the rate of change of core inlet NaK temperature ($T_{cin}$) will exceed 150°F/minute. The initial Hg rise time ($t_{1M}$) has little effect on the maximum or minimum values of core outlet coolant temperature ($T_{c5}$) (Figures 11 to 18).

The rate of change of NaK flow has a similar but less pronounced effect. The time for NaK flow to increase from 50 to 100% of reference flow ($t_c$) must be at least 25 seconds in order to avoid exceeding 150°F/minute rate of change of fuel or coolant temperatures. Again, the rate of change of NaK flow has little effect on the range of core outlet coolant temperature (Figures 19 to 22).

The initial level of NaK flow ($w_{c0}/w_{cr}$), at the beginning of PCS startup, is designated in percentage of the reference NaK flow level. This initial NaK flow has a two-way effect on system output variables. An initial flow level that is too low will result in excessive temperature rates of change, while a level that is too high will increase the maximum core outlet coolant temperature during PCS startup to beyond the acceptable limits. Increasing NaK flow prior to PCS startup also obviously increases pumping power requirements. Assuming that rates of change of all fuel and coolant temperatures must be held below 150°F/minute, the initial NaK flow must be above 35% of the reference flow,

for an initial power level of 50 kw. This limitation is imposed by the rate of change of core inlet coolant temperature. Also for the same initial power level, the initial NaK flow must be less than 60% to avoid excessively high values of core outlet coolant temperature during the PCS startup transient (Figures 23 to 29).

The initial thermal power level ($P_0$) and the initial core temperature difference ($\Theta_{core,0}$) are interrelated, the relationship being directly dependent on NaK flow level. Many reactor output variables exhibit minima with respect to these parameters, but the minima are strongly dependent on flow as well as the initial thermal power ($P_0$). $P_0$ (or $\Theta_{core,0}$) has a strong effect on both rates of change and extremes of core temperatures. Parameter studies indicate that, for 40 to 60% initial NaK flow, $P_0$ must be between 40 and 120 kwt corresponding to initial core temperature differences of 40 to 150°F. The lower limits are due to maximum core outlet coolant temperature, and the upper limits are due to coolant temperature rates of change (Figures 30 to 43).

As long as the interval between successive control drum steps in the same direction ($T_{\Delta R}$) is greater than 200 seconds, changing this interval has little effect on PCS startup. However, if $T_{\Delta R}$ is much below 200 seconds, it is possible that unnecessary and undesirable reactivity steps could occur. For a $T_{\Delta R}$ of 120 seconds, these undesirable steps increase both the magnitude and the rate of change of $T_{c5}$ beyond acceptable limits (see Figures 44 to 51).

## C. SECONDARY EFFECTS

The majority of the system parameters that were varied during the study of the PCS startup transient had relatively little effect on the transient, at least within the ranges studied. These parameters and the range of variation considered are listed in Table 2.

As can be seen in Figures 52, 54, and 55, the control drum step size ($\Delta R$) has practically no effect on the maximum core outlet NaK temperature or on the maximum rates of change of either coolant or fuel temperatures. Increasing $\Delta R$ leads to a small increase in the first minimum of core outlet coolant temperature ($T_{c5min1}$) before Hg flow reaches 100%. Figure 53 shows a variation in the minimum of core outlet coolant temperature after mercury flow reaches 100% ($T_{c5min2}$), but this result is meaningless because all values of $T_{c5min2}$ are within the control deadband.

As long as the time for the second increase in mercury flow ($t_{2M}$) is at least 250 seconds, changes in this parameter have very little effect on any of the maxima or minima considered here (see Figures 56 to 59). If $t_{2M}$ is less than 250 seconds, decreasing it will adversely affect the maxima and minima of core outlet coolant temperature as well as the rates of change of all core temperatures.

The ratio of mercury flow rate at the end of the injection phase to the reference flow rate ($w_{MI}/w_{Mr}$) has little effect on rates of change of core temperatures, as long as the rate of increase of flow is held constant. However, increasing $w_{MI}/w_{Mr}$ tends to increase the maximum core outlet coolant temperature ($T_{c5max}$) and decrease the first minimum of core outlet temperature (Figures 60 to 63).

The delay before NaK flow starts to increase ($\tau_c$) has very little effect on the extremes of core outlet coolant temperature ($T_{c5}$) as long as $\tau_c$ is less than 40 seconds. However, an increase in $\tau_c$ produces an increase in the rates of change of fuel and coolant temperatures (Figures 64 to 67).

The initial value of core outlet coolant temperature ($T_{c50}$) was assumed to be within the control deadband of 1270 to 1330°F, and most of this study was done with $T_{c50}$ = 1300°F. A check of the effect of a 20°F increase in $T_{c50}$ shows average increases of about 15°F in the maxima and minima of $T_{c5}$. Very little effect was observed in the rates of change of core temperatures (see Figures 68 to 71).

The temperature coefficients of reactivity for the reactor fuel and grid plates ($\alpha_f$, $\alpha_{\ell g}$, $\alpha_{ug}$), being negative, exhibit a stabilizing effect on the system during PCS startup. If the sum of these coefficients is made 60% more negative (by tripling the value of $\alpha_f$) the range of core outlet coolant temperature will be reduced to about 2/3 of its previous range. Rates of change of fuel and coolant temperatures will be reduced about 10 to 20%. If the PCS startup transient were driven by reactivity insertion rather than by changes in core inlet coolant temperature, the effect of the lower grid plate coefficient could not be lumped with the others. Its effect would be delayed by the primary NaK loop transport time.

The delay before mercury flow is increased from the injection level ($\tau_M$) has practically no effect on the maximum rates of change of fuel and coolant temperatures. Increasing $\tau_M$ beyond 100 seconds appears to decrease slightly both the maximum and minimum values of core outlet coolant temperature.

## IV. CONCLUSION

The overall optimization of parameters achieved by this study provides a PCS startup transient that is well within all presently known limitations. The permissible range of parameters studied and the present choice of design levels were given previously in Table 1. The variables listed in Table 2 had relatively small effects on the transients, and their values are primarily set by considerations other than PCS startup. If these variables, or many others not considered here, were to be changed beyond the range studied, the effect might be sufficient to necessitate changes in the design levels chosen.

As previously indicated, the method of simulation of the system on the analog computer can have a very strong effect on the results. This is particularly true of the intermediate heat exchanger and the reactor core heat transfer models. Alternate analytical methods and experimental results are presently being studied in order to confirm the validity of the present analog computer simulation.

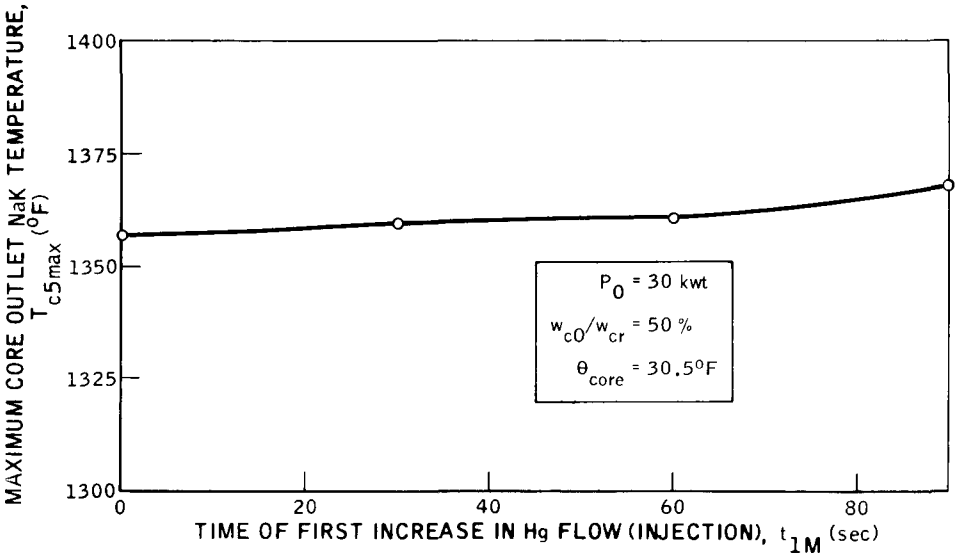


3-18-64 7568-0946

Figure 11. Effect of Time for First Increase in Mercury Flow on Maximum Core Outlet NaK Temperature, 30-kwt Initial Power

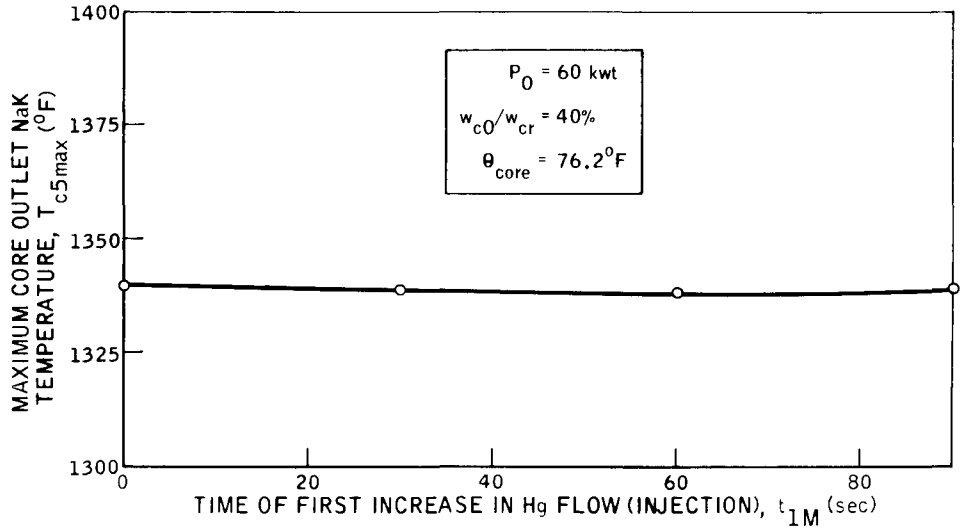


3-18-64 7568-0947

Figure 12. Effect of Time for First Increase in Mercury Flow on Maximum Core Outlet NaK Temperature, 60-kwt Initial Power

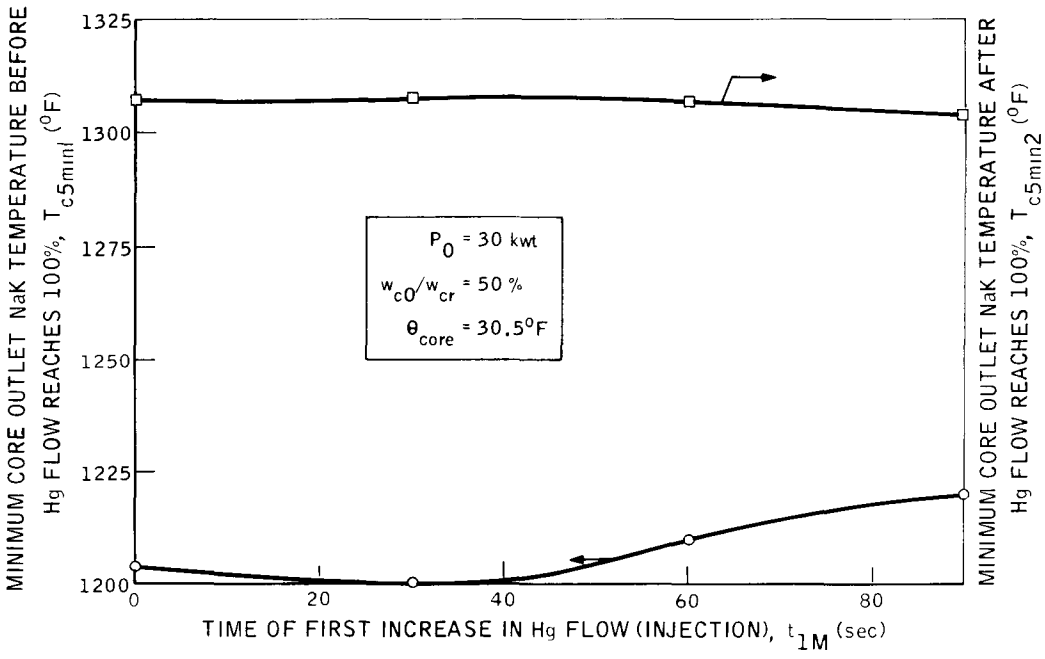


3-18-64 7568-0948

Figure 13. Effect of Time for First Increase in Mercury Flow on Minimum Core Outlet NaK Temperature, 30-kwt Initial Power

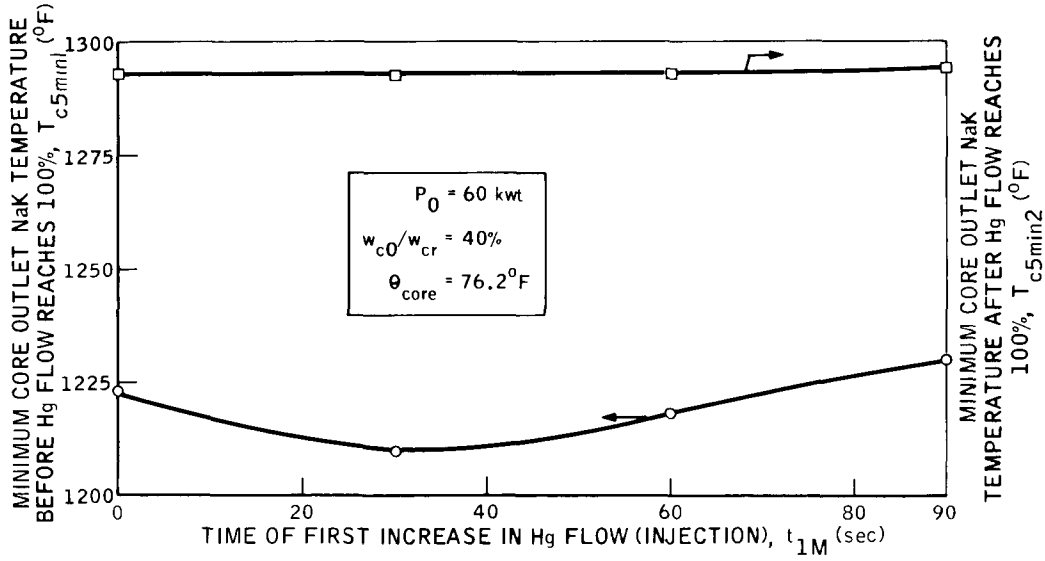


3-18-64 7568-0949

Figure 14. Effect of Time for First Increase in Mercury Flow on Minimum Core Outlet NaK Temperature, 60-kwt Initial Power

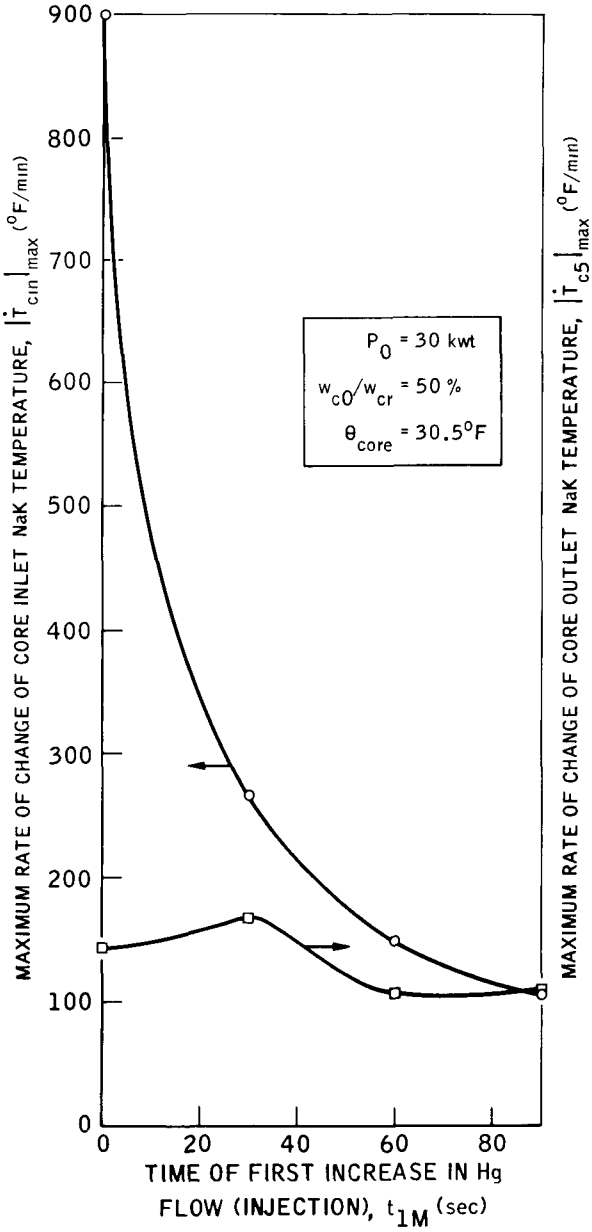


3-18-64 7568-0950

Figure 15. Effect of Time of First Increase in Mercury Flow on Maximum Rate of Change of Core Inlet and Outlet NaK Temperatures, 30-kwt Initial Power

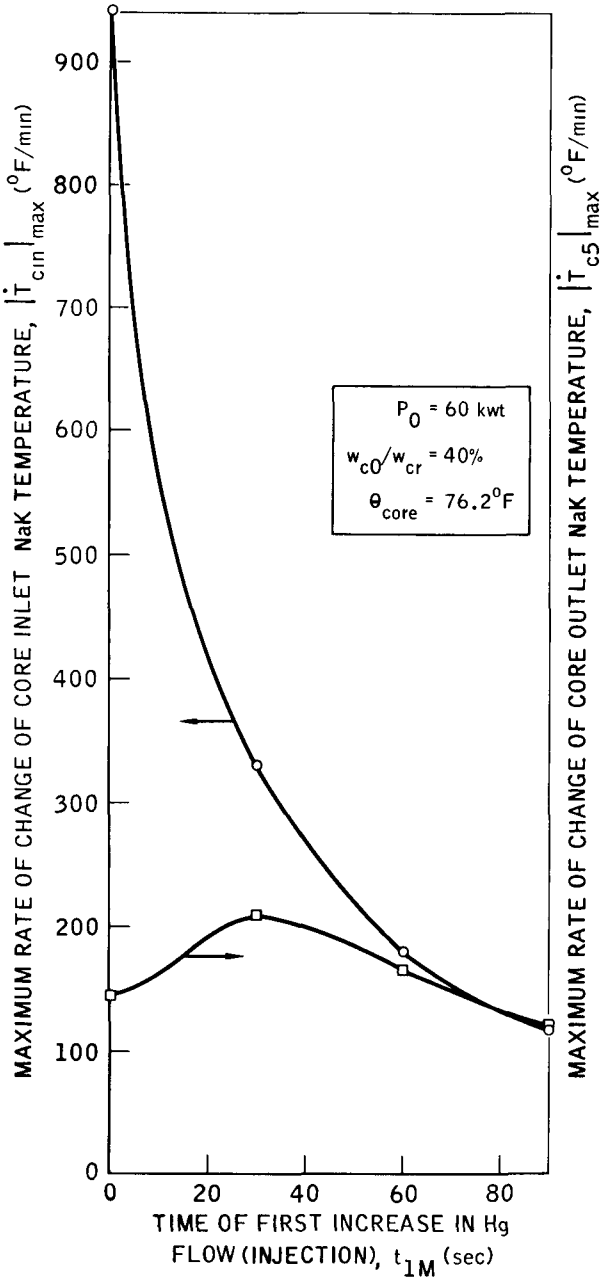


3-18-64 7568-0951

Figure 16. Effect of Time of First Increase in Mercury Flow on Maximum Rate of Change of Core Inlet and Outlet NaK Temperatures, 60-kwt Initial Power

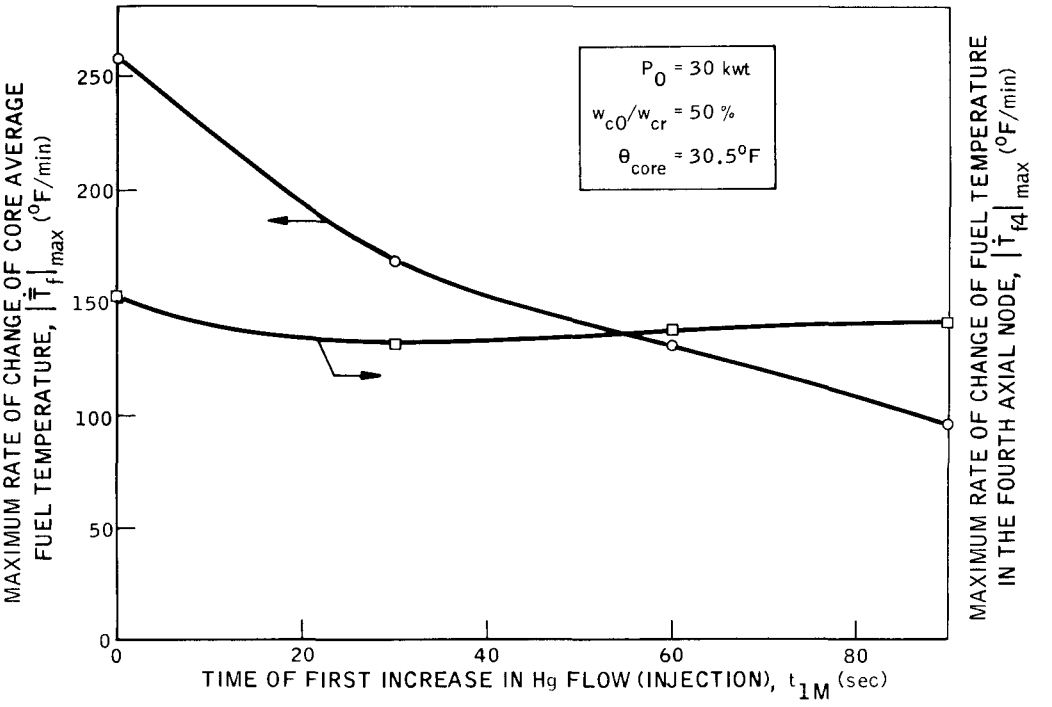


3-18-64 7568-0952

Figure 17. Effect of Time of First Increase in Mercury Flow on Maximum Rate of Change of Core Average and Fourth Axial Node Fuel Temperatures, 30-kwt Initial Power

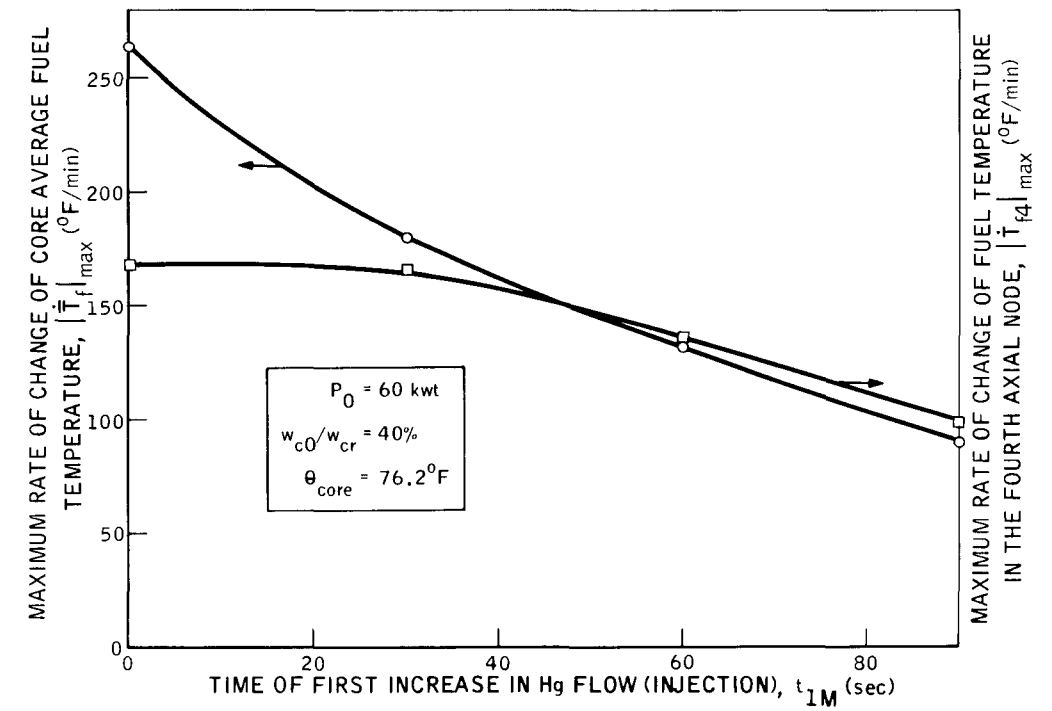


3-18-64 7568-0953

Figure 18. Effect of Time of First Increase in Mercury Flow on Maximum Rate of Change of Core Average and Fourth Axial Node Fuel Temperatures, 60-kwt Initial Power

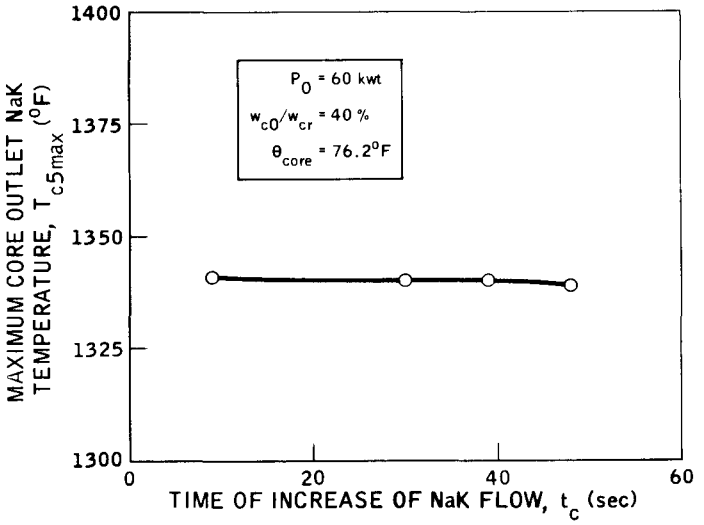


3-18-64 7568-0954

Figure 19. Effect of Time of Increase of NaK Flow on Maximum Core Outlet NaK Temperature

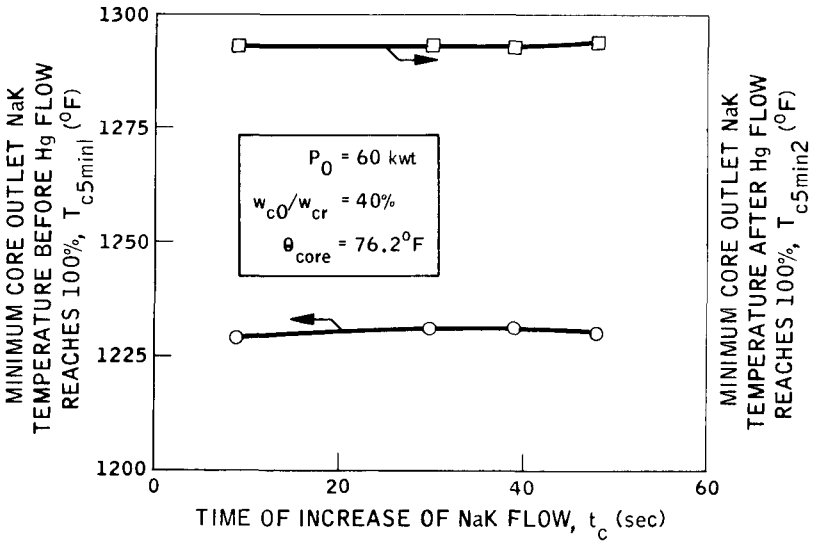


3-18-64 7568-0955

Figure 20. Effect of Time of Increase of NaK Flow on Minimum Core Outlet NaK Temperature

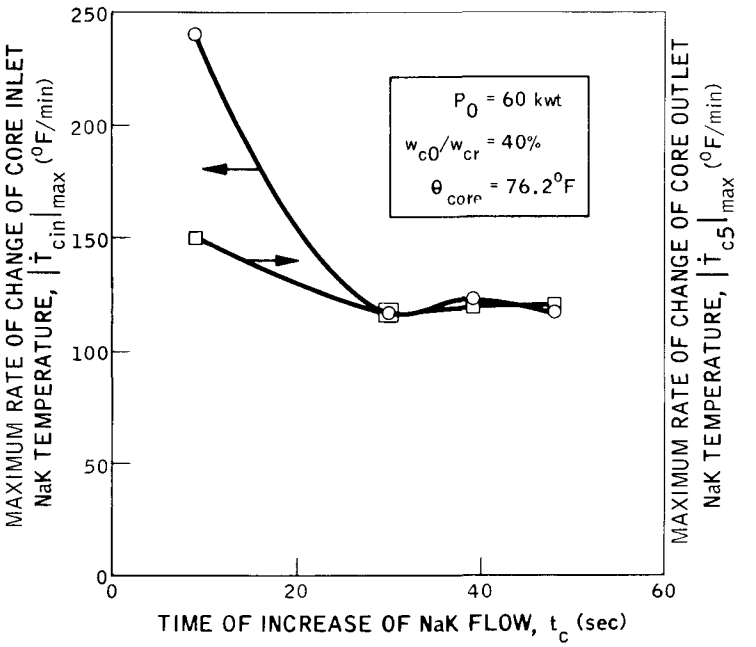


3-18-64 7568-0956

Figure 21. Effect of Time of Increase of NaK Flow on Maximum Rate of Change of Core Inlet and Outlet NaK Temperatures

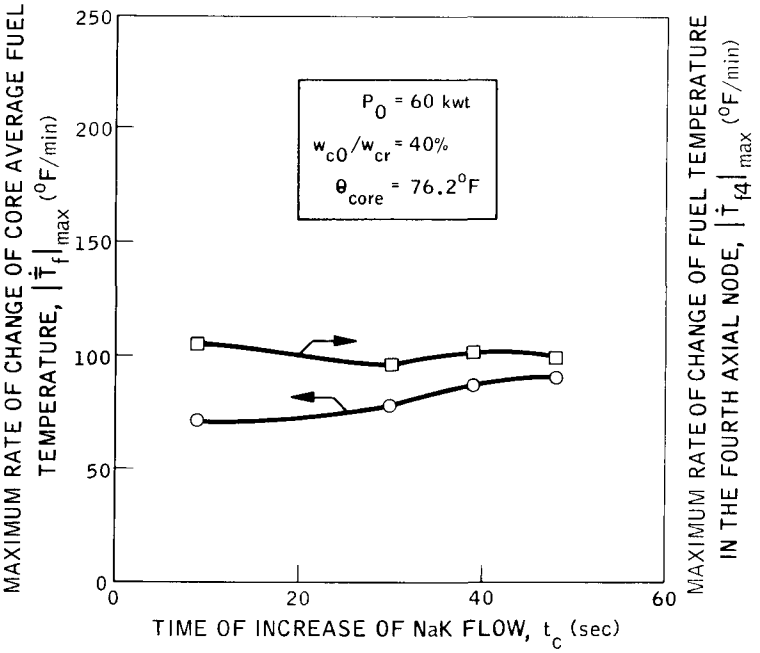


3-18-64 7568-0957

Figure 22. Effect of Time of Increase of NaK Flow on Maximum Rate of Change of Core Average and Fourth Axial Node Fuel Temperatures

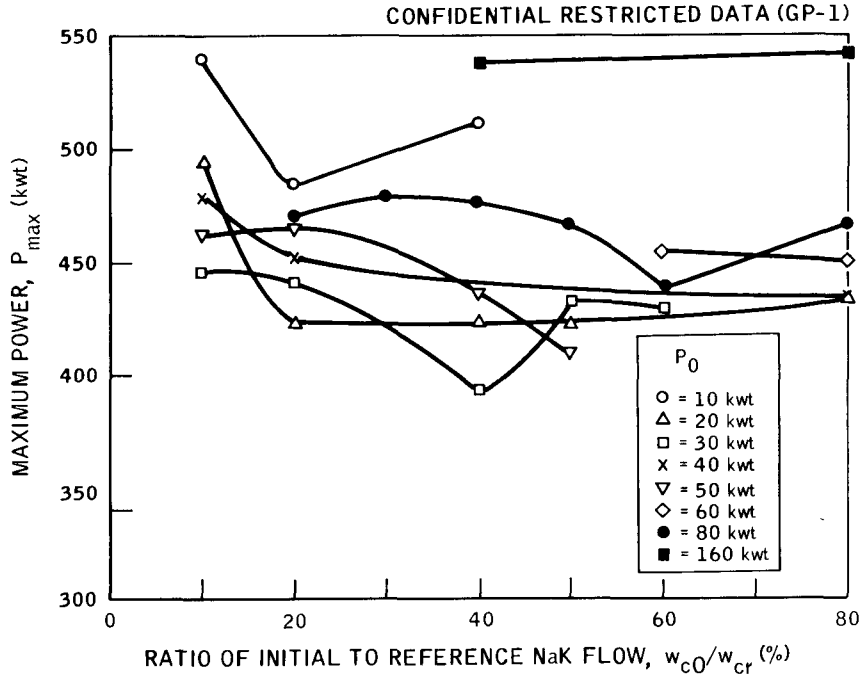


3-18-64 7568-0921

Figure 23. Effect of Initial NaK Flow on Maximum Power

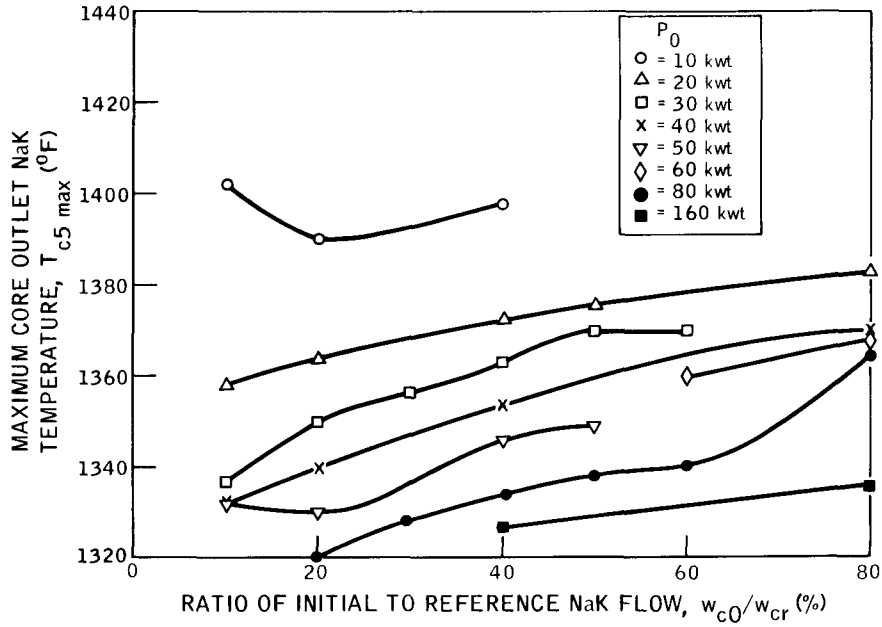


3-18-64 7568-0922

Figure 24. Effect of Initial NaK Flow on Maximum Core Outlet NaK Temperature

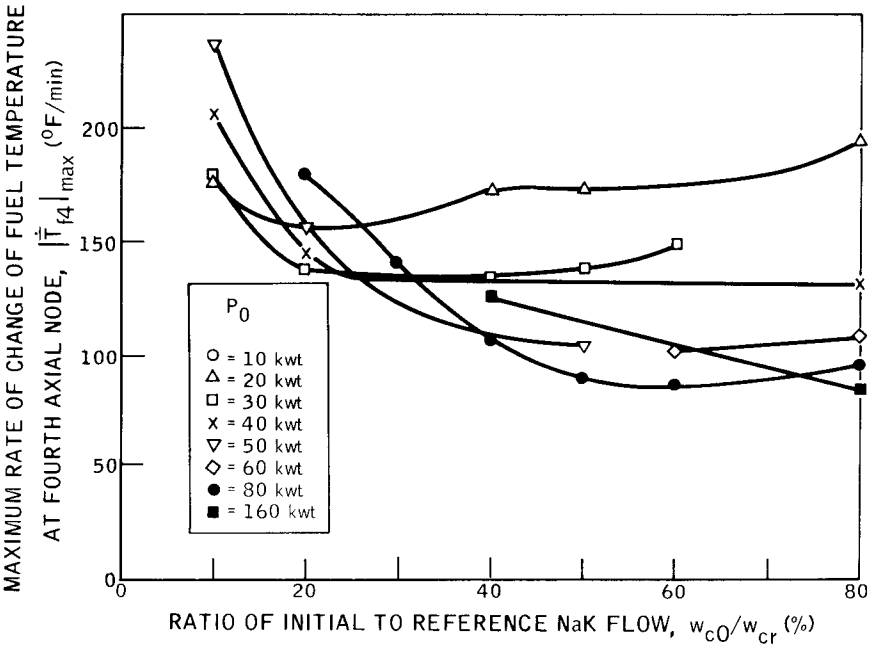


3-18-64 7568-0923

Figure 25. Effect of Initial NaK Flow on Maximum Rate of Change of Fuel Temperature at Fourth Axial Node

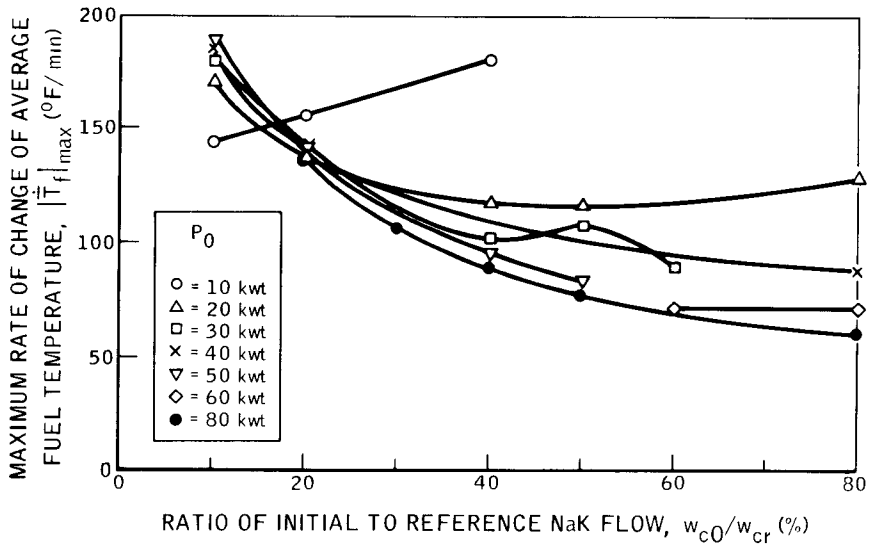


3-18-64 7568-0924

Figure 26. Effect of Initial NaK Flow on Maximum Rate of Change of Average Fuel Temperature

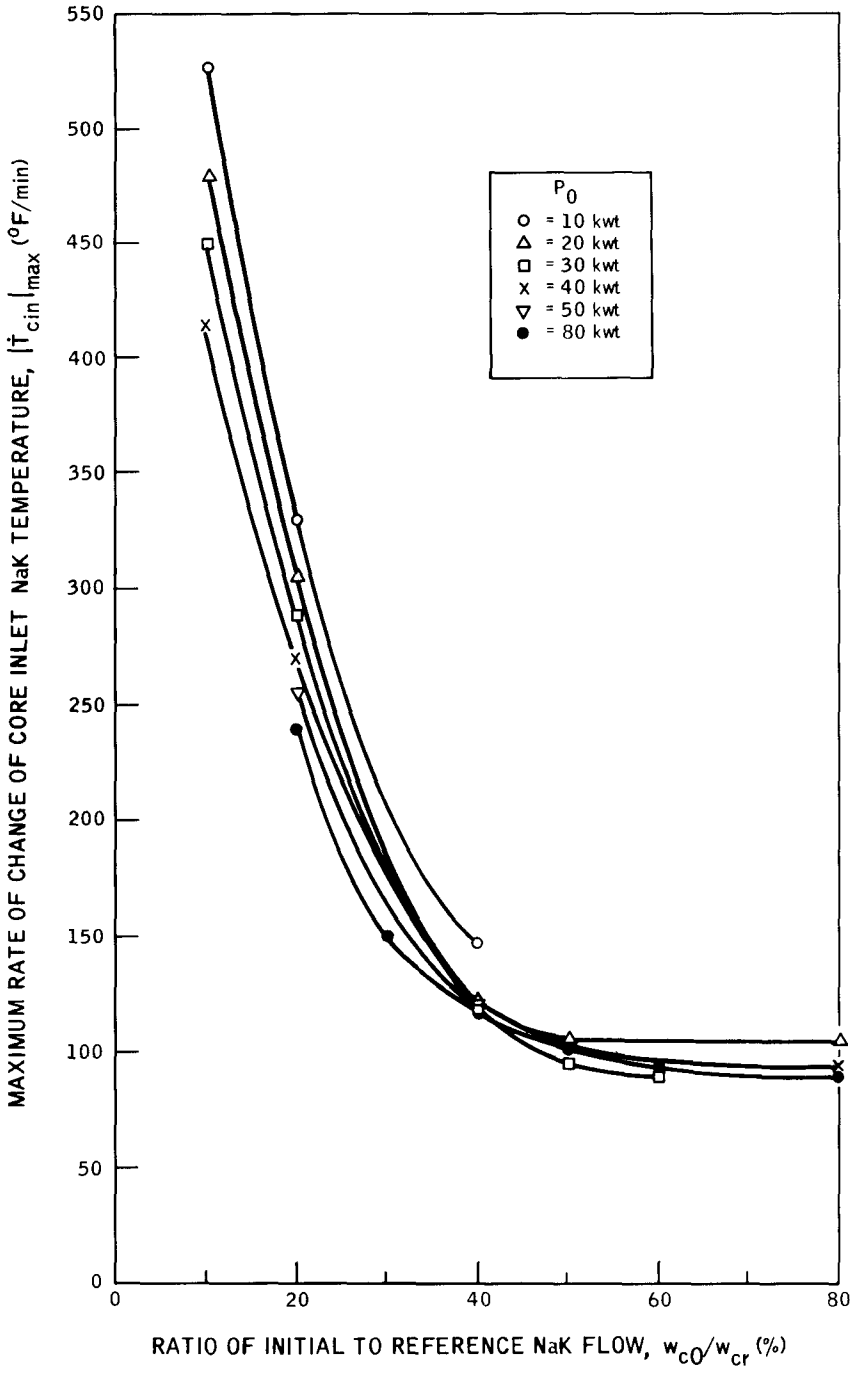


3-18-64 7568-0925

Figure 27. Effect of Initial NaK Flow on Maximum Rate of Change of Core Inlet NaK Temperature

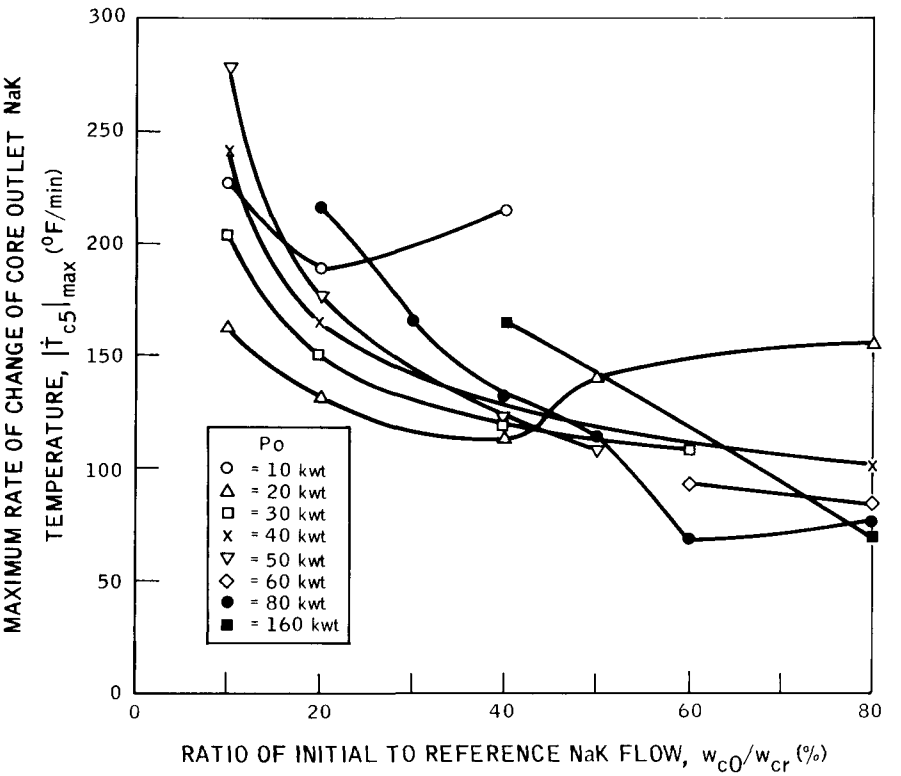


3-18-64 7568-0926

Figure 28. Effect of Initial NaK Flow on Maximum Rate of Change of Core Outlet NaK Temperature

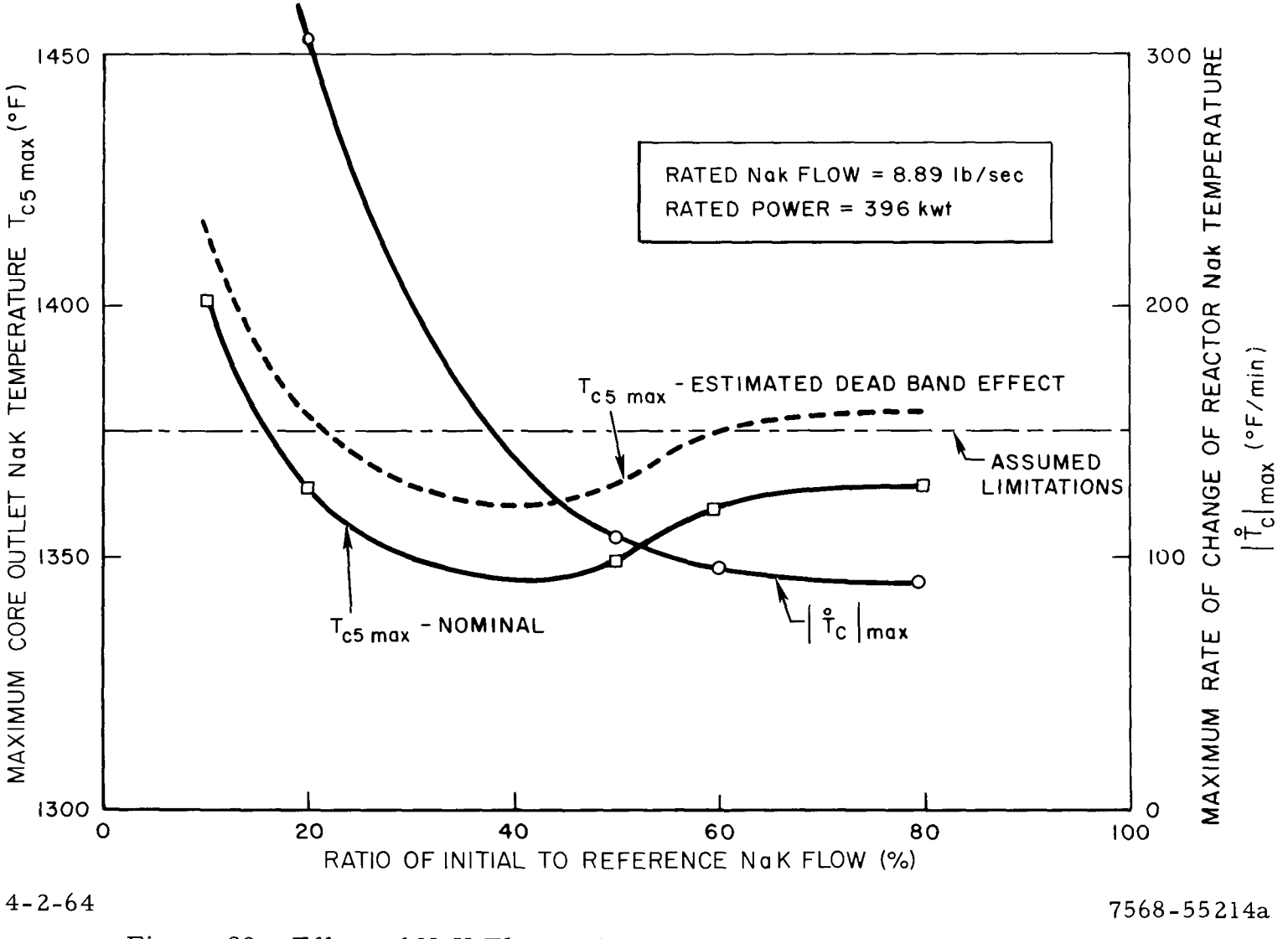


4-2-64

7568-55214a

Figure 29. Effect of NaK Flow on Maximum Core Outlet NaK Temperature and on Maximum Rate of Change of Reactor NaK Temperature

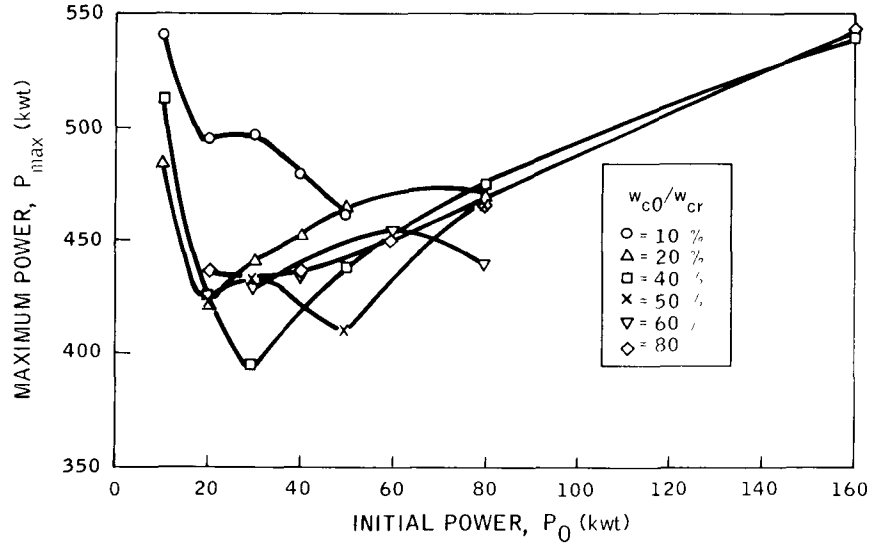


3-18-64 7568-0909

Figure 30. Effect of Initial Power on Maximum Power

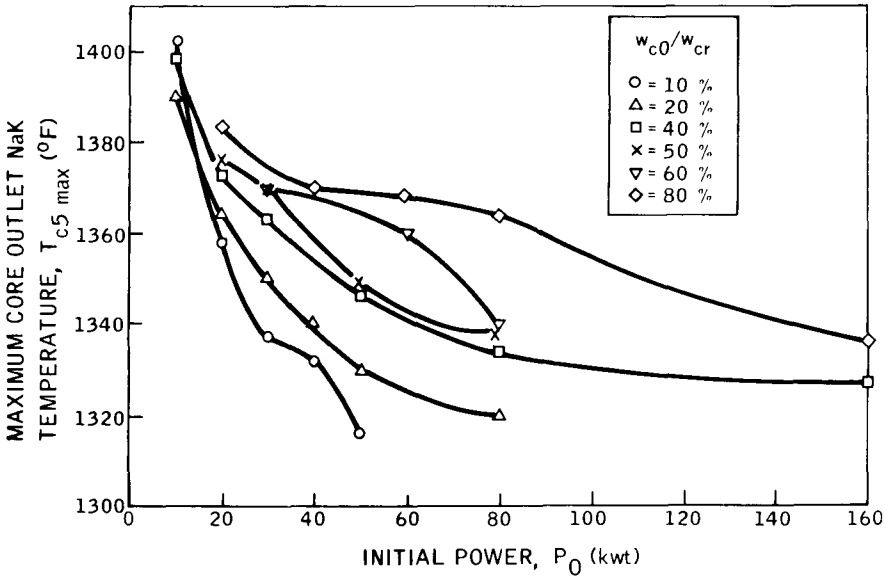


3-18-64 7568-0910

Figure 31. Effect of Initial Power on Maximum Core Outlet NaK Temperature

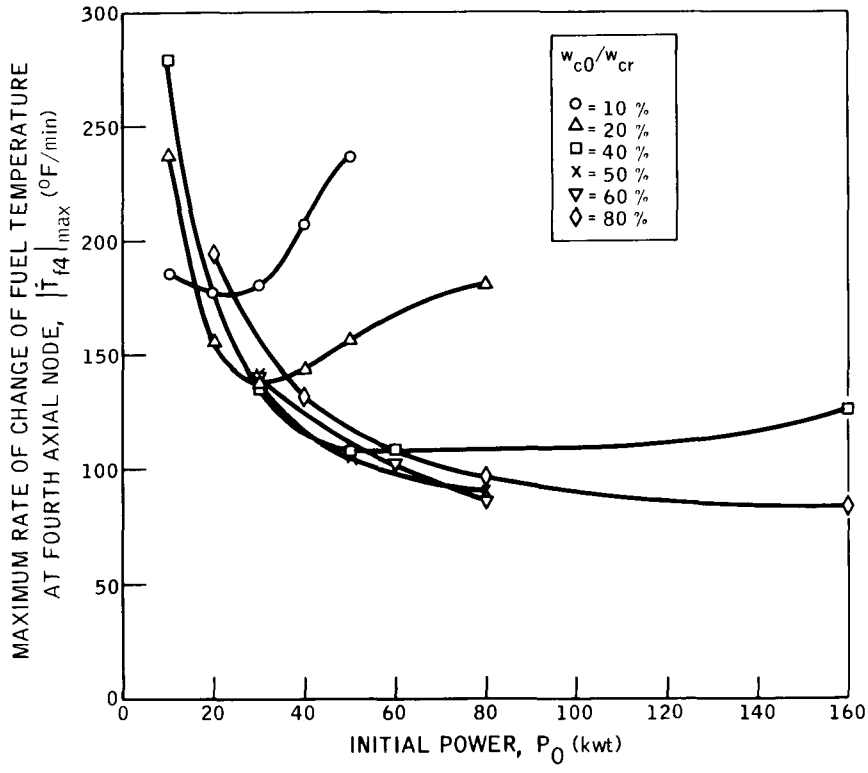


3-18-64 7568-0911

Figure 32. Effect of Initial Power on Maximum Rate of Change of Fuel Temperature at Fourth Axial Node

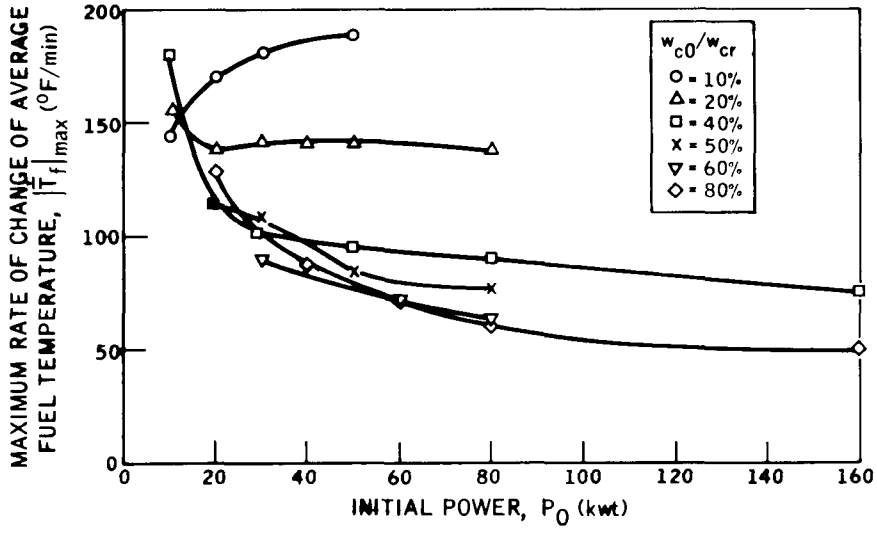


3-18-64 7568-0912

Figure 33. Effect of Initial Power on Maximum Rate of Change of Average Fuel Temperature

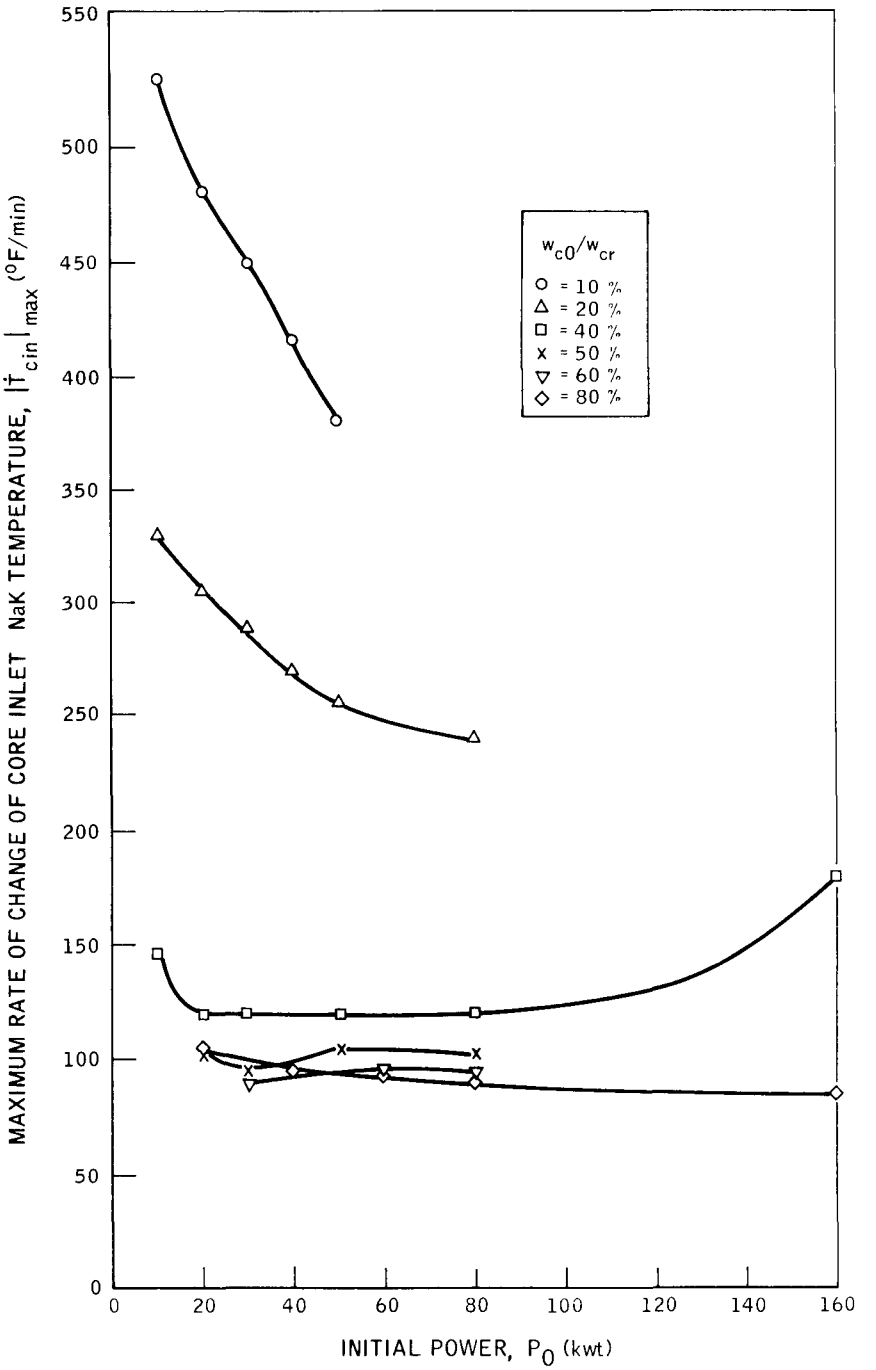


3-18-64 7568-0913

Figure 34. Effect of Initial Power on Maximum Rate of Change of Core Inlet NaK Temperature

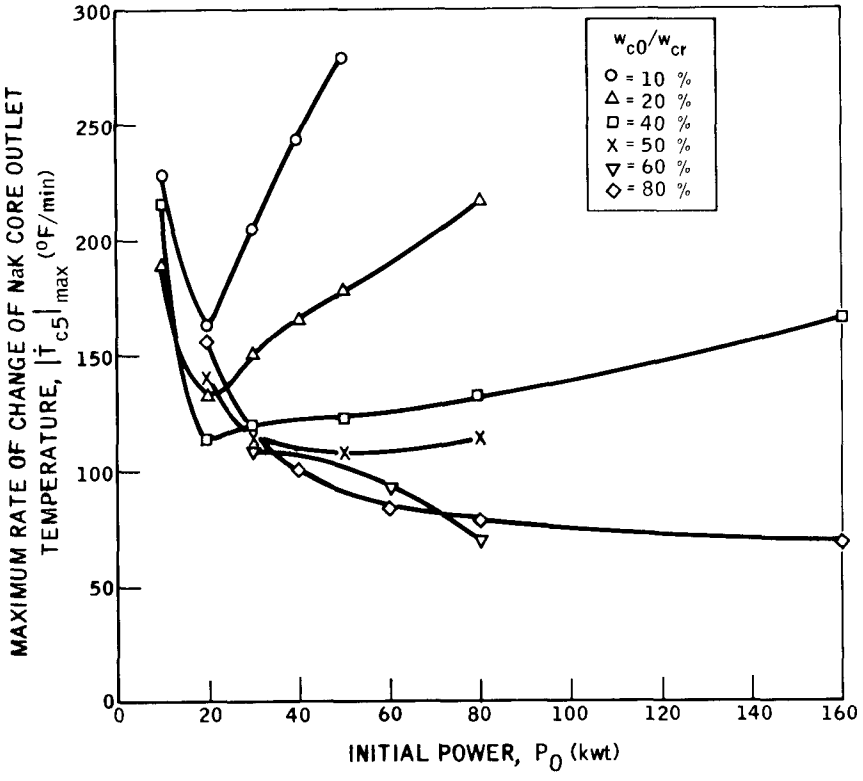


3-18-64 7568-0914

Figure 35. Effect of Initial Power on Maximum Rate of Change of Core Outlet NaK Temperature

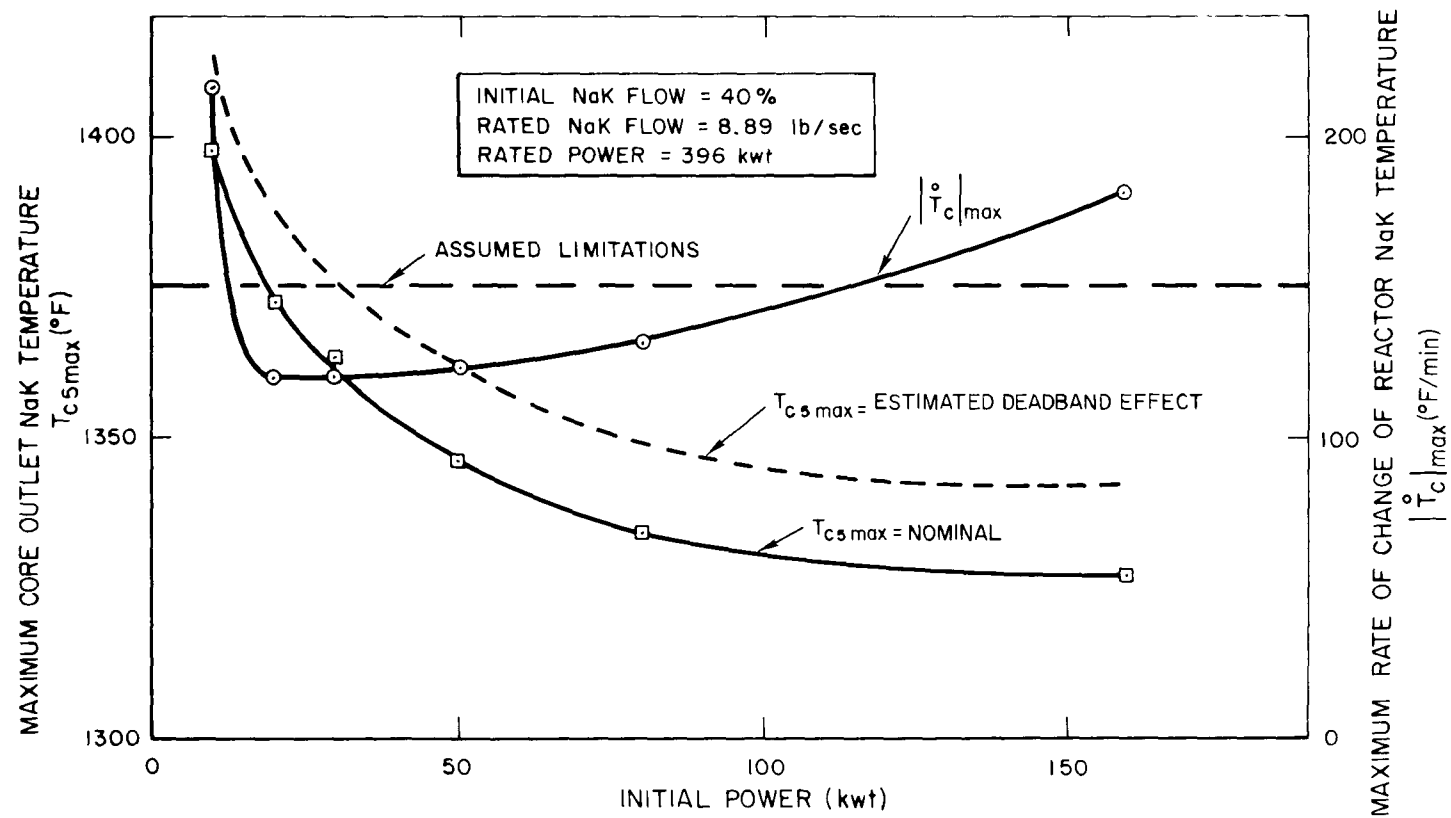


4-2-64

7568-55209a

Figure 36. Effect of Initial Power Level on Maximum Core Outlet NaK Temperature and on Maximum Rate of Change of Reactor NaK Temperature

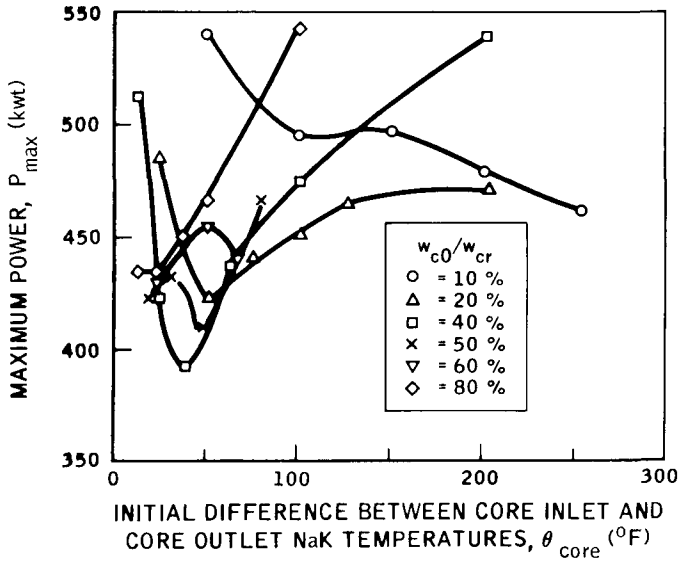


3-18-64 7568-0915

Figure 37. Effect of Initial Core Temperature Difference on Maximum Power

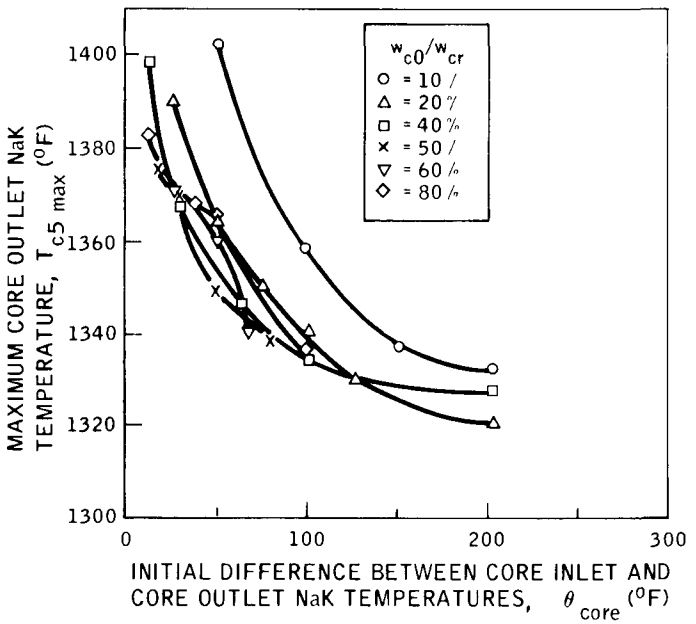


3-18-64 7568-0916

Figure 38. Effect of Initial Core Temperature Difference on Maximum Core Outlet NaK Temperature

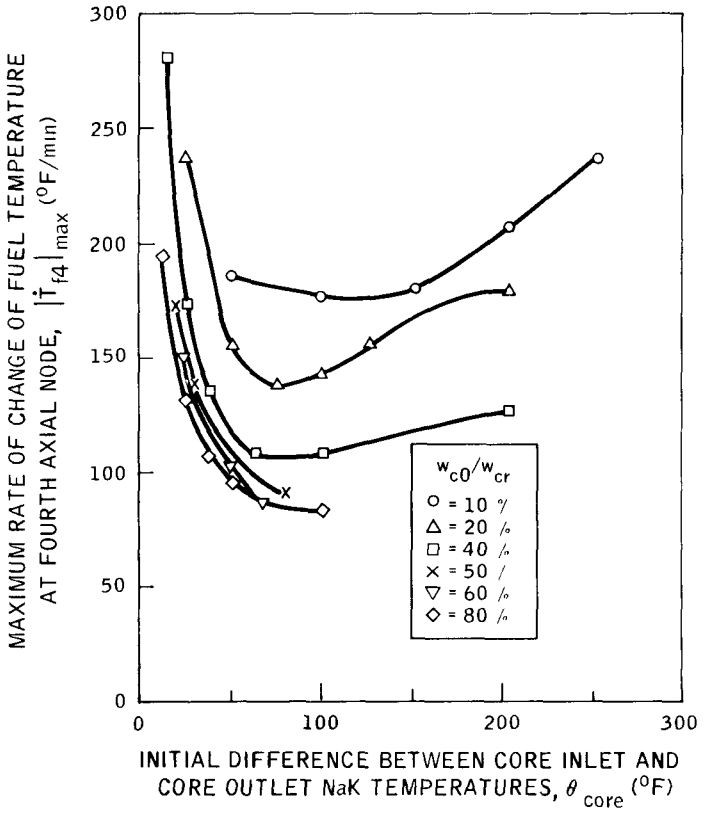


3-18-64 7568-0917

Figure 39. Effect of Initial Core Temperature Difference on Maximum Rate of Change of Fuel Temperature at Fourth Axial Node

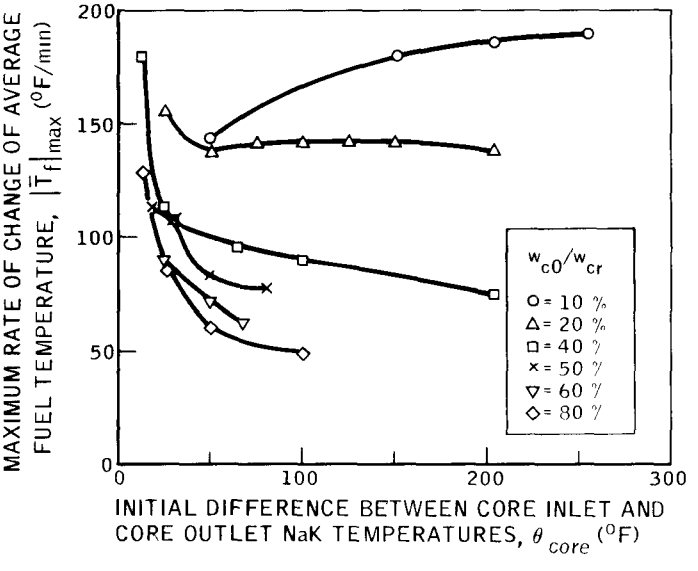


3-18-64 7568-0918

Figure 40. Effect of Initial Core Temperature Difference on Maximum Rate of Change of Average Fuel Temperature

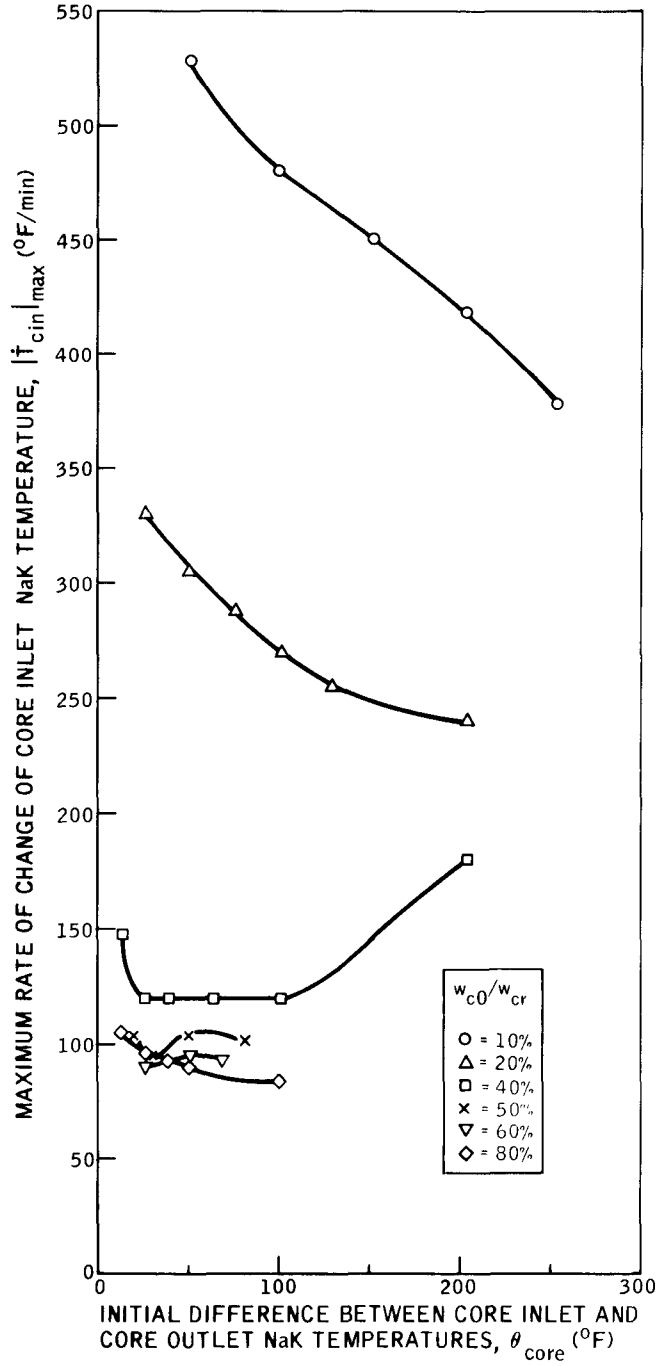


3-18-64 7568-0919

Figure 41. Effect of Initial Core Temperature Difference on Maximum Rate of Change of Core Inlet NaK Temperature

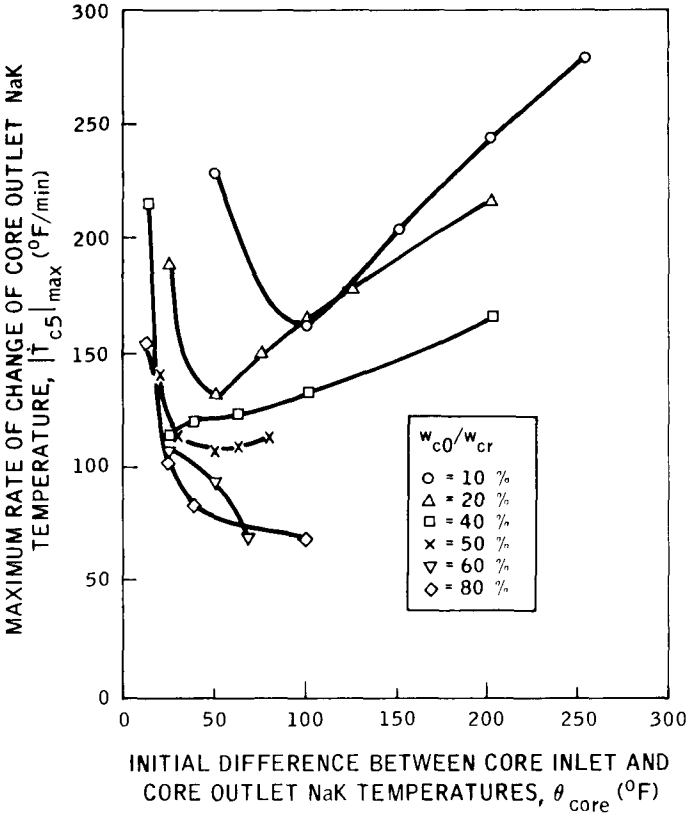


3-18-64 7568-0920

Figure 42. Effect of Initial Core Temperature Difference on Maximum Rate of Change of Core Outlet NaK Temperature

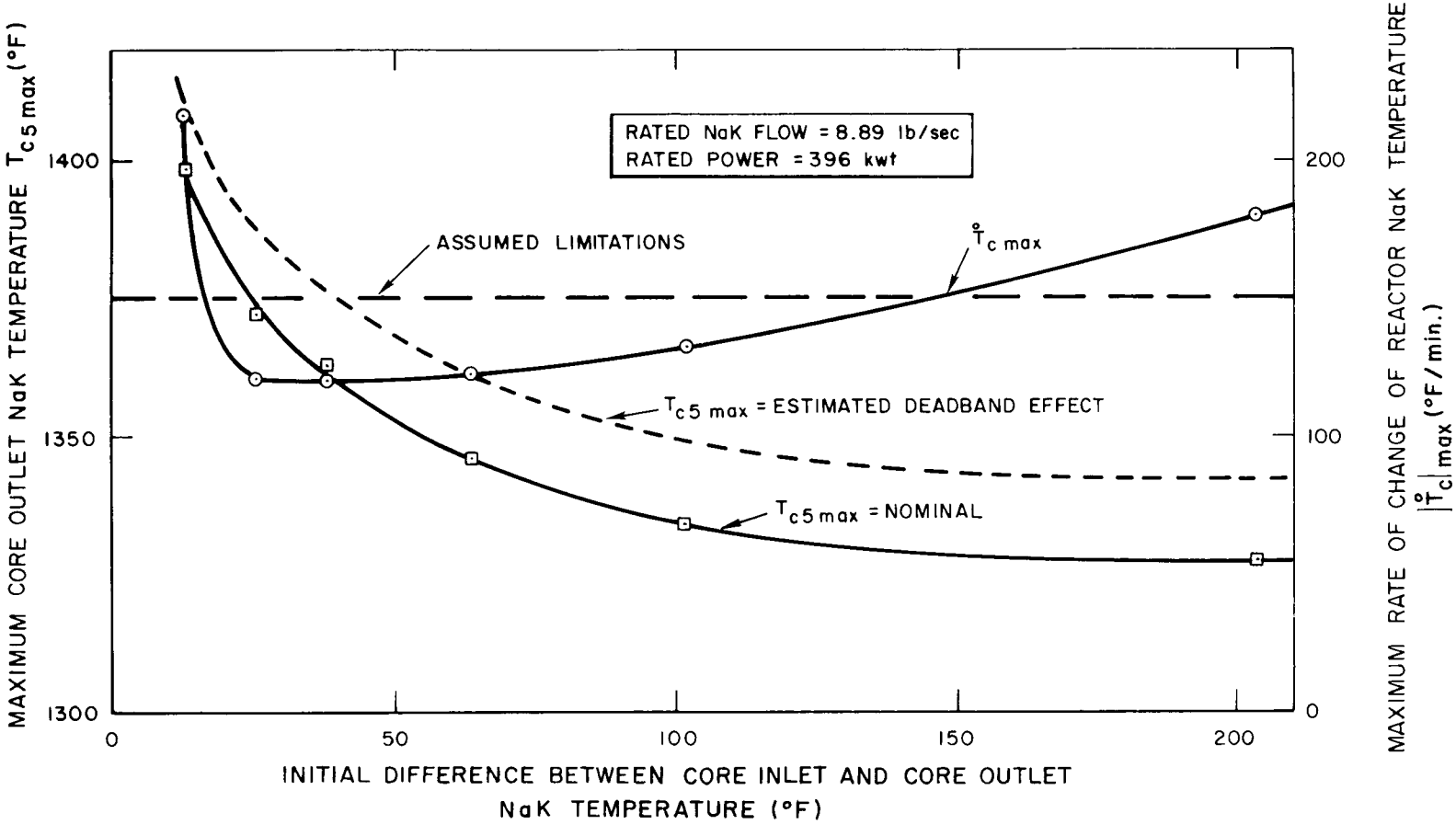


4-2-64

7568-55208a

Figure 43. Effect of Initial Core Temperature Difference on Maximum Core Outlet NaK Temperature and on Maximum Rate of Change of NaK Temperature

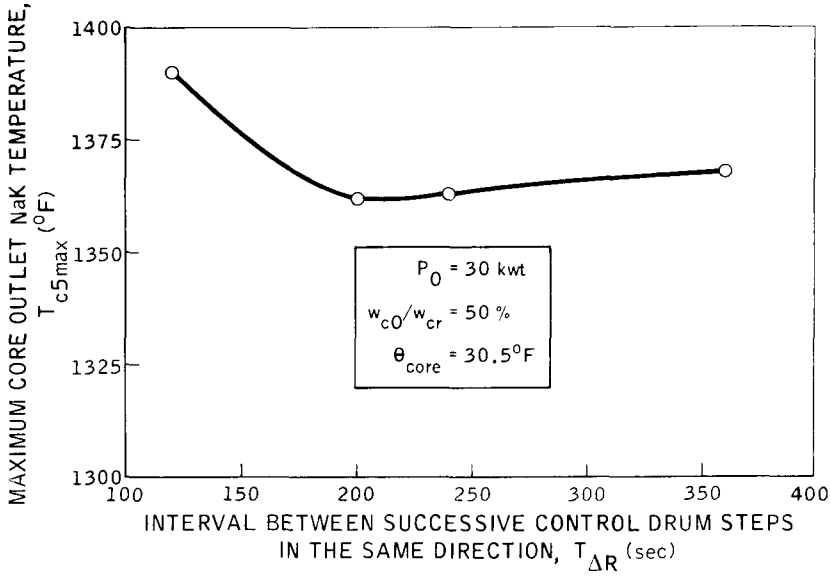


3-18-64 7568-0958

Figure 44. Effect of the Interval Between Successive Control Drum Steps on Maximum Core Outlet NaK Temperature, 30-kwt Initial Power

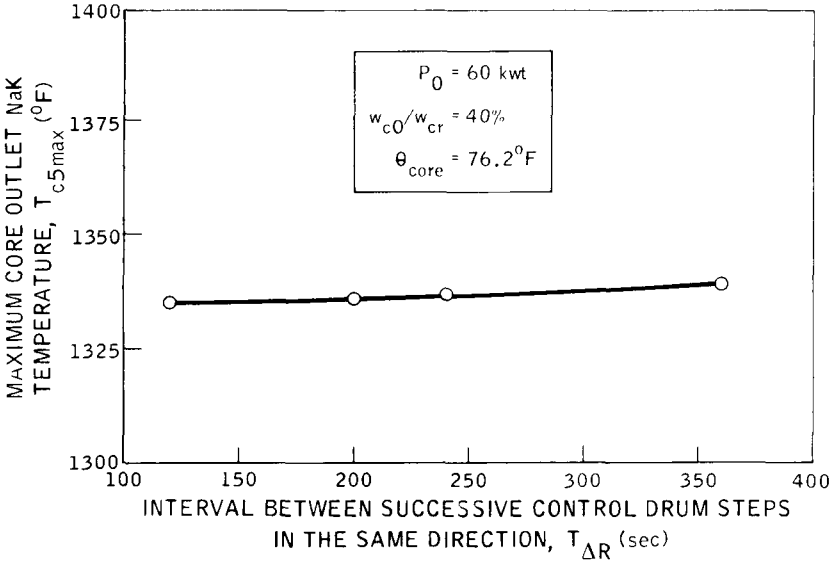


3-18-64 7568-0959

Figure 45. Effect of the Interval Between Successive Control Drum Steps on Maximum Core Outlet NaK Temperature, 60-kwt Initial Power

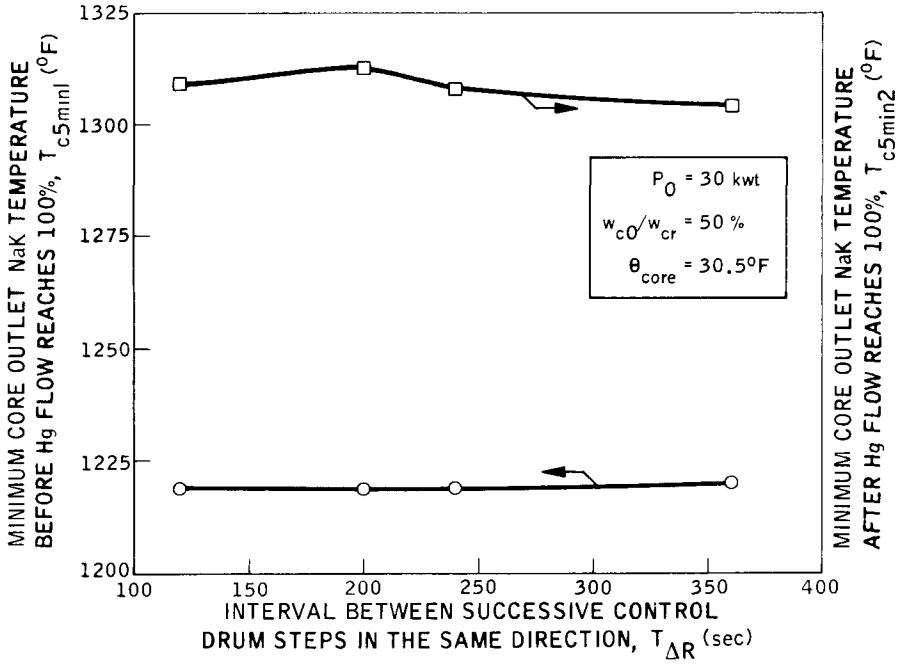


3-18-64 7568-0960

Figure 46. Effect of the Interval Between Successive Control Drum Steps on Minimum Core Outlet NaK Temperature, 30-kwt Initial Power

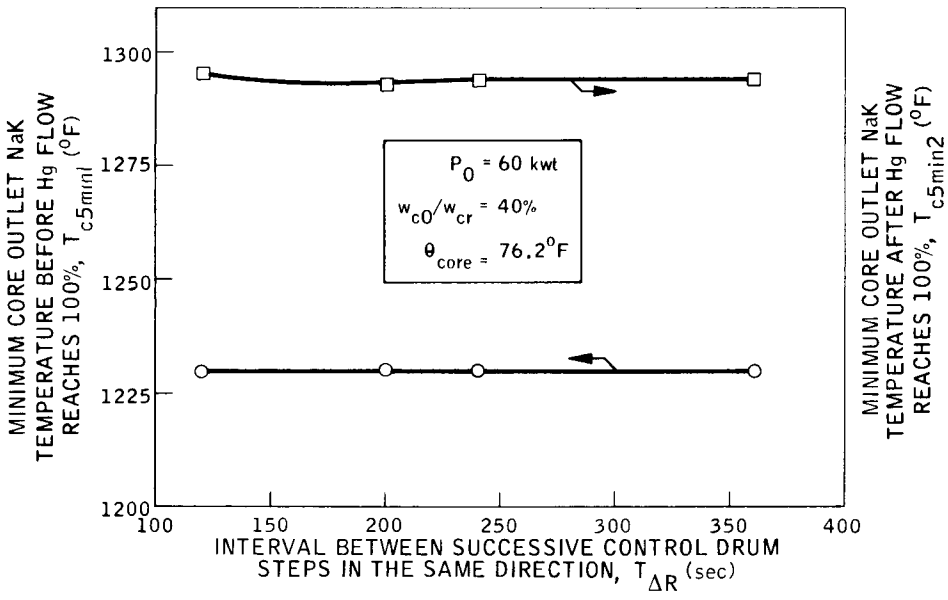


3-18-64 7568-0961

Figure 47. Effect of the Interval Between Successive Control Drum Steps on Minimum Core Outlet NaK Temperature, 60-kwt Initial Power

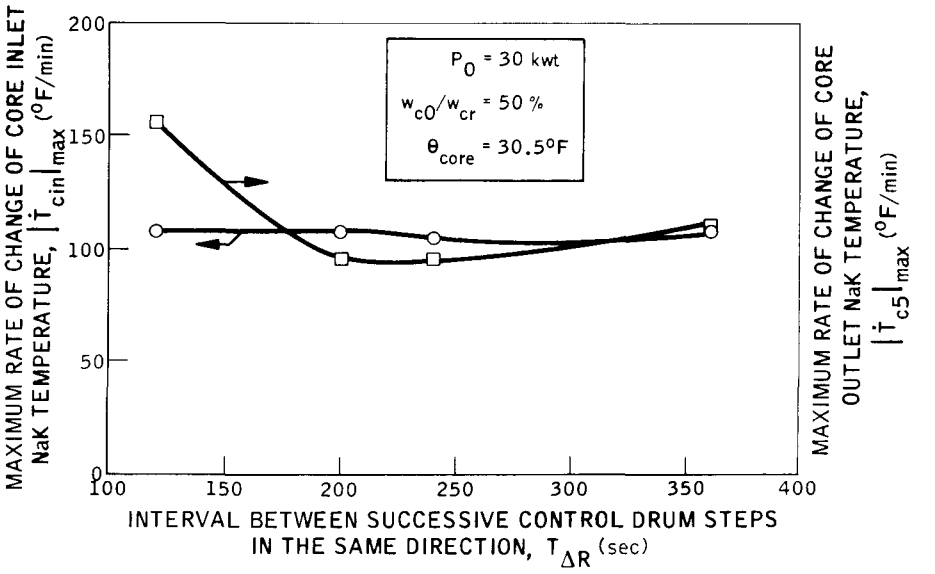


3-18-64 7568-0962

Figure 48. Effect of the Interval Between Successive Control Drum Steps on Maximum Rate of Change of Core Inlet and Outlet NaK Temperatures, 30-kwt Initial Power

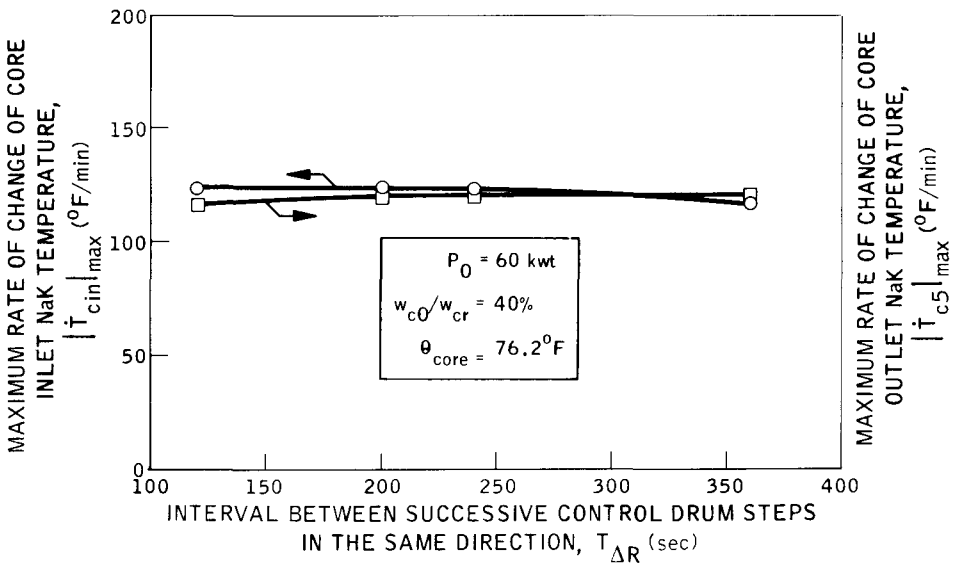


3-18-64 7568-0963

Figure 49. Effect of the Interval Between Successive Control Drum Steps on Maximum Rate of Change of Core Inlet and Outlet NaK Temperatures, 60-kwt Initial Power

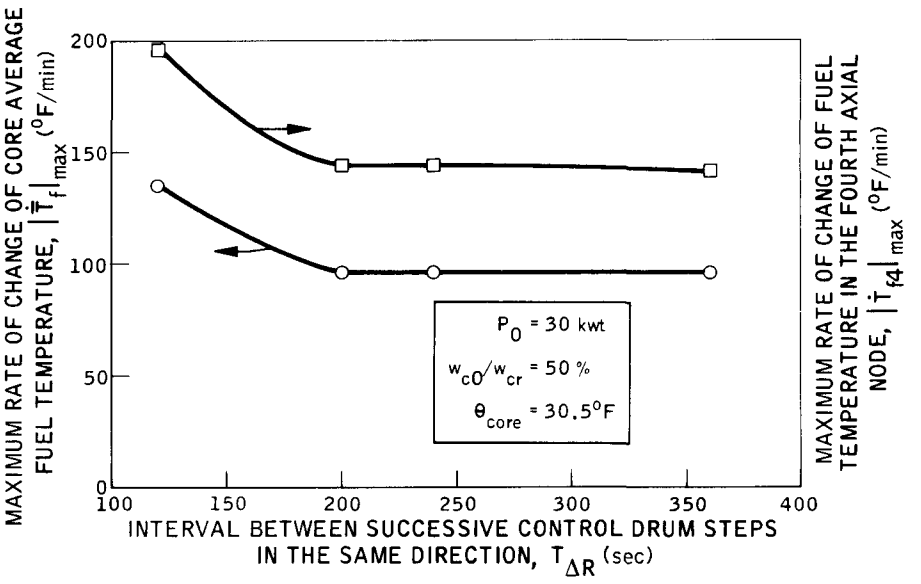


3-18-64 7568-0964

Figure 50. Effect of the Interval Between Successive Control Drum Steps on Maximum Rate of Change of Core Average and Fourth Axial Node Fuel Temperatures, 30-kwt Initial Power

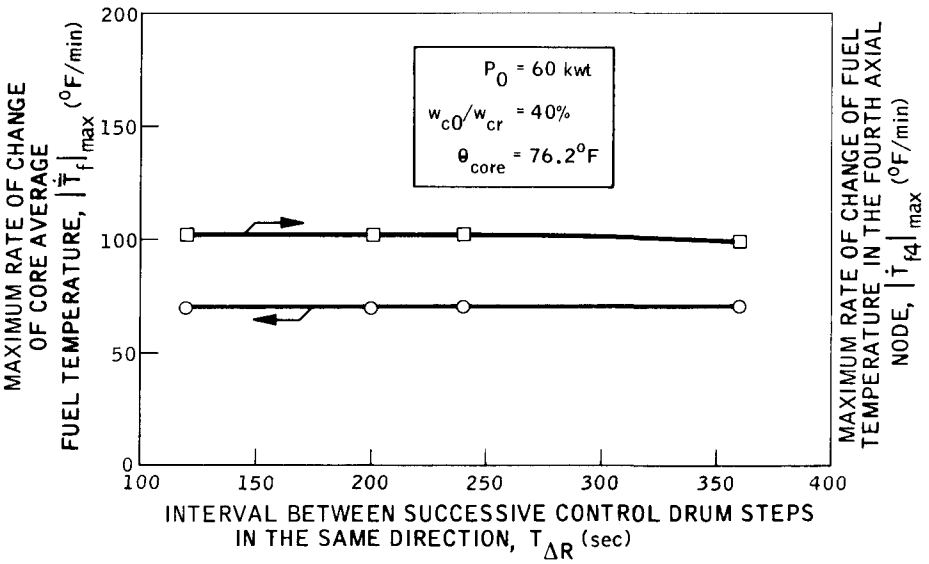


3-18-64 7568-0965

Figure 51. Effect of the Interval Between Successive Control Drum Steps on Maximum Rate of Change of Core Average and Fourth Axial Node Fuel Temperatures, 60-kwt Initial Power

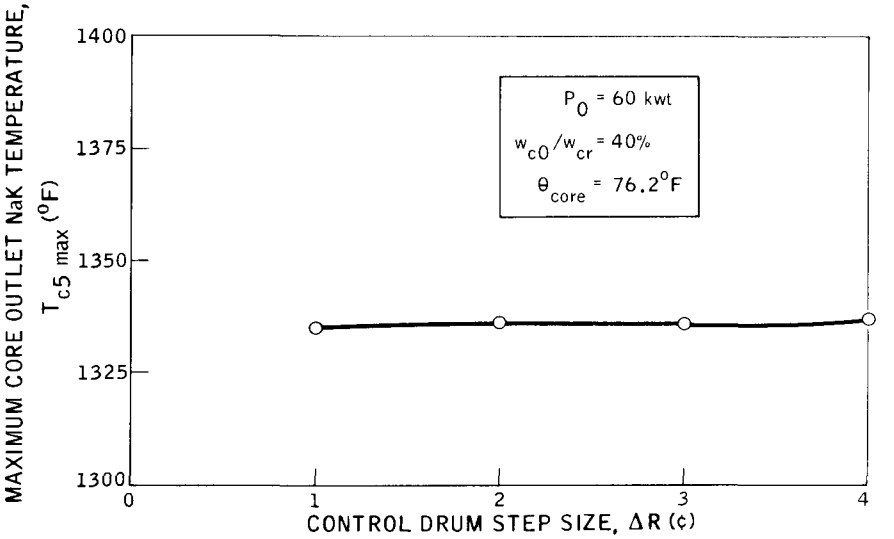


3-18-64 7568-0966

Figure 52. Effect of Control Drum Step Size on Maximum Core Outlet NaK Temperature

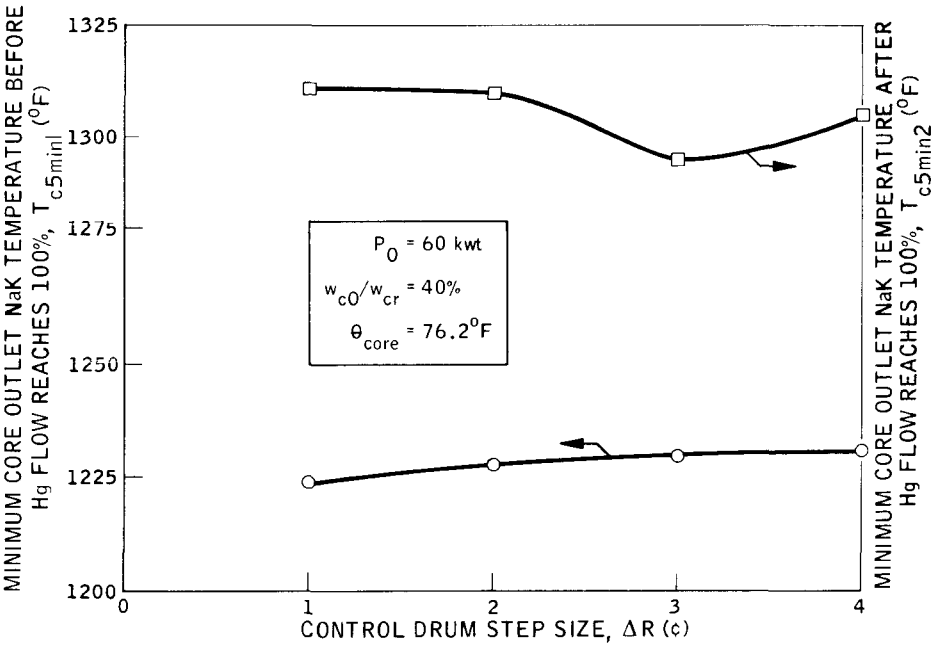


3-18-64 7568-0967

Figure 53. Effect of Control Drum Step Size on Minimum Core Outlet NaK Temperature

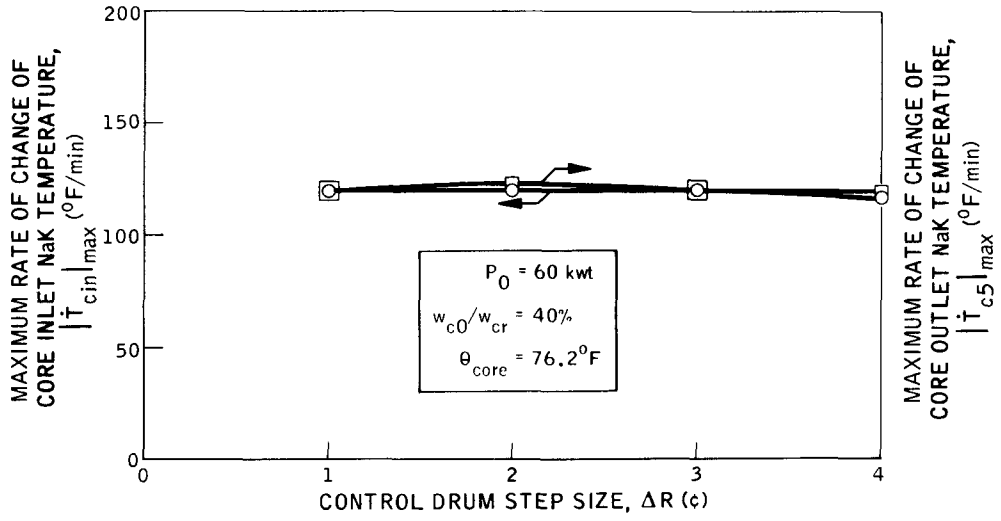


3-18-64 7568-0968

Figure 54. Effect of Control Drum Step Size on Maximum Rate of Change of Core Inlet and Outlet NaK Temperatures

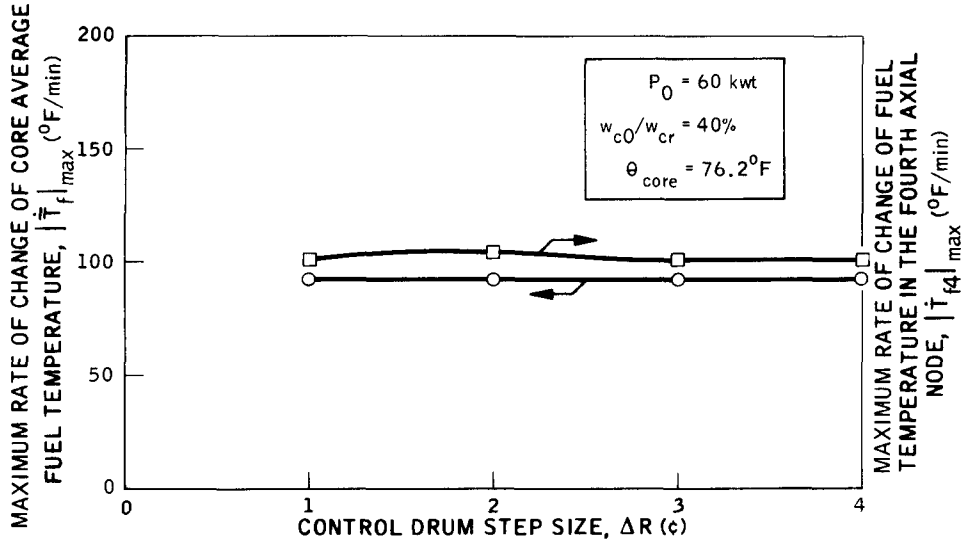


3-18-64 7568-0969

Figure 55. Effect of Control Drum Step Size on Maximum Rate of Change of Core Average and Fourth Axial Node Fuel Temperatures

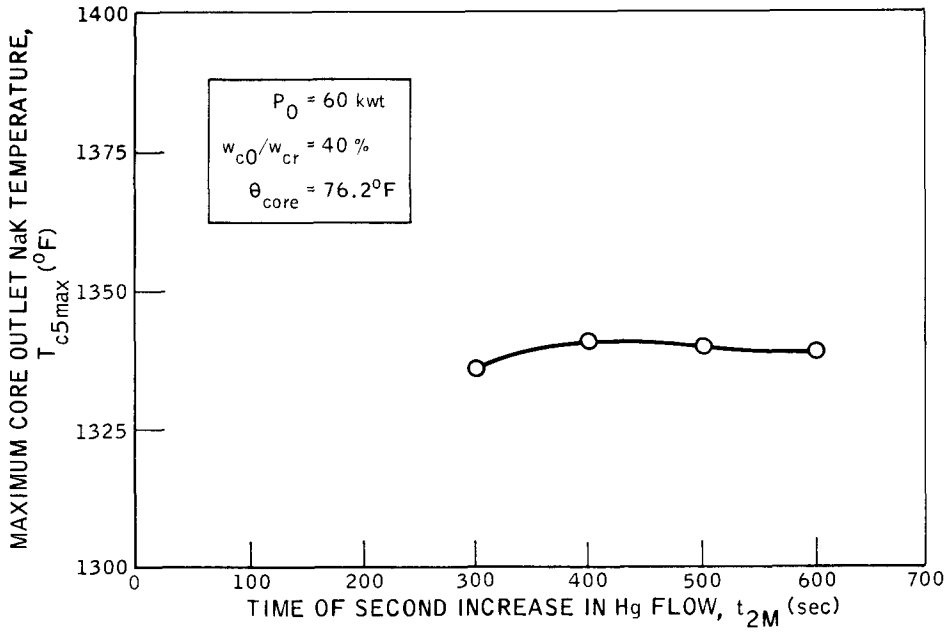


3-18-64 7568-0970

Figure 56. Effect of Time for Second Increase in Mercury Flow on Maximum Core Outlet Temperature

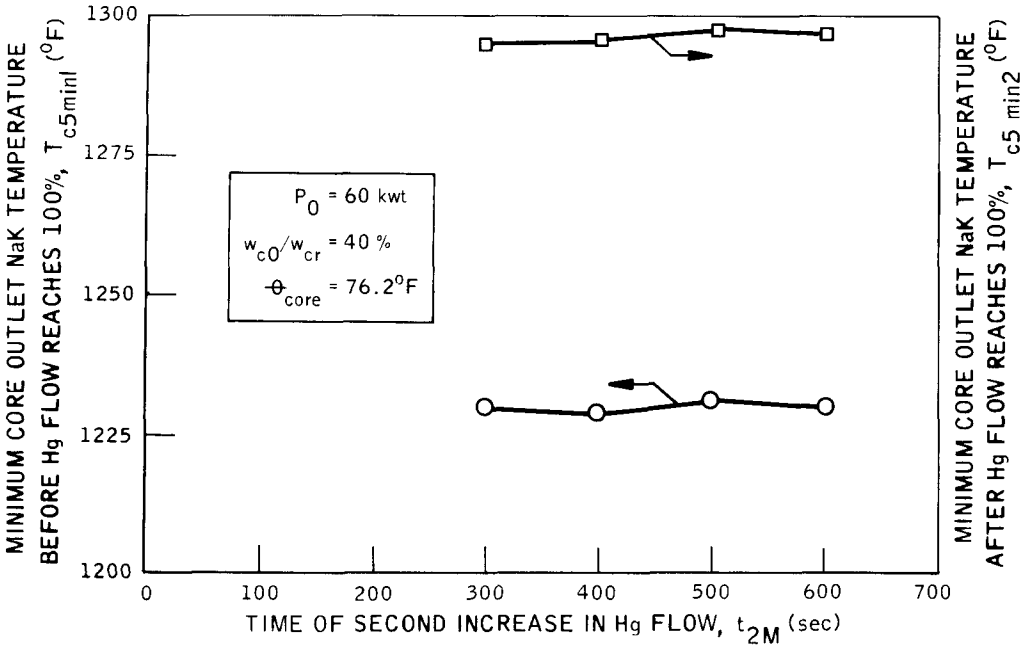


3-18-64 7568-0971

Figure 57. Effect of Time for Second Increase in Mercury Flow on Minimum Core Outlet Temperature

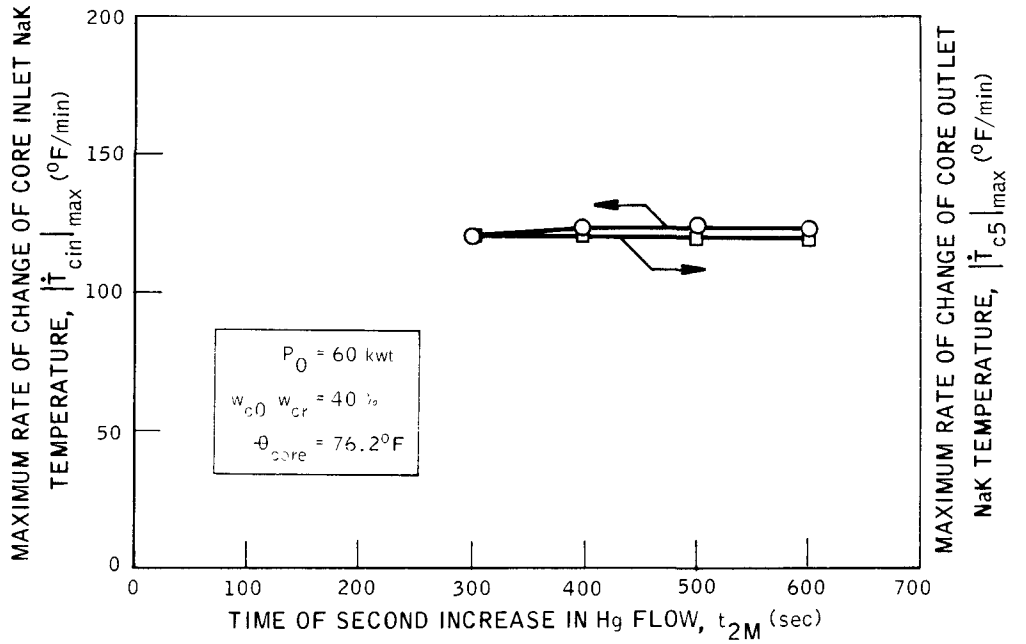


3-18-64 7568-0972

Figure 58. Effect of Time for Second Increase in Mercury Flow on Maximum Rate of Change of Core Inlet and Outlet NaK Temperatures

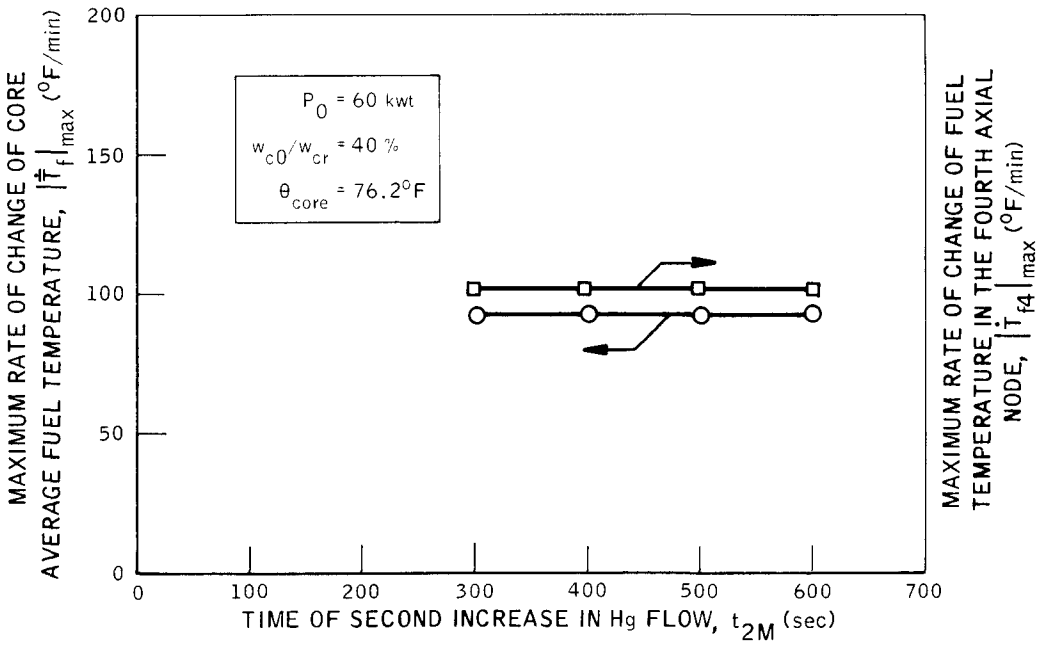


3-18-64 7568-0973

Figure 59. Effect of Time for Second Increase in Mercury Flow on Maximum Rate of Change of Core Average and Fourth Axial Node Fuel Temperatures

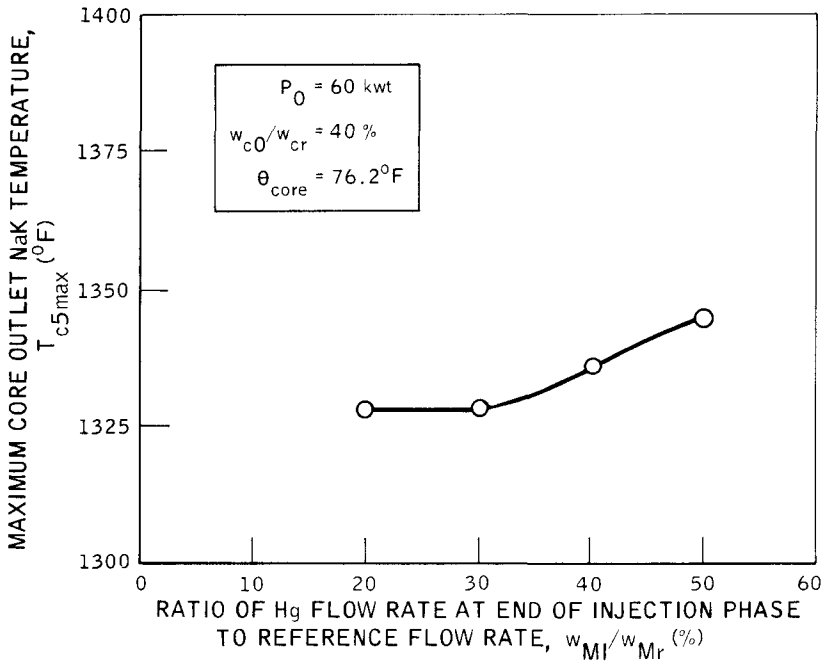


3-18-64 7568-0974

Figure 60. Effect of Mercury Flow Injection Level on Maximum Core Outlet NaK Temperature

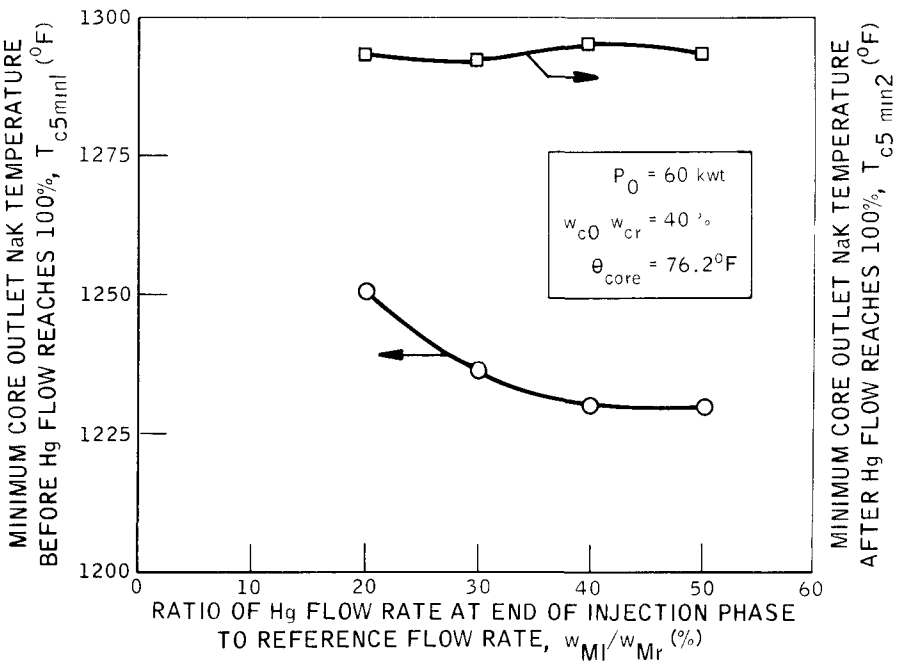


3-18-64 7568-0975

Figure 61. Effect of Mercury Flow Injection Level on Minimum Core Outlet NaK Temperature

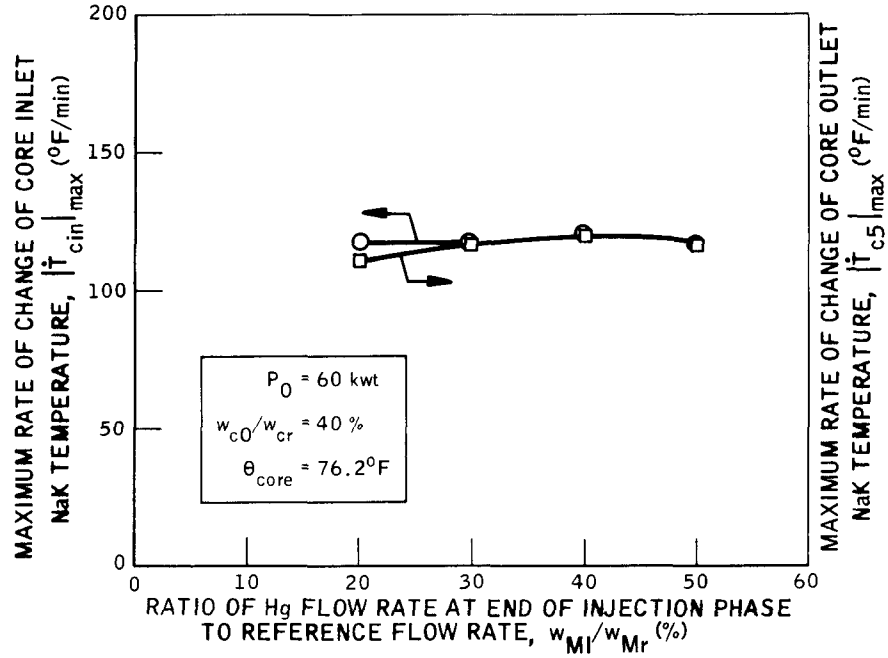


3-18-64 7568-0976

Figure 62. Effect of Mercury Flow Injection Level on Maximum Rate of Change of Core Inlet and Outlet NaK Temperatures

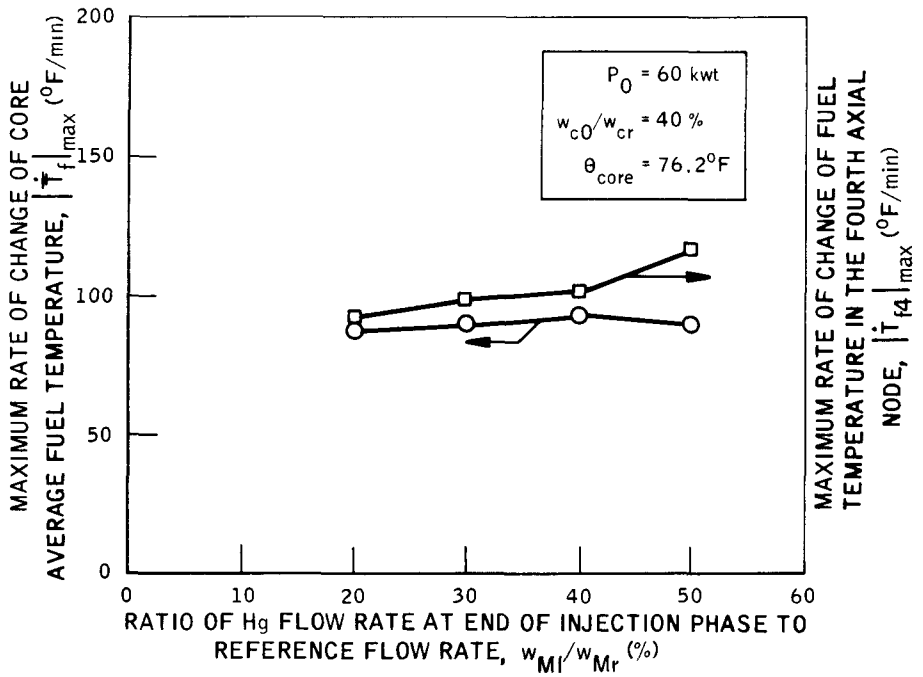


3-18-64 7568-0977

Figure 63. Effect of Mercury Flow Injection Level on Maximum Rate of Change of Core Average and Fourth Axial Node Fuel Temperatures

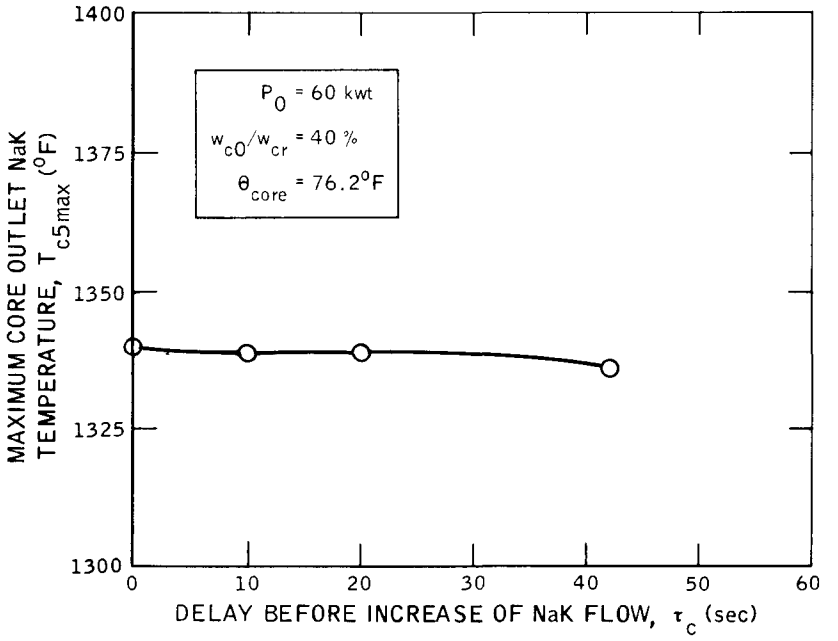


3-18-64 7568-0978

Figure 64. Effect of Delay Before Increase of NaK Flow on Maximum Core Outlet NaK Temperature

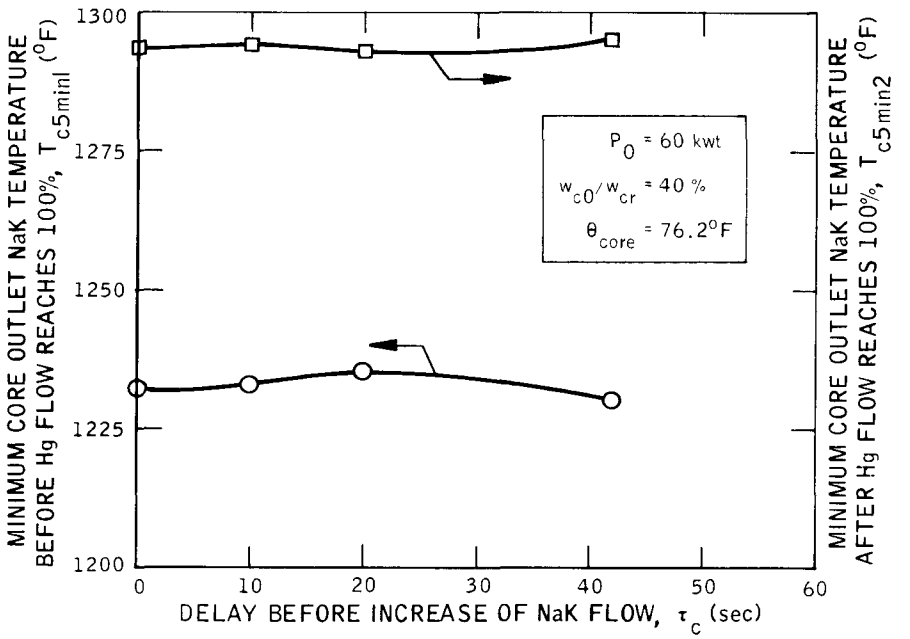


3-18-64 7568-0979

Figure 65. Effect of Delay Before Increase of NaK Flow on Minimum Core Outlet NaK Temperature

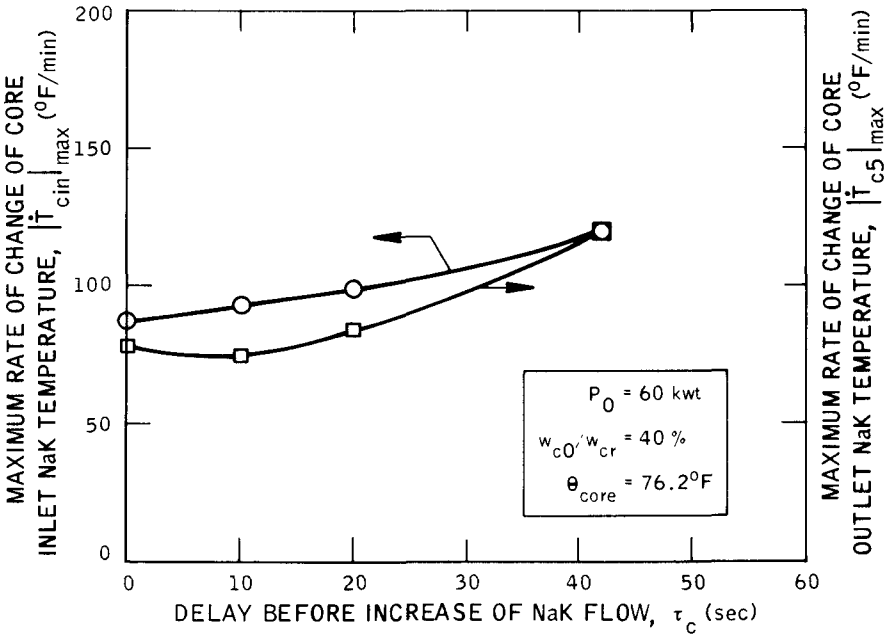


3-18-64 7568-0980

Figure 66. Effect of Delay Before Increase of NaK Flow on Maximum Rate of Change of Core Inlet and Outlet NaK Temperatures

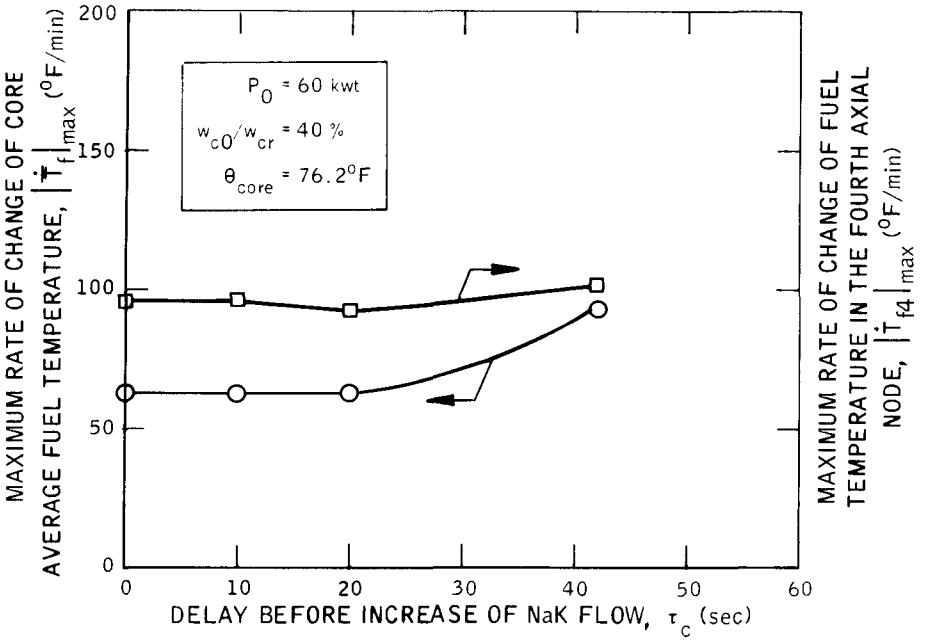


3-18-64 7568-0981

Figure 67. Effect of Delay Before Increase of NaK Flow on Maximum Rate of Change of Core Average and Fourth Axial Node Fuel Temperatures

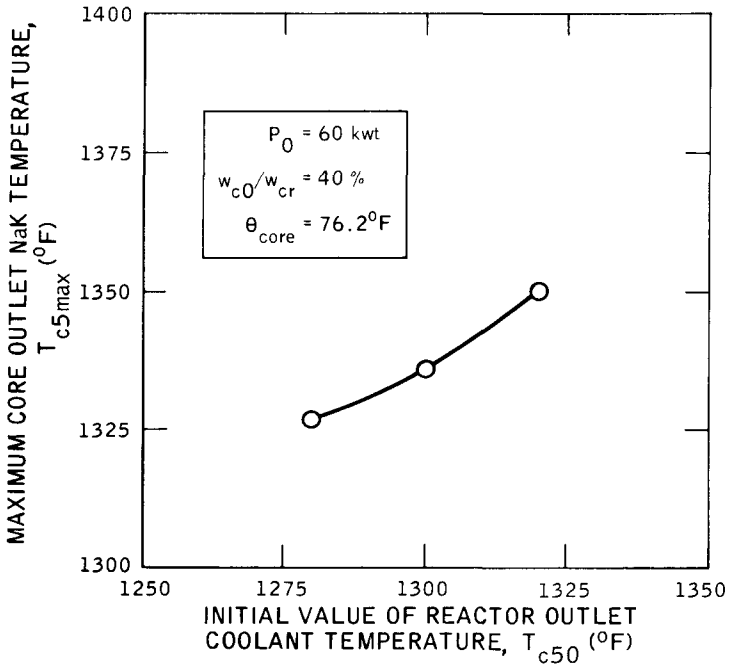


3-18-64 7568-0982

Figure 68. Effect of Initial Core Outlet NaK Temperature on Maximum Core Outlet NaK Temperature

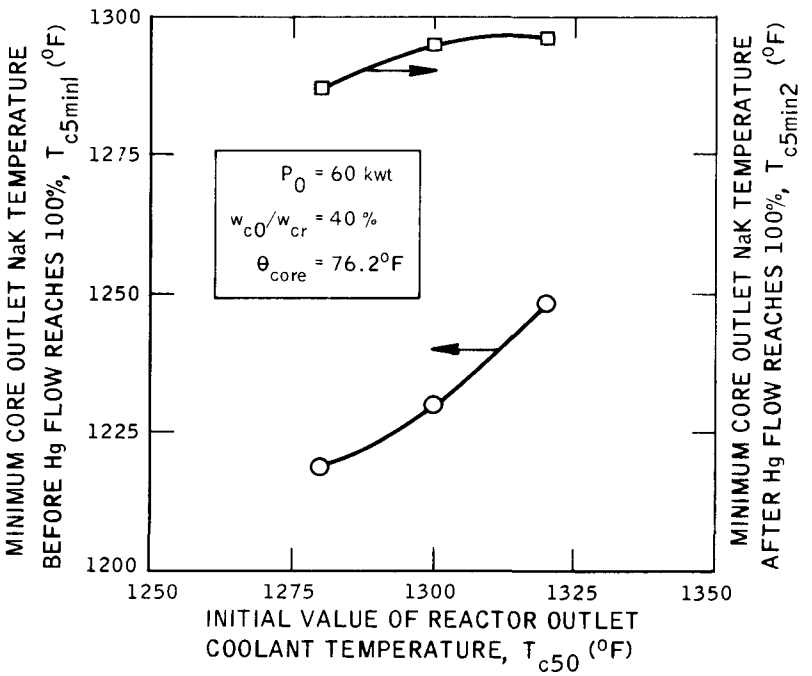


3-18-64 7568-0983

Figure 69. Effect of Initial Core Outlet NaK Temperature on Minimum Core Outlet NaK Temperature

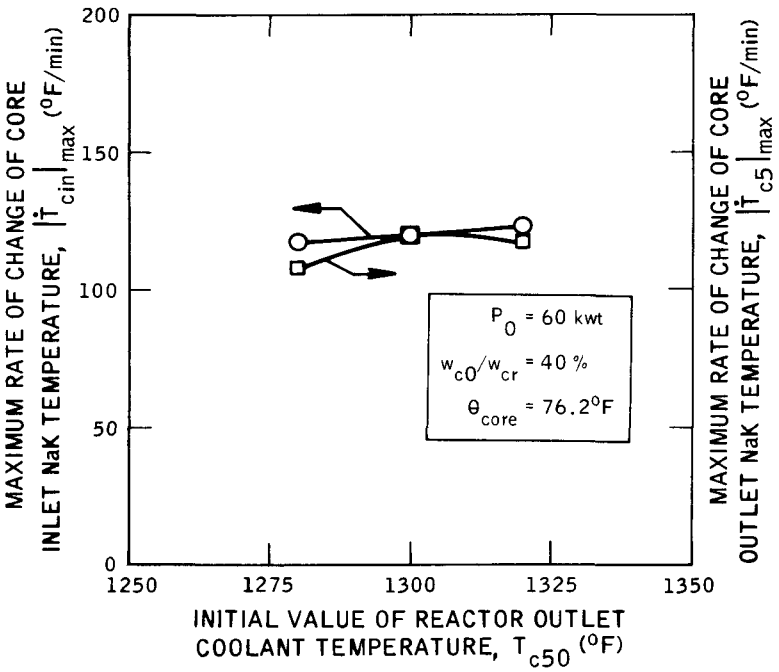


3-18-64 7568-0984

Figure 70. Effect of Initial Core Outlet NaK Temperature on Maximum Rate of Change of Core Inlet and Outlet NaK Temperatures

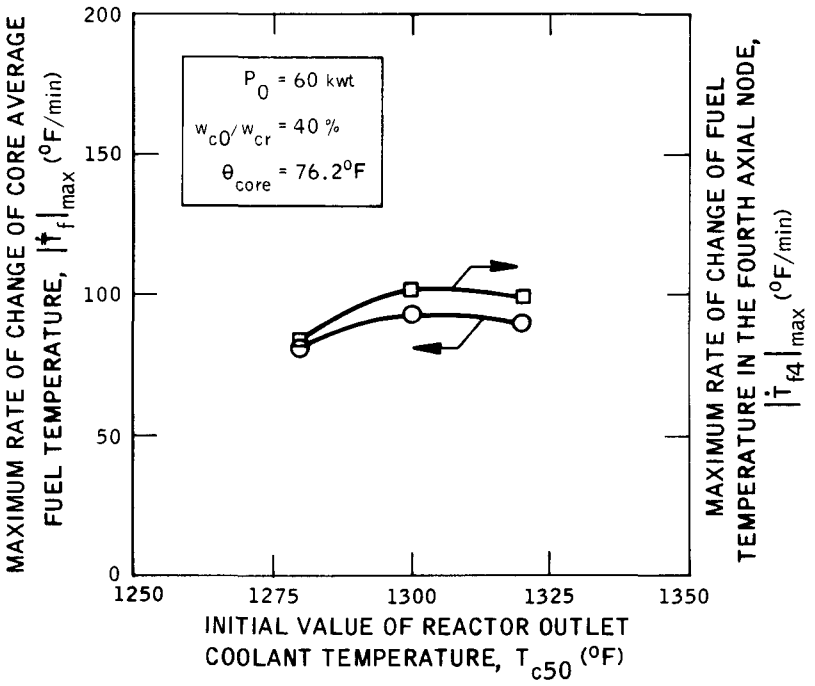


3-18-64 7568-0985

Figure 71. Effect of Initial Core Outlet NaK Temperature on Maximum Rate of Change of Core Average and Fourth Axial Node Fuel Temperatures

## REFERENCES


1. R. G. Geimer, "Preliminary SNAP 8 Startup Investigations," AGC-TM-345: 63-1-134 (CDI), September 9, 1963

2. R. L. Murray, Nuclear Reactor Physics, Prentice Hall, 1957

3. D. G. Mason and R. W. Winson, "A Reactor Transient Heat Transfer Model," NAA-SR-7938, March 1, 1964

4. C. E. Johnson, "SNAP 8 Quarterly Progress Report, July-September 1963," NAA-SR-8992 (SRD), November 15, 1963

5. C. E. Johnson, "SNAP 8 Quarterly Progress Report, February-April 1964," NAA-SR-9592 (SRD), to be published

6. D. G. Mason, "SNAP 8 Reactor Control System," NAA-SR-MEMO-7233 (SRD), March 20, 1962

7. S. Birken, "Analysis of SNAP 8 Nuclear System Startup," NAA-SR-9646 (CRD), to be published

8. D. G. Mason, "SNAP 8 Design Description," NAA-SR-MEMO-8740 (CRD), August 1, 1963

9. C. E. Johnson and C. A. Goetz, "SNAP 8 Reactor and Shield," AIAA Journal Vol 1, No. 10, October 1963

BLANK

# APPENDICES

BLANK

# APPENDIX A
# EQUATIONS

## 1. REACTOR KINETICS

The standard reactor kinetics equations can be written as

$$\frac{dn}{dt} = \dot{n} = \frac{R^{\$}\beta - \beta}{\ell^*} n + \sum_{i=1}^{6} \lambda_i C_i \qquad \ldots (1)$$

$$\frac{dC_i}{dt} = \dot{C}_i = \frac{\beta_i}{\ell^*} n - \lambda_i C_i \qquad \ldots (2)$$

where

$n$ = neutron level

$C_i$ = concentration of delayed neutron precursors in the $i^{\underline{th}}$ group

$R^{\$}$ = reactivity (dollars)

$\beta$ = effective fraction of delayed neutrons

$\beta_i$ = effective fraction of delayed neutrons in the $i^{\underline{th}}$ group

$\ell^*$ = effective prompt neutron lifetime (sec)

$\lambda_i$ = decay constant for delayed neutron precursors in the $i^{\underline{th}}$ group (1/sec)

These equations were normalized, converted to a delta ($\Delta$) model, and rewritten for the analog simulation as follows:

$$\frac{\Delta\dot{n}}{n_r} = \frac{\beta}{\ell^*} \left[ R^{\$} \frac{n}{n_r} - \frac{\Delta n}{n_r} + \sum_{i=1}^{6} \frac{\beta_i}{\beta} \left( \frac{\Delta C_i}{C_{ir}} \right) \right] \qquad \ldots (3)$$

$$\frac{\dot{\Delta C_i}}{C_{ir}} = \lambda_i \left( \frac{\Delta n}{n_r} \right) - \lambda_i \left( \frac{\Delta C_i}{C_{ir}} \right) \qquad \ldots (4)$$

where

$$\frac{n}{n_r} = \frac{n_0}{n_r} + \frac{\Delta n}{n_r}$$

$$\frac{C_i}{C_{ir}} = \frac{C_{i0}}{C_{ir}} + \frac{\Delta C_i}{C_{ir}}$$

The subscript r indicates the reference level and the subscript 0 indicates the initial level of the variable concerned. The symbol $\Delta$ indicates a change in the variable from its initial value.

The reactivity is computed from

$$R^{\$} = R^{\$}_d + \alpha_f \left(\Delta \overline{T}_f\right) + \alpha_{\ell g} \left(\Delta T_{\ell g}\right) + \alpha_{ug} \left(\Delta T_{ug}\right) \quad \ldots (5)$$

where

$R^{\$}_d$ = reactivity inserted by the reactor control drums (dollars)

$\alpha_f$ = temperature coefficient of reactivity for the reactor fuel (dollars/°F)

$\Delta \overline{T}_f$ = change in the core average fuel temperature (°F)

$\alpha_{\ell g}$, $\alpha_{ug}$ = temperature coefficients of reactivity for the reactor lower grid plate and upper grid plate, respectively (dollars/°F)

$\Delta T_{\ell g}$, $\Delta T_{ug}$ = change in temperatures of the lower grid plate and upper grid plate, respectively (°F)

## 2. CORE HEAT TRANSFER

The basic core heat transfer equations for heat balance between fuel and coolant are

$$\frac{d}{dt}\left(T_{fj}\right) = \frac{G_j}{M_{fj}C_f}\left(\frac{n}{n_r}\right) - \frac{U_{fc}A_{fcj}}{M_{fj}C_f}\left(T_{fj} - T_{cj}\right) \quad \ldots (6)$$

$$\frac{d}{dt}\left(T_{cj}\right) = \frac{U_{fc}A_{fcj}}{M_{cj}C_c}\left(T_{fj} - T_{cj}\right) - \frac{w_c C_c}{M_{cj}C_c}\left(T_{cj} - T_{c,j-1}\right) \quad \ldots (7)$$

where

$T_{fj}$ = fuel temperature in the $j^{\underline{th}}$ axial node (°F)

$T_{cj}$ = coolant temperature in the $j^{\underline{th}}$ axial node (°F)

$G_j$ = heat generation rate in the $j^{\underline{th}}$ axial node (°F)

$M_{fj}$ = mass of fuel in the $j^{\underline{th}}$ axial node (lb)

$C_f$ = heat capacity of fuel (Btu/lb-°F)

$n$ = neutron level

$n_r$ = reference neutron level

$U_{fc}$ = overall heat transfer coefficient from reactor fuel to coolant (Btu/sec-ft$^2$-°F)

$A_{fcj}$ = heat transfer area between fuel and coolant (outside surface area of fuel cladding) for the $j^{\underline{th}}$ axial node (ft$^2$)

$M_{cj}$ = mass of coolant in the $j^{\underline{th}}$ axial node (lb)

$C_c$ = heat capacity of reactor coolant (Btu/lb-°F)

$w_c$ = NaK coolant flow rate (lb/sec)

These equations were converted to a Δ model for the PCS startup analog simulation and rewritten as follows:

$$\dot{\Delta T}_{fj} = \frac{G_j}{M_{fj}C_f}\left(\frac{\Delta n}{n_r}\right) - \frac{U_{fc}A_{fcj}}{M_{fj}C_f}\left(\Delta T_{fj} - \Delta T_{cj}\right) \qquad \ldots (8)$$

$$\dot{\Delta T}_{cj} = \frac{U_{fc}A_{fcj}}{M_{cj}C_c}\left(\Delta T_{fj} - \Delta T_{cj}\right) - \frac{w_c}{w_{cr}}\,\frac{w_{cr}}{M_{cj}}\left(\Delta T_{cj} - \Delta T_{c,j-1}\right)$$

$$- \left(\frac{\Delta w_c}{w_{cr}}\right) O_{cjw} \qquad \ldots (9)$$

$$O_{cjw} = \frac{w_{cr}}{M_{cj}}\left(T_{cj0} - T_{c,j-1,0}\right) = \frac{G_j}{M_{cj}C_c}\left(\frac{n_0}{n_r}\right)\left(\frac{w_{cr}}{w_{c0}}\right) \qquad \ldots (10)$$

where

$\dot{T}_{fj}$ = time rate of change of fuel temperature in the $j^{th}$ axial node (°F/sec)

$\dot{T}_{cj}$ = time rate of change of coolant temperature in the $j^{th}$ axial node (°F/sec)

$\Delta$ = change in variable from its initial value

$w_{cr}$ = reference level of NaK coolant flow rate (lb/sec)

$w_{c0}$ = initial level of NaK coolant flow rate (lb/sec)

$n_0$ = initial neutron level

$T_{cj0}$ = initial value of nodal coolant temperature (°F)

The fuel temperature in the entrance fuel node is computed from

$$\Delta\dot{T}_{fe} = \frac{G_e}{M_{fe}C_f}\left(\frac{\Delta n}{n_r}\right) - \frac{U_{fc}A_{fce}}{M_{fe}C_f}\left(\Delta T_{fe} - \Delta T_{cin}\right) \qquad \ldots (11)$$

where $T_{cin}$ is the NaK coolant temperature at the core inlet, and the subscript e indicates values for the entrance node.

The change in core average fuel temperature is

$$\Delta\overline{T}_f = \frac{1}{6}\left(\Delta T_{fe} + \sum_{j=1}^{5} \Delta T_{fj}\right) \qquad \ldots (12)$$

The temperatures of the lower and upper grid plates are calculated from the respective coolant temperatures by using effective values for heat conduction area and path length.

$$\Delta\dot{T}_{\ell g} = \frac{K_{\ell g}}{M_{\ell g}C_{\ell g}}\left(\frac{A}{L}\right)_{\ell g}\left(\Delta T_{cin} - \Delta T_{\ell g}\right) \qquad \ldots (13)$$

$$\Delta\dot{T}_{ug} = \frac{K_{ug}}{M_{ug}C_{ug}}\left(\frac{A}{L}\right)_{ug}\left(\Delta T_{c5} - \Delta T_{ug}\right) \qquad \ldots (14)$$

where

$\dot{T}_{\ell g}$ = time rate of change of temperature of lower grid plate (°F/sec)

$\dot{T}_{ug}$ = time rate of change of temperature of upper grid plate (°F/sec)

$\Delta$ = change of variable from its initial value

$k_{\ell g}$ = thermal conductivity of the lower grid plate (Btu/sec-ft-°F)

$M_{\ell g}$ = mass of lower grid plate (lb)

$C_{\ell g}$ = heat capacity of lower grid plate (Btu/lb-°F)

$\left(\frac{A}{L}\right)_{\ell g}$ = ratio of effective heat conduction area to effective heat conduction path length for lower grid plate (ft)

$T_{cin}$ = core inlet coolant temperature (°F)

$T_{\ell g}$ = temperature of lower grid plate (°F)

$K_{ug}$ = thermal conductivity of the upper grid plate (Btu/sec-ft-°F)

$M_{ug}$ = mass of upper grid plate (lb)

$C_{ug}$ = heat capacity of upper grid plate (Btu/lb-°F)

$\left(\frac{A}{L}\right)_{ug}$ = ratio of effective heat conduction area to effective heat conduction path length for upper grid plate (ft)

$T_{c5}$ = coolant temperature at the outlet of the fifth axial node (core outlet) (°F)

$T_{ug}$ = temperature of upper grid plate (°F)

3. INTERMEDIATE HEAT EXCHANGER (IHX) (See Figure 8)

The equations supplied by Aerojet-General Corporation simulate the intermediate (NaK-Hg) heat exchanger as follows:

a. Preheater Section Heat Balance

$$\frac{d}{dt}\left(T_{c\,pout}\right) = \frac{w_c C_c \left(T_{cpb} - T_{c\,pout}\right) - \pi D_i Z L_p U_p \left(LMTD\right)_p}{M_{IHX} C_{IHX} \left(\frac{L_p}{L_{IHX}}\right)} \quad \ldots (15)$$

where:

$T_{cpout}$ = NaK coolant temperature at the NaK outlet of the preheater section (°F)

$w_c$ = NaK coolant flow rate (lb/sec)

$C_c$ = heat capacity of NaK coolant at constant pressure (Btu/lb-°F)

$T_{cpb}$ = NaK coolant temperature at the interface between preheater and boiler sections (°F)

$D_i$ = internal diameter of mercury flow tubes (ft)

$Z$ = number of mercury flow tubes

$L_p$ = variable length of the preheater section (ft)

$U_p$ = overall heat transfer coefficient for the preheater section (Btu/sec-ft$^2$-°F)

$(LMTD)_p$ = log mean temperature difference in the preheater section (°F)

$M_{IHX}$ = mass of NaK and metal in the intermediate heat exchanger (lb)

$C_{IHX}$ = heat capacity of metal and NaK in the intermediate heat exchanger (Btu/lb-°F)

$L_{IHX}$ = length of the intermediate heat exchanger flow tubes (ft)

The length of the preheater section is computed as

$$L_p = \frac{w_{ML} C_{ML} \left(T_{Mpb} - T_{Mpin}\right)}{\pi D_i Z U_p (LMTD)_p} \qquad \ldots (16)$$

where

$w_{ML}$ = liquid mercury flow rate (lb/sec)

$C_{ML}$ = heat capacity of mercury liquid at constant pressure (Btu/lb-°F)

$T_{Mpb}$ = mercury temperature at the interface between preheater and boiler sections (°F)

$T_{Mpin}$ = mercury temperature at the mercury inlet to the preheater section (°F)

The log mean temperature difference in the preheater section is

$$(LMTD)_p = \frac{\left(T_{cpb} - T_{Mpb}\right) - \left(T_{cpout} - T_{Mpin}\right)}{\ln\left(\frac{T_{cpb} - T_{Mpb}}{T_{cpout} - T_{Mpin}}\right)} \quad \ldots (17)$$

The mercury temperature at the preheater-boiler interface is the saturation temperature corresponding to the saturation pressure.

$$T_{Mpb} = f\left(P_{Mpb}\right) \quad \ldots (18)$$

where $P_{Mpb}$ is the mercury saturation pressure at the interface between the boiler and preheater section ($lb/ft^2$).

The overall heat transfer coefficient for the preheater section is

$$U_p = \frac{1}{\frac{1}{h_{Mp}} + \frac{t_t}{K_t} + \frac{1}{h_c}} \quad \ldots (19)$$

where

$h_{Mp}$ = convective heat transfer coefficient for mercury in the preheater section ($Btu/sec\text{-}ft^2\text{-}°F$)

$h_c$ = convective heat transfer coefficient for NaK in the IHX ($Btu/sec\text{-}ft^2\text{-}°F$)

$K_t$ = thermal conductivity of the mercury flow tubes ($Btu/sec\text{-}ft\text{-}°F$)

$t_t$ = thickness of mercury flow tubes (ft)

The convective heat transfer coefficient for mercury in the preheater section is given by

$$h_{Mp} = \frac{7\,K_{ML}}{D_i} + \frac{0.025\,K_{ML}}{D_i}\left(\frac{4\,w_{ML}C_{ML}}{\pi D_i Z K_{ML}}\right)^{0.8} \quad \ldots (20)$$

where

$K_{ML}$ = thermal conductivity of liquid mercury ($Btu/hr\text{-}ft\text{-}°F$)

b. Boiler Section Heat Balance

$$\frac{d}{dt}\left(T_{cpb}\right) = \frac{w_c C_c \left(T_{cbs} - T_{cpb}\right) - H_M w_{ML}}{M_{IHX} C_{IHX} \left(\frac{L_b}{L_{IHX}}\right)} \quad \ldots (21)$$

where

$T_{cpb}$ = NaK coolant temperature at the interface between preheater and boiler sections (°F)

$T_{cps}$ = NaK coolant temperature at the interface between boiler and superheater sections (°F)

$H_M$ = heat of vaporization of mercury (Btu/lb)

$L_b$ = length of the boiler section (ft)

The length of the boiler section is computed from

$$\frac{d}{dt}\left(L_b\right) = \epsilon_b \left[ - \frac{w_c C_c}{\pi D_i Z U_b} \ln \left(1 - \frac{T_{cbs} - T_{cpb}}{T_{cps} - T_{Mpb}}\right) - L_b \right] \quad \ldots (22)$$

where

$\epsilon_b$ = a small constant used for analog stability

$U_b$ = overall heat transfer coefficient for the boiler section (Btu/sec-ft$^2$-°F)

and

$$U_b^* = h_{Mb} = \frac{K_{MV}}{D_i} B_1 \left(\frac{4 w_{MV}}{\pi D_i Z \mu_{MV}}\right)^{0.8} \left(\frac{\mu_{MV} H_M}{K_{MV} (LMTD)_b}\right)^{1.75} \quad \ldots (23)$$

---

*$U_b$ was assumed to be constant (at the reference level)

where

$h_{Mb}$ = convective heat transfer coefficient for mercury in the boiler section (Btu/sec-ft$^2$-°F)

$K_{MV}$ = thermal conductivity of mercury vapor (Btu/sec-ft-°F)

$B_1$ = a correlation constant

$w_{MV}$ = mercury vapor flow rate (lb/sec)

$\mu_{MV}$ = absolute viscosity of mercury vapor (lb/ft-sec)

$(LMTD)_b$ = log mean temperature difference for the boiler section (°F)

The log mean temperature difference for the boiler section can be written as

$$(LMTD)_b^* = \frac{\left(T_{cpb} - T_{Mpb}\right) - \left(T_{cbs} - T_{Mbs}\right)}{\ln\left(\frac{T_{cpb} - T_{Mpb}}{T_{cbs} - T_{Mbs}}\right)} \qquad \ldots (24)$$

where

$T_{Mbs}$ = mercury temperature at the interface between the boiler and superheater sections (°F)

The boiler section two-phase pressure drop is defined by the relationship

$$P_{Mpb} = P_{Mbs} + \frac{B_2 f_{MV}}{2_g D_i A_t^2 Z^2}\left(\frac{L_b w_{MV}^2}{\rho_{MV}}\right) \qquad \ldots (25)$$

where

$P_{Mpb}$ = mercury pressure at the interface between the preheater and boiler sections (lb/ft$^2$)

$P_{Mbs}$ = mercury pressure at the interface between the boiler and superheater sections (lb/ft$^2$)

$B_2$ = a correlation constant

---

*$(LMTD)_b$ was assumed to be constant (at the reference level)

$f_{MV}$ = friction factor for mercury vapor

$g$ = acceleration due to gravity ($ft/sec^2$)

$D_i$ = internal diameter of mercury flow tubes (ft)

$A_t$ = flow area of mercury tube ($ft^2$)

$Z$ = number of mercury flow tubes

$L_b$ = length of the boiler section (ft)

$w_{MV}$ = mercury vapor flow rate (lb/sec)

$\rho_{MV}$ = density of mercury vapor ($lb/ft^3$)

The mercury temperature at the boiler-superheater interface is the saturation temperature corresponding to the saturation pressure,

$$T_{Mbs} = f\left(P_{Mbs}\right) \qquad \ldots (26)$$

c. Superheater Section Heat Balance

$$\frac{d}{dt}\left(T_{cbs}\right) = \frac{w_c C_c \left(T_{csin} - T_{cbs}\right) - Q_s}{M_{IHX} C_{IHX} \left(\frac{L_s}{L_{IHX}}\right)} \qquad \ldots (27)$$

where

$T_{cbs}$ = NaK coolant temperature at the interface between the boiler and superheater sections (°F)

$T_{csin}$ = NaK coolant temperature at the NaK inlet to the superheater section (°F)

$Q_s$ = heat absorbed by the mercury vapor in the superheater section (Btu/sec)

$L_s$ = length of the superheater section (ft)

$L_{IHX}$ = length of the intermediate heat exchanger flow tubes (ft)

The length of the superheater section is computed from

$$L_s = L_{IHX} - L_b - L_p \qquad \ldots (28)$$

The heat absorbed by mercury vapor in the superheater section is

$$Q_s = {}^{w}{}_{MV} C_{MV} \left( T_{csin} - T_{Mbs} \right) \left( 1 - e^{-B_3 L_s} \right) \qquad \ldots (29)$$

where $B_3$ is a correlation factor

$$B_3 = \pi D_i Z U_s \left( \frac{1}{w_{MV} C_{MV}} - \frac{1}{w_c C_c} \right) \qquad \ldots (30)$$

where

$U_s$ = overall heat transfer coefficient for the superheater section (Btu/sec-ft$^2$-°F)

and

$$U_s = h_{Ms} = \frac{B_4 K_{MV}}{D_i} \left( \frac{4 w_{MV}}{\pi D_i Z \mu_{MV}} \right)^{0.8} \left( \frac{\mu_{MV} C_{MV}}{K_{MV}} \right)^{0.4} \qquad \ldots (31)$$

where

$h_{Ms}$ = convective heat transfer coefficient for mercury in the superheater section (Btu/sec-ft$^2$-°F)

$B_4$ = a correlation constant

The superheater mercury pressure drop is

$$\Delta P_{Ms} = \frac{f_{MV}}{2 g D_i A_t{}^2 Z^2} \left( \frac{L_s w_{MV}{}^2}{\rho_{MV}} \right) \qquad \ldots (32)$$

The mercury temperature at the mercury outlet of the superheater section is given by

$$T_{Msout} = T_{Mbs} + \frac{Q_s}{w_{MV} C_{MV}} \qquad \ldots (33)$$

The density of mercury vapor follows the relationship

$$\frac{d}{dt}\left(\rho_{MV}\right) = \epsilon_s \left\{ \left[ \frac{1}{V_{MV}} \int \left( w_{ML} - w_{MV} \right) dt \right] + \frac{16.04}{V_{MV}} \right.$$

$$\left. - \frac{\pi}{4} \left( D_i^2 - D_P^2 \right) \frac{Z \rho_{ML}}{V_{MV}} \left( L_p + 0.01\, L_b \right) - \rho_{MV} \right\} \qquad \ldots (34)$$

where

$\epsilon_s$ = a small constant used for analog stability

$V_{MV}$ = volume of mercury vapor ($ft^3$)

$w_{ML}$ = mercury liquid flow rate (lb/sec)

$w_{MV}$ = mercury vapor flow rate (lb/sec)

$\rho_{ML}$ = density of mercury liquid ($lb/ft^3$)

$D_P$ = diameter of plug in mercury flow tubes (ft)

The average mercury pressure in the superheater section is assumed to follow the perfect gas law,

$$P_{Ms} = \rho_{MV} R T_{Ms} \qquad \ldots (35)$$

where R is the ideal gas constant (ft-lb/lb-°F).

The average mercury temperature in the superheater section is

$$T_{Ms} = 1/2 \left( T_{Mbs} + T_{Msout} \right) \qquad \ldots (36)$$

The mercury pressure at the mercury outlet of the superheater section is computed from

$$P_{Msout} = P_{Ms} - \frac{\Delta P_{Ms}}{2} \qquad \ldots (37)$$

and the mercury pressure at the interface between the boiler and superheater regions is

$$P_{Mbs} = P_{Msout} + \Delta P_{Ms} \qquad \ldots (38)$$

The mercury vapor flow rate is computed from

$$w_{MV} = \frac{w_{MVr} \sqrt{T_{Msoutr}}}{P_{Msoutr}} \left( \frac{P_{Msout}}{\sqrt{T_{Msout}}} \right) \qquad \ldots (39)$$

where the subscript r denotes the reference level of the variable subscripted.

BLANK

# APPENDIX B
## ANALOG COMPUTER CIRCUITS AND POTENTIOMETER SETTINGS

The circuits used in the analog simulation of PCS startup are presented in Figures 72 to 81. The numerical settings and symbolic descriptions for the analog potentiometers (pots) are given in Tables 4 and 5. The simulation used three analog computer consoles designated here as Consoles A, B, and C. Most of the equipment used was located on Consoles B or C (PACE 231R), and this location is indicated on the circuit diagrams. Equipment located on Console A (PACE 1631) is indicated by the letter A preceding the number of the item.

Nomenclature used in this appendix is the same as previously used in the equations with the following additions:

P = potentiometers of series P ( letter P omitted on circuit diagrams for clarity)

Q = potentiometers of series Q (letter Q shown on circuit diagrams)

g = direct connection to grid of amplifier

IC = initial condition on amplifier

J = junction of leads from two consoles

K = 1000 ohms resistance

FG = function generator — approximates a curve with a series of straight line segments

LIM = limiter, restricts voltage to a given quantity

Multiplier = electronic multiplying device

SJ = connection to summing junction of amplifier

SW = switch

$\mu$f = microfarads

$\tau$ = computer time, a factor of 10 faster than real time, t

Figure 72 illustrates the symbols used in the analog circuit diagrams of Figures 73 through 81.

Figure 73 is the simulation of the six-group reactor kinetics equations including the reactivity feedback terms from the average fuel and grid plate temperatures.

| NAME | SYMBOL | MATHEMATICAL REPRESENTATION |
|---|---|---|
| 1. AMPLIFIER | 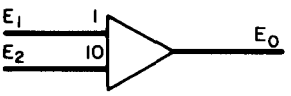 | $E_0 = -(E_1 + 10E_2)$ |
| 2. INTEGRATOR | 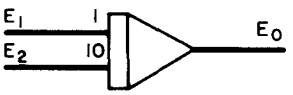 | $E_0 = -\int(E_1 + 10E_2)dt$ |
| 3 POTENTIOMETER (POT) | 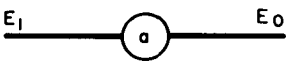 | $E_0 = aE_1$<br>$a$ = CONSTANT $0<a<1.0$ |
| 4 SERVOMECHANISM (MULTIPLICATION) | 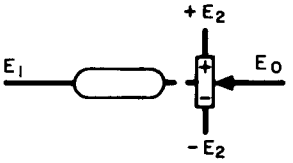 | $E_0 = E_1E_2/100$, $E_1, E_2 \pm$ |
| | 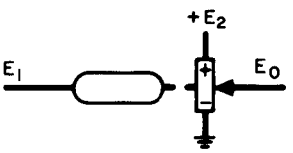 | $E_0 = E_1E_2/100$; $E_2 \pm$, $E_1$ + ONLY |
| (DIVISION) | 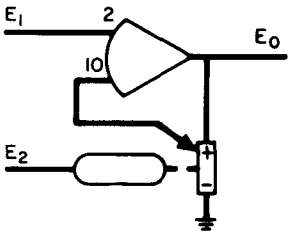 | $E_0 = -100\left(\frac{2E_1}{10E_2}\right)$; $E_1 \pm$, $E_2$ + ONLY |
| 5 ELECTRONIC MULTIPLIER | 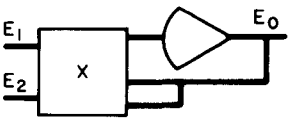 | $E_0 = -E_1E_2/100$ |
| 6 HIGH GAIN AMPLIFIER | 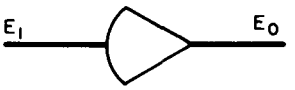 | $E_0 = -10^6$ (approx) $E_1$<br>NEVER USED AS REPRESENTED HERE, ALWAYS HAS FEEDBACK PATH FROM OUTPUT TO INPUT |
| 7 INITIAL CONDITION ON INTEGRATOR | 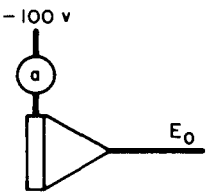 | $E_0$, AT $t = 0$, $= -(-100)a$<br>$a$ = CONSTANT $0<a<1.0$ |

3-30-64 7568-0986

Figure 72. Analog Computer Circuitry Symbols

Figure 74 shows the simulation of the five-node entrance fuel node core heat transfer model.

Figure 75 is the simulated controller which generates step changes in reactivity.

Figure 76 shows the circuits used to generate changes in NaK coolant flow and to compute the rates of change of fuel and coolant temperatures.

Figure 77 is an abbreviated simulation of coolant transport delays and load changes.

Figure 78 combines Figures 72 through 74 to show the complete simulation of the nuclear system.

Figure 79 gives the full circuit used for transport delays and load changes in the primary coolant loop from reactor outlet back to reactor inlet. This figure also shows the generation of flow changes and the computation of temperature rates of change.

Figure 80 is the analog circuit diagram for the preheater and boiler section of the intermediate (NaK-Hg) heat exchanger.

Figure 81 completes the circuit by presenting the diagram for the superheater section of the intermediate heat exchanger.

The circuit for the entire simulation is a combination of figures 78 through 81.

BLANK

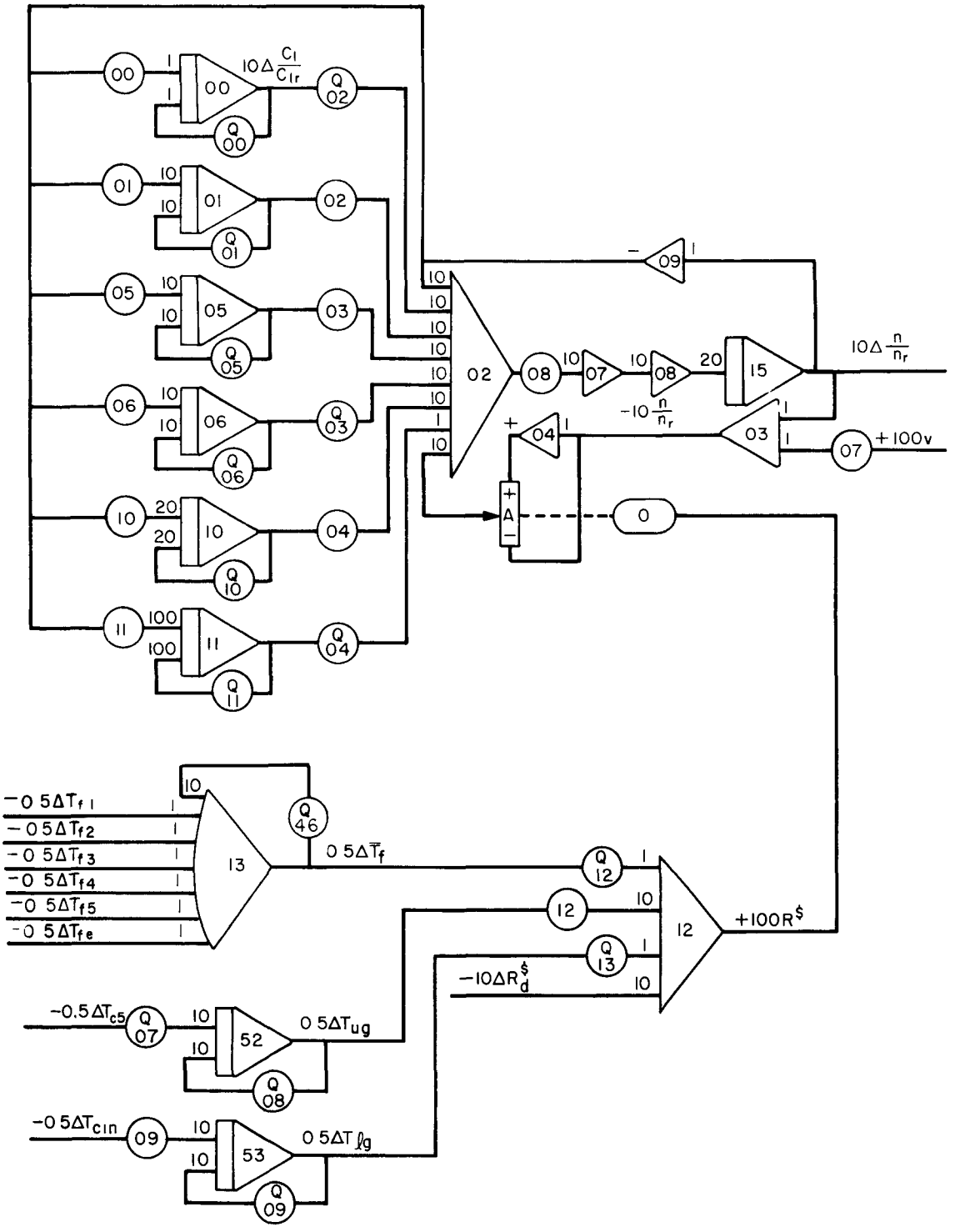


3-4-64 7568-0930

Figure 73. Analog Circuit Diagram, Reactor Kinetics

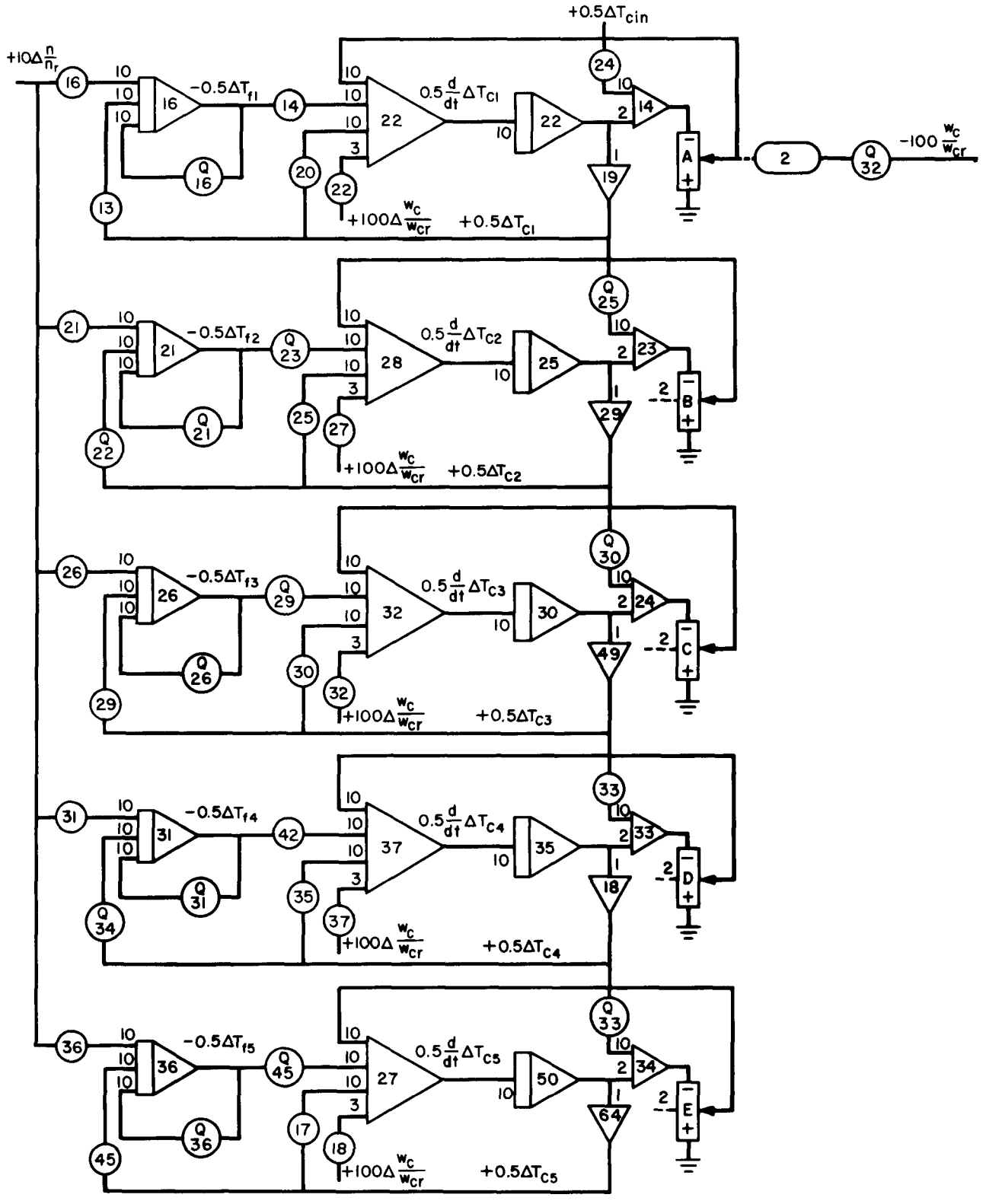


3-4-64

7568-0931

Figure 74. Analog Circuit Diagram, Core Heat Transfer

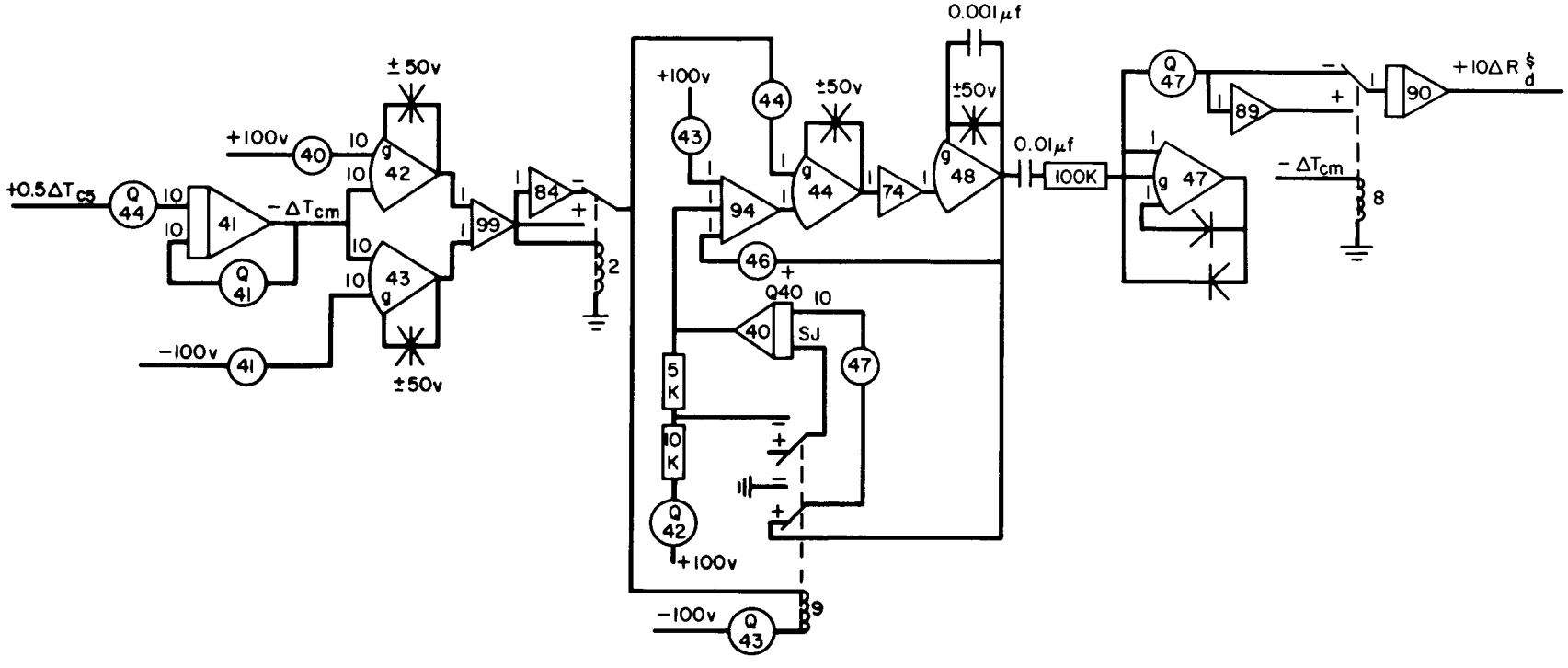


3-4-64

7568-0928

Figure 75. Analog Circuit Diagram, Controller

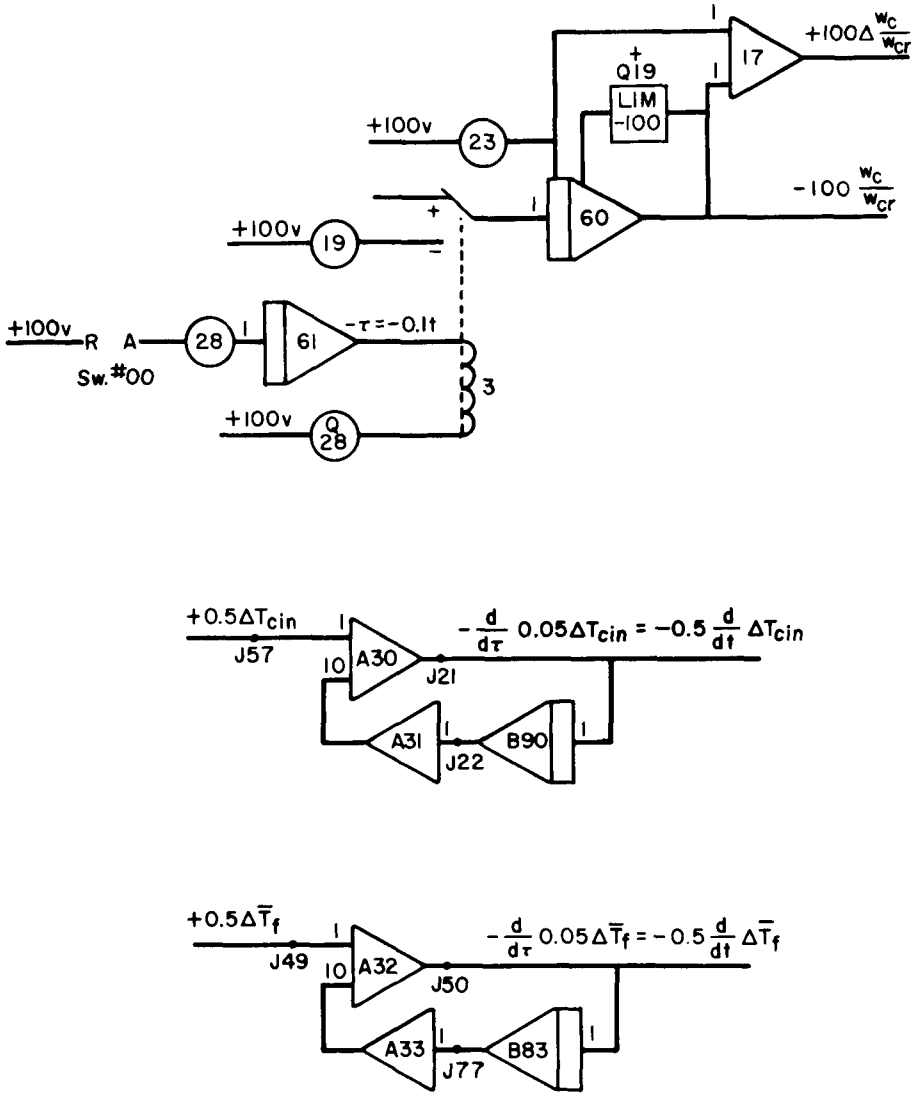


3-4-64 7568-0929

Figure 76. Analog Circuit Diagram, NaK Flow Rate Change and Temperature Differentiation

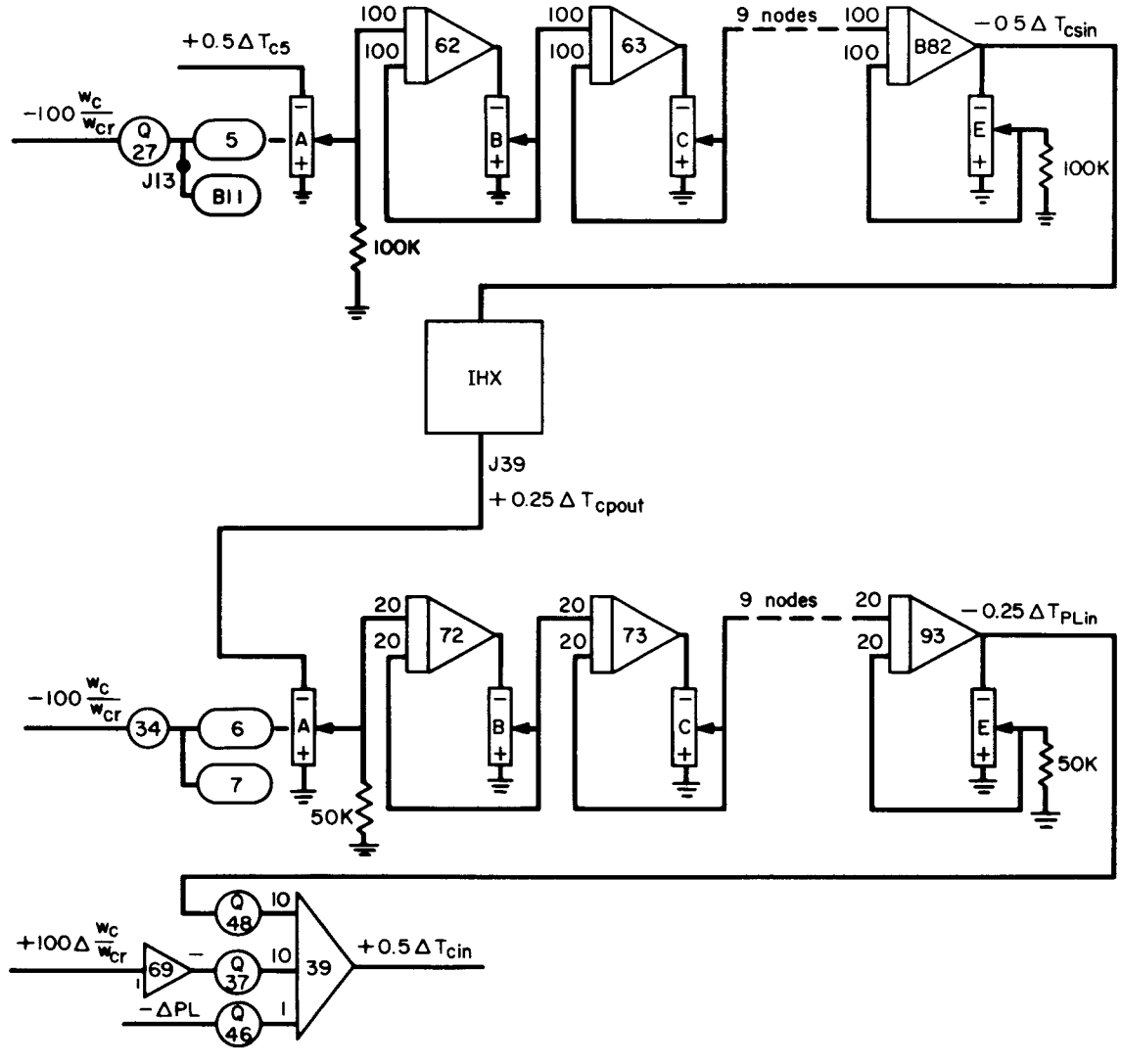


Figure 77. Analog Circuit Diagrams, Coolant Transport Delays and Heat Loads

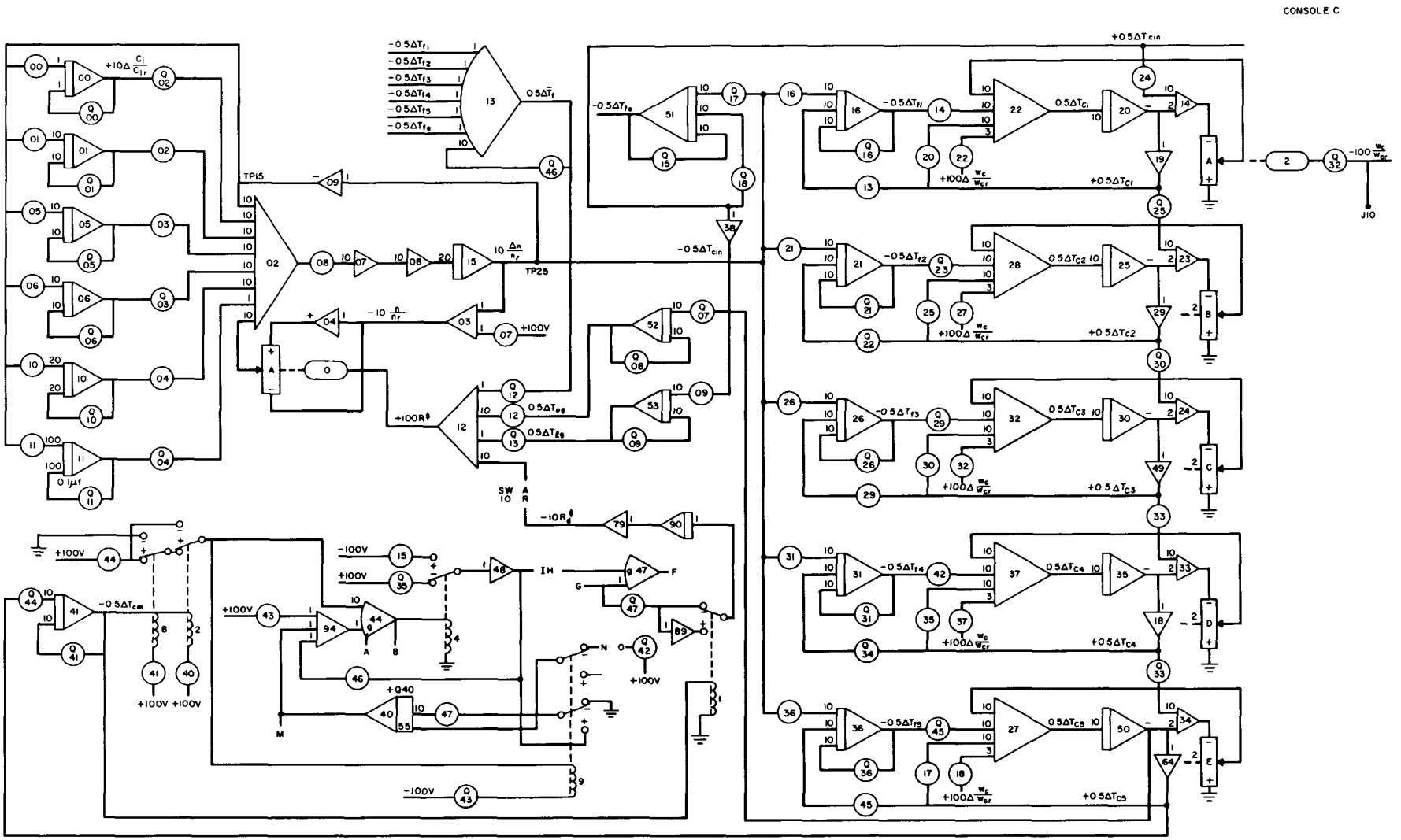


Figure 78. Analog Circuit Diagram, Reactor

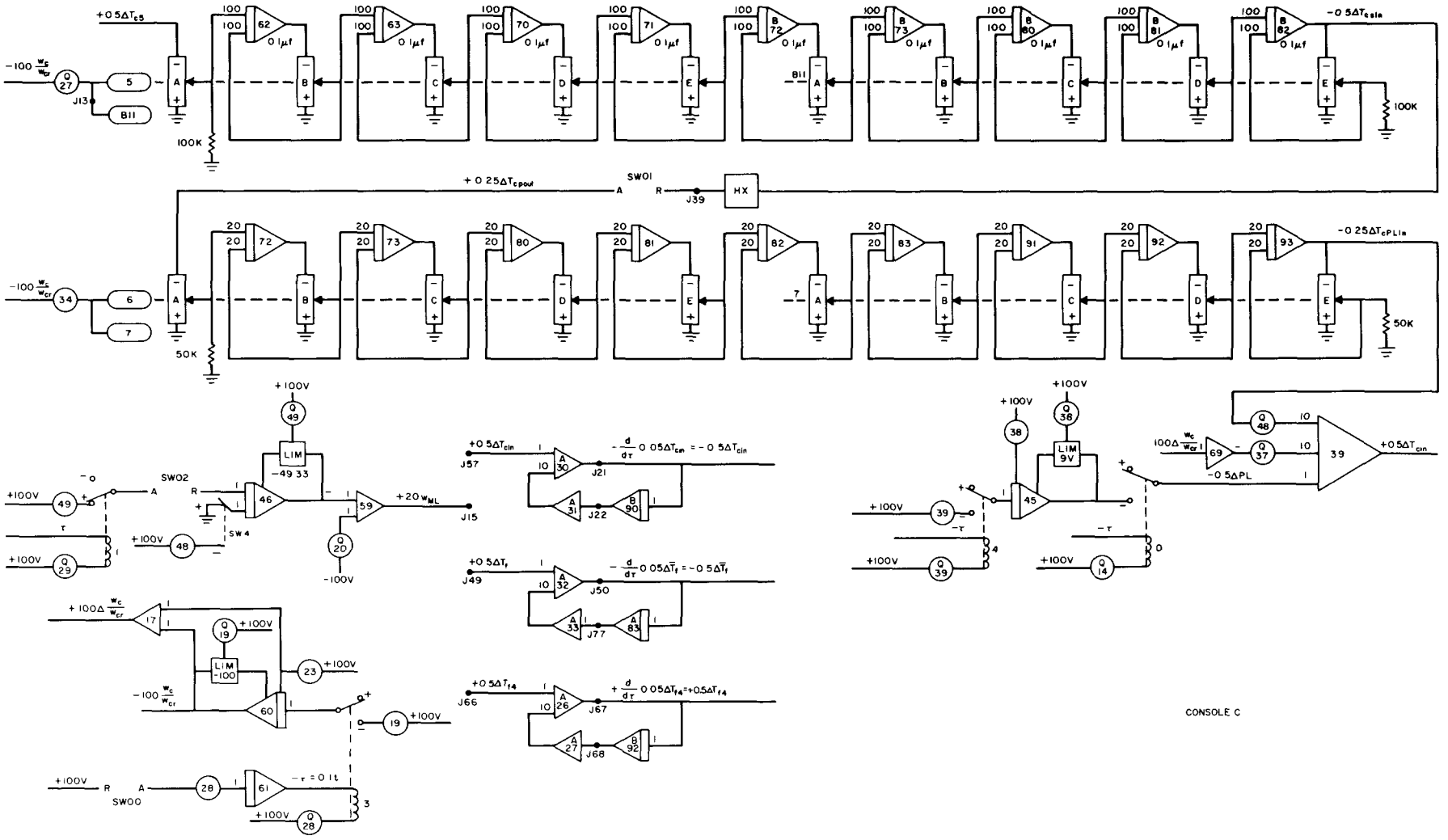


3-24-64

7568-01006

Figure 79. Analog Circuit Diagram, Primary Coolant Loop

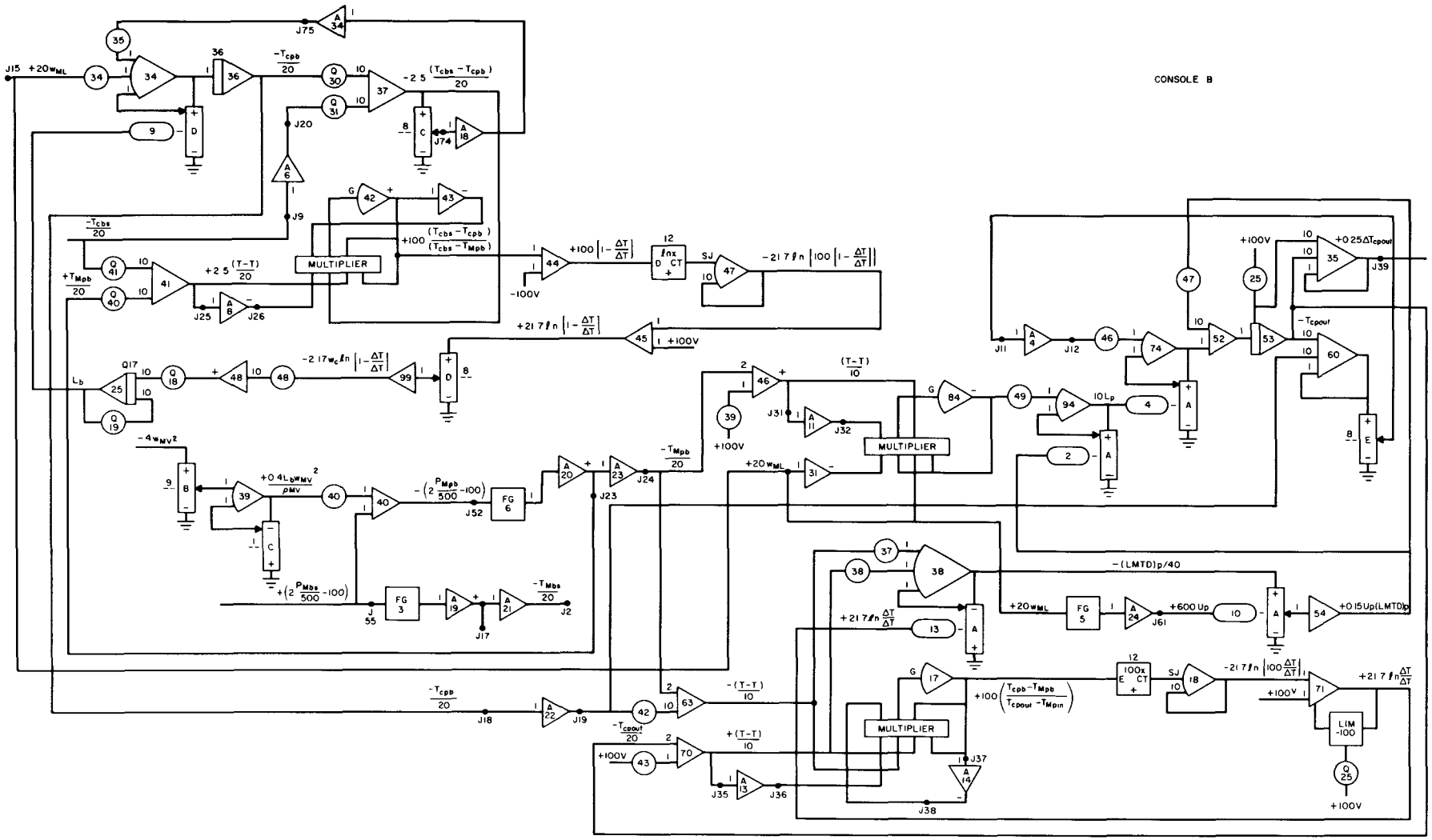


Figure 80. Analog Circuit Diagram, Preheater and Boiler Sections of the NaK-Mercury Heat Exchanger

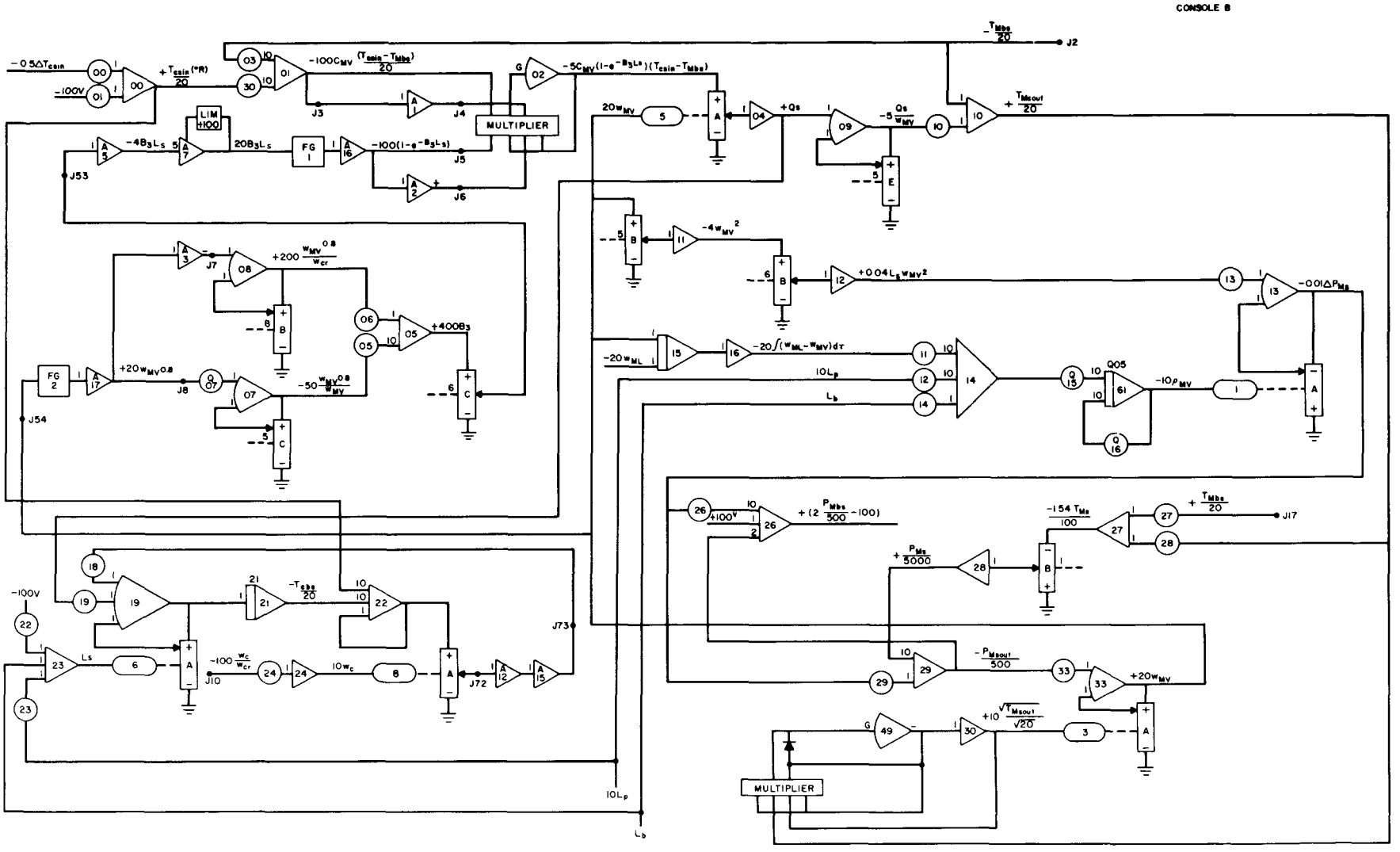


3-24-64

7568-01004

Figure 81. Analog Circuit Diagram, Superheater Section of the NaK-Mercury Heat Exchanger

# TABLE 4

## CONSOLE B POTENTIOMETER SETTINGS

| Console and Potentiometer Number | Description | Setting | Console and Potentiometer Number | Description | Setting |
|---|---|---|---|---|---|
| BP00 | 1/10 | 1000 | BP18 | $\frac{0.2\ C_c}{M_{IHX}\ C_{IHX}\ \frac{1}{L_{IHX}}}$ | 0481 |
| BP01 | $(T_{csin0} + 460)/2000$ | 8800 | | | |
| BP03 | $10\ C_{MV}$ | 2550 | BQ18 | $\epsilon_b$ | 2368 |
| BP05 | $\frac{8}{10 C_{MV}}\left(\frac{\pi D_1 Z B_4 K_{MV}}{D_1}\right)\left(\frac{4}{\pi D_1 Z \mu_{MV}}\right)^{0.8}\left(\frac{\mu_{MV} C_{MV}}{K_{MV}}\right)^{0.4}$ | 1573 | BP19 | $\frac{0.005}{M_{IHX}\ C_{IHX}\ \frac{1}{L_{IHX}}}$ | 0057 |
| BQ05 | $\rho_{MV0}$ | * | BQ19 | $\epsilon_b$ | 2368 |
| BP06 | $\frac{2}{C_c}\left(\frac{\pi D_1 Z B_4 K_{MV}}{D_1}\right)\left(\frac{4}{\pi D_1 Z \mu_{MV}}\right)^{0.8}\left(\frac{\mu_{MV} C_{MV}}{K_{MV}}\right)^{0.4}$ | 0475 | BP21 | $-\left(\frac{T_{cbs0} + 460}{20}\right)$ | A21 IC |
| BQ07 | 1/2 | 5000 | BP22 | $10^{-2}\ L_{IHX}$ | 6770 |
| BP10 | $1/100\ C_{MV}$ | 3922 | BP23 | 1/10 | 1000 |
| BP11 | $1/2\ V_{MV}$ | 4425 | BP24 | $10^{-1}\ w_{c0}$ | 8900 |
| BP12 | $10^{-1}\frac{\pi}{4}(D_1^2 - D_p^2)Z\frac{\rho_{ML}}{V_{MV}}$ | 5062 | BP25 | $-\left(\frac{T_{cpout} + 460}{20}\right)$ | A53 IC |
| | | | BQ25 | Limit A71 -100 V | - |
| BP13 | $\frac{0\ 025\ f_{MV}}{2_g D_1 A_t^2 Z^2}$ | 5625 | BP26 | $\frac{2}{50}$ | 0400 |
| BP14 | $10^{-1}\frac{\pi}{4}(D_1^2 - D_p^2)Z\frac{\rho_{ML}}{V_{MV}}$ | 5062 | BP27 | $\frac{R}{50}$ | 1540 |
| | | | BP28 | $\frac{R}{50}$ | 1540 |
| BQ15 | $\epsilon_s$ | 2368 | BP29 | $\frac{1}{10}$ | 1000 |
| BQ16 | $\epsilon_s$ | 2368 | BP30 | $10\ C_{MV}$ | 2550 |
| BQ17 | $L_{b0}$ | * | BQ30 | $\frac{1}{4}$ | 2500 |

*Varies with initial condition

TABLE 4 (Continued)

CONSOLE B POTENTIOMETER SETTINGS

| Console and Potentiometer Number | Description | Setting | Console and Potentiometer Number | Description | Setting |
|---|---|---|---|---|---|
| BQ31 | $\frac{1}{4}$ | 2500 | BQ40 | $\frac{1}{4}$ | 2500 |
| BP33 | $\frac{10^3}{\sqrt{20}} \frac{w_{MVr} \sqrt{T_{Msoutr}}}{P_{Msoutr}}$ | 6037 | BQ41 | $\frac{1}{4}$ | 2500 |
| | | | BP42 | $\frac{2}{10}$ | 2000 |
| BP34 | $\frac{H_M}{4000\, M_{IHX}\, C_{IHX}\left(\frac{1}{L_{IHX}}\right)}$ | 0351 | BP43 | $10^{-3}\, T_{Mpin}$ | 9730 |
| BP35 | $\frac{0.4\, C_c}{M_{IHX}\, C_{IHX}\left(\frac{1}{L_{IHX}}\right)}$ | 0962 | BP46 | $\frac{2C_c}{M_{IHX}\, C_{IHX}\left(\frac{1}{L_{IHX}}\right)}$ | 4811 |
| BP36 | $-\left(\frac{T_{cpb} + 460}{20}\right)$ | A36 IC | BP47 | $\frac{\pi D_1 Z}{3\, M_{IHX}\, C_{IHX}\left(\frac{1}{L_{IHX}}\right)}$ | 3694 |
| BP37 | $\frac{21.7}{400}$ | 0542 | | | |
| BP38 | $\frac{21.7}{400}$ | 0542 | BP48 | $\frac{1}{21.7}\left(\frac{C_c}{\pi D_1 Z U_b}\right)$ | 1344 |
| BP39 | $10^{-3}\, T_{Mpin}$ | 9730 | BP49 | $5\,(0.15)\left(\frac{C_{ML}}{\pi D_1 Z}\right)$ | 0257 |
| BP40 | $10^{-2}\left(\frac{B_2 F_{MV}}{2 g D_1 A_t^2 Z^2}\right)$ | 4330 | | | |

# TABLE 5

## CONSOLE C POTENTIOMETER SETTINGS

| Console and Potentiometer Number | Description | Setting | Console and Potentiometer Number | Description | Setting | Console and Potentiometer Number | Description | Setting |
|---|---|---|---|---|---|---|---|---|
| CP00 | $10\lambda_1$ | 1240 | CP09 | $K_{\ell g}$ | 3446 | CP18 | $\frac{O_{c5w}}{600}$ | * |
| CQ00 | $10\lambda_1$ | 1240 | CQ09 | $K_{\ell g}$ | 3446 | CQ18 | $\frac{UA_j\dagger}{M_{fj}C_f}$ | 1655 |
| CP01 | $\lambda_2$ | 0305 | CP10 | $0\,5\,\lambda_5$ | 5650 | CP19 | Flow Ramp Rate | * |
| CQ01 | $\lambda_2$ | 0305 | CQ10 | $0.5\,\lambda_5$ | 5650 | CQ19 | Limit A60 to -100 v | * |
| CP02 | $\frac{\beta_2}{\beta}$ | 2194 | CP11 | $10^{-1}\lambda_6$ | 3000 | CP20 | $\frac{UA_j\dagger}{10\,M_{cj}C_c}$ | 5799 |
| CQ02 | $\frac{\beta_1}{\beta}$ | 0330 | CQ11 | $10^{-1}\lambda_6$ | 3000 | CQ20 | $0.2\,w_{ML0}$ | 0127 |
| CP03 | $\frac{\beta_3}{\beta}$ | 1960 | CP12 | $20\,\alpha_{ug}$ | 0120 | CP21 | $\frac{0.5\,G_2}{10\,M_{fj}C_f}$ | 7040 |
| CQ03 | $\frac{\beta_4}{\beta}$ | 3947 | CQ12 | $200\,\alpha_f$ | 1000 | CQ21 | $\frac{UA_j\dagger}{M_{fj}C_f}$ | 1655 |
| CP04 | $\frac{\beta_5}{\beta}$ | 1150 | CP13 | $\frac{UA_j\dagger}{M_{fj}C_f}$ | 1655 | CP22 | $\frac{O_{c1w}}{600}$ | * |
| CQ04 | $\frac{10\beta_6}{\beta}$ | 4193 | CQ13 | $200\,\alpha_{\ell g}$ | 0800 | CQ22 | $\frac{UA_j\dagger}{M_{fj}C_f}$ | 1655 |
| CP05 | $\lambda_3$ | 1110 | CP14 | $\frac{UA_j\dagger}{10\,M_{cj}C_c}$ | 5799 | CP23 | $\frac{100\,w_{c0}}{w_{cr}}$ | A60 IC |
| CQ05 | $\lambda_3$ | 1110 | CQ14 | $10^{-3}(\tau_c + t_c)$ | * | CQ23 | $\frac{UA_j\dagger}{10\,M_{cj}C_c}$ | 5799 |
| CP06 | $\lambda_4$ | 3010 | CP15 | (set under load) | 5000 | CP24 | $\frac{1}{5}$ | 2000 |
| CQ06 | $\lambda_4$ | 3010 | CQ15 | $\frac{UA_j\dagger}{M_{fj}C_f}$ | 1655 | CQ24 | $10^{-3}(t_{1M} + \tau_M)$ | * |
| CP07 | $\frac{10^{-1}\,n_0}{n_r}$ | * | CP16 | $\frac{0.5\,G_1}{10\,M_{fj}C_f}$ | 3581 | CP25 | $\frac{UA_j\dagger}{10\,M_{cj}C_c}$ | 5799 |
| CQ07 | $K_{ug}$ | 4915 | CQ16 | $\frac{UA_j\dagger}{M_{fj}C_f}$ | 1655 | CQ25 | $\frac{1}{5}$ | 2000 |
| CP08 | $\frac{\beta}{2000\,\ell^*}$ | 4750 | CP17 | $\frac{UA_j\dagger}{10\,M_{cj}C_c}$ | 5799 | | | |
| CQ08 | $K_{ug}$ | 4915 | CQ17 | $\frac{0.5\,G_e}{10\,M_{fe}C_f}$ | 3581 | | | |

*Varies with initial condition
†$UA_j$ stands for $U_{fc}\,A_{fcj}$

## TABLE 5 (Continued)

## CONSOLE C POTENTIOMETER SETTINGS

| Console and Potentiometer Number | Description | Setting |
|---|---|---|
| CP26 | $\frac{0.5\ G_3}{10\ M_{fj} C_f}$ | 8436 |
| CQ26 | $\frac{UA_j\dagger}{M_{fj} C_f}$ | 1655 |
| CP27 | $\frac{O_{c2w}}{600}$ | |
| CQ27 | $\frac{n}{100\ \tau_{TRI}}$ | 2500 |
| CP28 | $1^V$ = 10 sec real time | 0100 |
| CQ28 | $10^{-3}\ \tau_c$ | |
| CP29 | $\frac{UA_j\dagger}{M_{fj} C_f}$ | 1655 |
| CQ29 | $\frac{UA_j\dagger}{10\ M_{cj} C_c}$ | 5799 |
| CP30 | $\frac{UA_j\dagger}{10\ M_{cj} C_c}$ | 5799 |
| CQ30 | $\frac{1}{5}$ | 2000 |
| CP31 | $\frac{0.5\ G_4}{10\ M_{fj} C_f}$ | 7313 |
| CQ31 | $\frac{UA_j\dagger}{M_{fj} C_f}$ | 1655 |
| CP32 | $\frac{O_{c3w}}{600}$ | * |
| CQ32 | $\frac{w_r}{20\ M_{cj}}$ | M2F = 5291 |
| CP33 | $\frac{1}{5}$ | 2000 |
| CQ33 | $\frac{1}{5}$ | 2000 |
| CP34 | $\frac{n}{20\ \tau_{TIR}}$ | 7692 |
| CQ34 | $\frac{UA_j\dagger}{M_{fj} C_f}$ | 1655 |
| CP35 | $\frac{UA_j\dagger}{10\ M_{cj} C_c}$ | 5799 |
| CQ35 | (set under load) | 5000 |
| CP36 | $\frac{0.5\ G_5}{10\ M_{fj} C_f}$ | 3975 |
| CQ36 | $\frac{UA_j\dagger}{M_{fj} C_f}$ | 1655 |
| CP37 | $\frac{O_{c4w}}{600}$ | |
| CQ37 | $\frac{0.5\ \theta_{AHX}}{10\ \Delta\frac{w}{w_r}(\%)}$ | * |
| CP38 | $0.5\ \Delta PL_0$ | A45 IC |
| CQ38 | LIM ΔPL A45 | |
| CP39 | ΔPL ramp rate | 0057 |
| CQ39 | $10^{-3}\ \tau_M$ | 1200 |
| CP40 | $1/2 \times 10^{-2}$ UDB | * |
| CQ40 | IC A40 | 2400 |
| CP41 | $1/2 \times 10^{-2}$ LDB | " |
| CQ41 | $\frac{1}{\tau_M}$ | 1000 |
| CP42 | $\frac{UA_j\dagger}{10\ M_{cj} C_c}$ | 5799 |
| CQ42 | Control | " |
| CP43 | Control | 5000 |
| CQ43 | Control | 0250 |
| CP44 | Control | 0514 |
| CQ44 | $\frac{1}{\tau_M}$ | 1000 |
| CP45 | $\frac{UA_j\dagger}{M_{fj} C_f}$ | 1655 |
| CQ45 | $\frac{UA_j\dagger}{10\ M_{cj} C_c}$ | 5799 |
| CP46 | Control | 5000 |
| CQ46 | 0.6 | 6000 |
| CP47 | step period | " |
| CQ47 | step amplitude | * |
| CP48 | $w_{ML}$ ramp rate II | " |
| CQ48 | $\frac{0.2}{1 - \frac{w_{ML0} w_{cr}}{w_{MLr} w_{c0}}}$ | " |
| CP49 | $w_{ML}$ ramp rate I | " |
| CQ49 | Limit A46 to -49.33 | " |

**Function Generators**

| | Input | Output |
|---|---|---|
| FG1 | $\frac{P_{Mbs}}{250} - 100$ | $-\frac{T_{Mbs}}{20}$ |
| FG2 | $\frac{P_{Mpb}}{250} - 100$ | $-\frac{T_{Mpb}}{20}$ |
| FG3 | $20\ B_3 L_s$ | $100(1 - e^{-B_3 L_s})$ |
| FG6 | $20\ W_{Mv}$ | $20\ W_{Mv}^{0.8}$ |

*Varies with initial condition
†$UA_j$ stands for $U_{fc} A_{fcj}$

BLANK

# APPENDIX C
# SYSTEM CONSTANTS AND REFERENCE LEVELS

The constants and reference levels given in Tables 6 through 9 are those used for the latest phase of the PCS startup study. They were valid for the SNAP 8 reference flight design at the time of this study.[4] Some of the constants have changed since then,[5] and more can be expected to change in the future. All of the items listed as "constants" were assumed to be invariant with respect to temperature over the relatively small temperature range of PCS startup. The values used were determined for their respective average temperatures.

For the calculation of $M_{fj}$ and $C_{fj}$, the fuel nodal mass and heat capacity, the fuel cladding was assumed to be "lumped" with the fuel itself. The nodal heat generation rates used are averages over the length of the node, as shown in Figure 82.

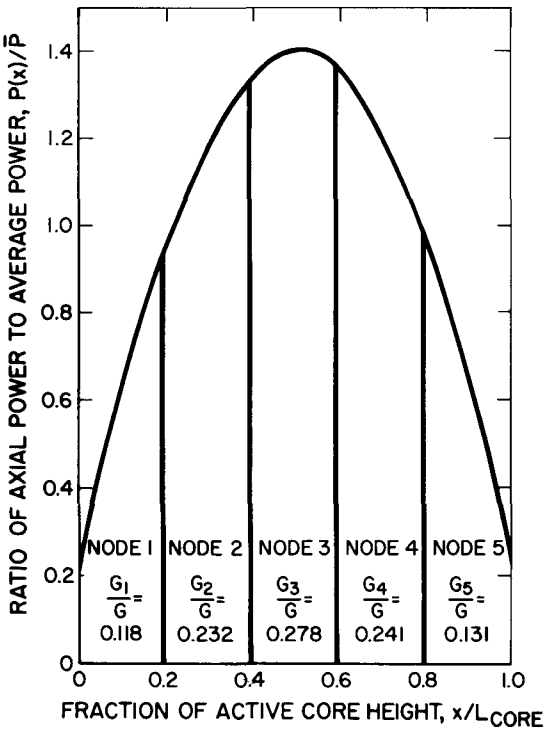


3-24-64 7568-01002

Figure 82. Normalized Axial Power Distribution

Computation of the ratio of conduction area to conduction path length for the grid plates was handled by assuming that two independent paths could be computed and then summed. One path is radial from the center of a typical "cell" to the coolant flow holes. The other is vertical from the horizontal centerline of the grid plate to the flat surfaces.

It was assumed that the expansion of the reactor vessel walls in response to changes in coolant temperature would take place with the same time constant as that of the corresponding grid plate. Therefore, the temperature coefficient of reactivity due to reactor vessel expansion was included with those of the grid plates.

Figure 83 presents the differential reactivity worth of the SNAP 8 control drums with respect to control drum position. It is expected that PCS startup will take place when the drums are near the position of maximum differential worth. The variation of control drum

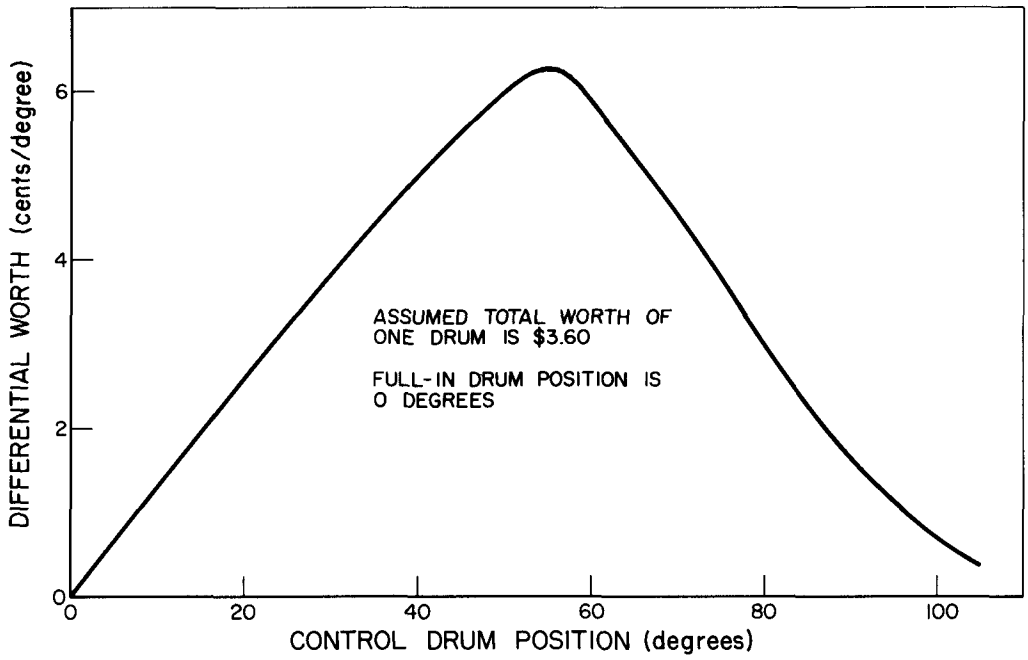


4-10-64 7568-01023

Figure 83. Control Drum Differential Reactivity Worth

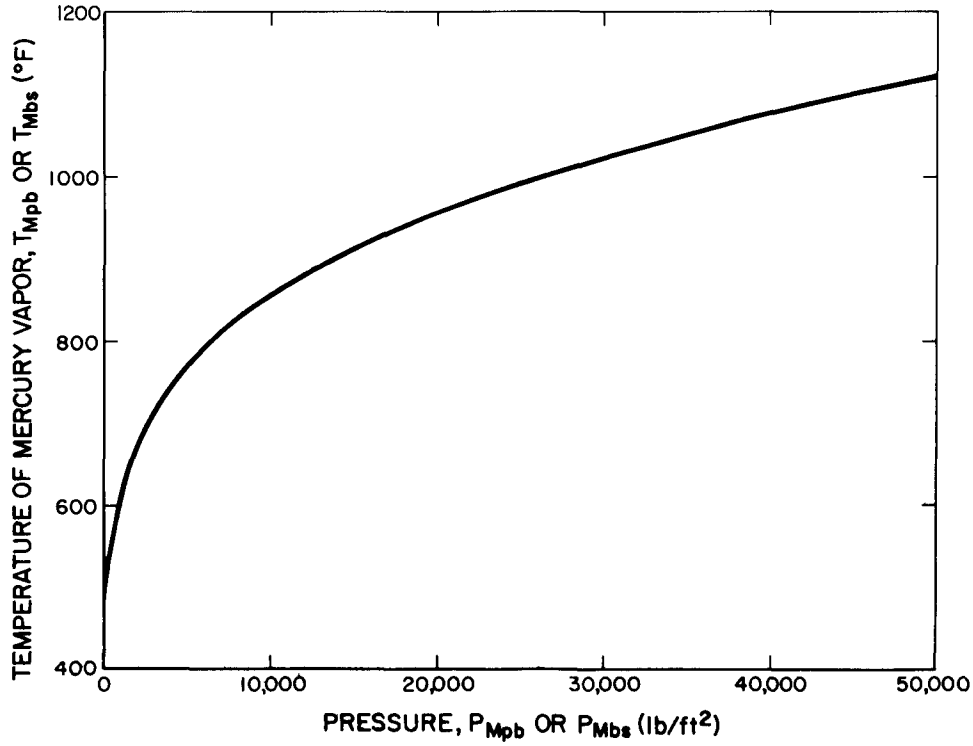


3-24-64 7568-01003

Figure 84. Relationship Between Pressure and Temperature of Mercury Vapor

step size is such that each step can have a reactivity worth between 2.6¢ and 3.8¢. Thus most of the PCS startup study assumed 3¢ per step. The range of step size was given in Table 2.

Figure 84 shows the relationship between the pressure and temperature of mercury vapor as used in the simulation of the intermediate heat exchanger.

TABLE 6

NUCLEAR SYSTEM CONSTANTS

| | | | | | |
|---|---|---|---|---|---|
| Reactor kinetics | | | | | |
| $\ell^*$ | $8.1 \times 10^{-6}$ | sec | $C_{clad}$ | 0.138 | Btu/lb-°F |
| $\beta$ | 0.0077 | | $M_c$ | 4.2 | lb |
| $\beta_1/\beta$ | 0.03297 | | $C_c$ | 0.210 | Btu/lb-°F |
| $\beta_2/\beta$ | 0.2194 | | G | 375.05 | Btu/sec |
| $\beta_3/\beta$ | 0.1960 | | $G_e/G$ | 0.118 | |
| $\beta_4/\beta$ | 0.3947 | | $G_1/G$ | 0.118 | |
| $\beta_5/\beta$ | 0.1150 | | $G_2/G$ | 0.232 | |
| $\beta_6/\beta$ | 0.04193 | | $G_3/G$ | 0.278 | |
| $\lambda_1$ | 0.0124 | $sec^{-1}$ | $G_4/G$ | 0.241 | |
| $\lambda_2$ | 0.0305 | $sec^{-1}$ | $G_5/G$ | 0.131 | |
| $\lambda_3$ | 0.1110 | $sec^{-1}$ | Grid plates | | |
| $\lambda_4$ | 0.3010 | $sec^{-1}$ | $K_{\ell g}$ | 0.00272 | Btu/sec-ft-°F |
| $\lambda_5$ | 1.1300 | $sec^{-1}$ | $M_{\ell g}$ | 7.47 | lb |
| $\lambda_6$ | 3.000 | $sec^{-1}$ | $C_{\ell g}$ | 0.131 | Btu/lb-°F |
| Core heat transfer | | | $(A/L)_{\ell g}$ | 124.0 | ft |
| $U_{fc}$ | 0.1167 | Btu/sec-$ft^2$-°F | $K_{ug}$ | 0.00389 | Btu/sec-ft-°F |
| $A_{fc}$ | 43.82 | $ft^2$ | $M_{ug}$ | 6.24 | lb |
| $M_f$ | 166.7 | lb | $C_{ug}$ | 0.180 | Btu/lb-°F |
| $C_f$ | 0.1655 | Btu/lb-°F | $(A/L)_{ug}$ | 141.9 | ft |
| $M_{clad}$ | 22.7 | lb | | | |

TABLE 7

NUCLEAR SYSTEM REFERENCE LEVELS

| | |
|---|---|
| $n_r$ | = 395.6 kwt |
| $w_{cr}$ | = 8.889 lb/sec |
| $T_{cinr}$ | = 1099°F |
| $T_{c1r}$ | = 1123°F |
| $T_{c2r}$ | = 1169°F |
| $T_{c3r}$ | = 1225°F |
| $T_{c4r}$ | = 1274°F |
| $T_{c5r}$ | = 1300°F |
| $T_{fer}$ | = 1142°F |
| $T_{f1r}$ | = 1166°F |
| $T_{f2r}$ | = 1255°F |
| $T_{f3r}$ | = 1327°F |
| $T_{f4r}$ | = 1362°F |
| $T_{f5r}$ | = 1348°F |
| $\overline{T}_{fr}$ | = 1267°F |
| $\tau_m$ | = 10 sec |

TABLE 8

INTERMEDIATE HEAT EXCHANGER CONSTANTS

| | | |
|---|---|---|
| $A_t$ | 0.00471 | $ft^2$ |
| $B_1$ | $3.33 \times 10^{-4}$ | (dimensionless) |
| $B_2$ | 1.9 | (dimensionless) |
| $B_4$ | 0.023 | (dimensionless) |
| $C_c$ | 0.211 | Btu/lb-°F |
| $C_{ML}$ | 0.0332 | Btu/lb-°F |
| $C_{MV}$ | 0.0255 | Btu/lb-°F |
| $D_i$ | 0.93 | inch |
| $D_P$ | 0.72 | inch |
| $f_{MV}$ | 0.04 | (dimensionless) |
| g | 32 | $ft/sec^2$ |
| $h_c$ | 0.556 | $Btu/sec-ft^2-°F$ |
| $H_M$ | 123.1 | Btu/lb |
| $K_{ML}$ | 0.0026 | Btu/sec-ft-°F |
| $K_{MV}$ | $3.25 \times 10^{-6}$ | Btu/sec-ft-°F |
| $K_t$ | 0.0033 | Btu/sec-ft-°F |
| $L_{IHX}$ | 67.7 | ft |
| $(MC)_{IHX}$ | 59.5 | Btu/°F |
| R | 7.7 | ft-lb/lb-°F |
| $t_t$ | 0.035 | inch |
| Z | 4 | tubes |
| $\epsilon_b$ | 0.2368 | (dimensionless) |
| $\epsilon_s$ | 0.2368 | (dimensionless) |
| $\mu_{MV}$ | $7.47 \times 10^{-5}$ | lb/ft-sec |
| $\rho_{ML}$ | 757 | $lb/ft^3$ |

TABLE 9

INTERMEDIATE HEAT EXCHANGER REFERENCE LEVELS

| | | | | | |
|---|---|---|---|---|---|
| $B_3$ | 14.58 | $ft^{-1}$ | $T_{cpout}$ | 1100 | °F |
| $h_{Mb}$ | 0.0744 | Btu/sec-$ft^2$-°F | $T_{csin}$ | 1300 | °F |
| $h_{Mp}$ | 0.277 | Btu/sec-$ft^2$-°F | $T_{Mbs}$ | 1081 | °F |
| $h_{Ms}$ | 0.01 | Btu/sec-$ft^2$-°F | $T_{Mpb}$ | 1095 | °F |
| $L_b$ | 51.2 | ft | $T_{Mpin}$ | 513 | °F |
| $(LMTD)_b$ | 91.05 | °F | $T_{Ms}$ | 1177 | °F |
| $(LMTD)_p$ | 191 | °F | $T_{Msout}$ | 1273 | °F |
| $L_p$ | 1.7 | ft | $U_b$ | 0.0744 | Btu/sec-$ft^2$-°F |
| $L_s$ | 14.8 | ft | $U_p$ | 0.159 | Btu/sec-$ft^2$-°F |
| $P_{Mbs}$ | 273 | psia | $U_s$ | 0.01 | Btu/sec-$ft^2$-°F |
| $P_{Mpb}$ | 306 | psia | $V_{MVs}$ | 1.13 | $ft^3$ |
| $P_{Ms}$ | 271.5 | psia | $w_c$ | 8.889 | lb/sec |
| $\Delta P_{Ms}$ | 3.0 | psia | $w_{ML}$ | 2.53 | lb/sec |
| $P_{Msout}$ | 270 | psia | $w_{MV}$ | 2.53 | lb/sec |
| $Q_b$ | 312 | Btu/sec | $\rho_{MV}$ | 3.14 | $lb/ft^3$ |
| $Q_p$ | 50.7 | Btu/sec | $\tau_{TRI}$ | 3.6 | sec |
| $Q_s$ | 12.8 | Btu/sec | $\tau_{TIR}$ | 5.85 | sec |
| $T_{cbs}$ | 1293 | °F | $\tau_M$ | 120 | sec |
| $T_{cpb}$ | 1127 | °F | | | |

BLANK

# APPENDIX D
# HISTORY OF PCS STARTUP STUDY

The original purpose of this study of PCS startup was to attempt to reduce the magnitude of the transients seen on the first analog simulation at Aerojet-General Corporation. The first brief study showed that the interval between control drum steps ($T_{\Delta R}$) needed to be increased from 60 seconds to at least 120 seconds in order to avoid reinforcing the temperature oscillations. This first phase of the PCS startup study also showed that the extremes of core temperatures during the startup transient are somewhat dependent on the initial values of the temperatures. It was also noted that control drum step size had little effect on the transient and that strong (more negative) temperature coefficients were generally beneficial.

The analog computer simulation for the first and second phases of the PCS startup study differed in two basic ways from the present simulation. For phases I and II, the effect of the power conversion system on the primary coolant (NaK) temperature was expressed as a "driving function." Changes in temperature difference between the core outlet and core inlet were simulated by a series of straight lines connecting "steady state" values. The steady-state values were computed on the basis of relative NaK flow, relative mercury flow, and relative thermal load on the reactor. Coolant transport delays for the first two phases were computed as first-order lags.

The results of phase II indicated that the control drum step interval should be increased still more, preferably to at least 240 seconds. The initial power level was found to be too low at 9 kwt, whereas 30 kwt appeared to be better. Coolant transport delay times seemed to be relatively unimportant. An increase in the fuel temperature coefficient of reactivity ($\alpha_f$) still showed beneficial results, but an increase of the lower grid plate ($\alpha_{\ell g}$) coefficient had rather erratic effects. Presumably this effect of $\alpha_{\ell g}$ was due to the coolant transport delay time from core outlet to core inlet causing $\alpha_{\ell g}$ to be delayed with respect to $\alpha_f$. Phase II results also indicated that the time for mercury flow to increase from the injection level to the reference level ($t_{2M}$) must be at least 20 seconds.

For phase III of the PCS startup study, simulation of the intermediate heat exchanger was changed from a "driving function" to a single-node heat transfer model. This model was subsequently shown to be inadequate because the lumped mass of the heat exchanger responded too slowly to changes in temperature,

thus holding back the calculated rates of change of coolant temperatures. The simulation of coolant transport delay was expanded from one first-order lag to a series of four cascaded lags. The present simulation uses the more realistic form of nine cascaded first-order lags.

Results of phase III indicate that the initial core temperature difference ($\theta_{core}$) should be less than 200°F, corresponding to <80 kwt initial power at 20% NaK flow or <200 kwt initial power at the present 50% initial NaK flow. Phase III results also showed that the time ($t_c$) for NaK flow to increase from the former initial level of 20% to the reference level must be at least 60 seconds. These results also indicated that the increase in NaK flow should be started as soon as possible after the beginning of mercury injection. Later studies have shown this to be less important than previously believed because mercury injection has been changed from a step to a ramp.

The detailed results of phases I, II, and III are not presented in this report for two reasons. The simulation of the intermediate heat exchanger presently used is quite different from the previous ones, and is felt to give much more accurate results. Also, the reference power and flow levels have changed considerably, as have the chosen initial flow and power levels. Thus, the numerical results of the first three phases have been rendered invalid. It should be noted, however, that the trends in parameter effects noted in the earlier phases have generally been confirmed by the most recent results.

# APPENDIX E

## SYMBOLS AND SUBSCRIPTS

SYMBOLS

A = area ($ft^2$)

A = analog console A

AHX = auxiliary heat exchanger

B = analog console B

$B_1$ = a constant in calculation of $U_b$

$B_2$ = a constant in calculation of $P_{Mpb}$

$B_3$ = a factor in calculation of $Q_s$ (1/ft)

C = delayed neutron precursor concentration

C = specific heat at constant pressure (Btu/lb-°F)

C = analog console C

D = diameter (ft)

f = friction factor

G = heat generation rate (Btu/sec)

g = acceleration due to gravity ($ft/sec^2$)

H = heat of vaporization (Btu/lb)

h = heat transfer coefficient ($Btu/sec-ft^2-°F$)

IC = initial condition on analog integrator

IHX = intermediate heat exchanger

J = analog junction

K = thermal conductivity (Btu/sec-ft-°F)

L = length (ft)

LDB = lower deadband setting (°F)

(LMTD) = log mean temperature difference

$\ell^*$ = effective mean prompt neutron lifetime

$\ell n$ = natural (Napierian) logarithm

M = mass (lb)

n = neutron level

O = a constant based on reference temperature levels

P = power (kwt)

P = pressure (psi)

PCS = power conversion system

PL = parasitic load

Q = heat flow rate (Btu/sec)

R = ideal gas constant (ft-lb/lb-°F)

$R^{\$}$ = reactivity (dollars)

Re = Reynolds number

T = temperature (°F)

$\dot{T}$ = time rate of change of temperature (°F/sec)

t = time (sec)

t = thickness (ft)

$t_1$ = time of first transient (sec)

$t_2$ = time of second transient (sec)

U = overall heat transfer coefficient ($Btu/sec-ft^2-°F$)

UDB = upper deadband setting (°F)

V = volume ($ft^3$)

w = flow rate (lb/sec)

Z = number of tubes in IHX

$\alpha$ = temperature coefficient of reactivity ($/°F)

$\beta$ = effective delayed neutron fraction

$\Delta$ = change of variable from initial value (used with symbol for variable)

$\epsilon$ = a small constant used for analog stability

$\theta$ = temperature difference (°F)

$\lambda$ = decay constant for delayed neutrons ($sec^{-1}$)

$\mu$ = absolute viscosity (lb/ft-sec)

$\rho$ = density ($lb/ft^3$)

$\tau$ = time constant or delay time (sec)

T = period (sec)

BLANK

## APPENDIX E (Continued)

SUBSCRIPTS

a = actual (at measuring device)

AHX = auxiliary heat exchanger

AP = AHX to parasitic load

b = boiler region of IHX

bs = boundary between boiler and superheater (IHX)

c = nuclear system coolant (NaK)

clad = fuel element cladding

core = nuclear system core

d = control drums

e = entrance node (core heat transfer)

f = fuel elements

I = injection level

i = $i^{\underline{th}}$ delayed neutron precursor group

IA = IHX to AHX

IHX = intermediate (NaK-Hg) heat exchanger

IR = IHX to reactor core inlet

in = reactor core inlet

j = $j^{\underline{th}}$ core heat transfer node

L = liquid

$\ell$g = lower grid plate

M = mercury

m = measured

max = peak or maximum value during transient

max1 = first maximum (before second mercury flow increase)

max2 = second maximum (after second mercury flow increase)

min = minimum value during transient

min1 = first minimum (before second mercury flow increase)

min2 = second minimum (after second mercury flow increase)

P = plug in IHX tubes

p = preheater

pb = boundary between preheater and boiler (IHX)

pin = preheater inlet (IHX)

PLin = inlet to parasitic load

PLout = outlet of parasitic load

pout = preheater outlet (IHX)

PR = parasitic load to reactor core inlet

RI = reactor core outlet to IHX

RIR = reactor core outlet to IHX to reactor core inlet

s = superheater region of IHX

sin = superheater inlet (IHX)

sout = superheater outlet (IHX)

T = fluid transport delay time

t = tube (IHX)

ug = upper grid plate

V = vapor

0 = initial value

1 = first core heat transfer node

$\Delta$R = control drum reactivity steps

BLANK

## APPENDIX F
## NOMENCLATURE

$A_{fce}$ = heat transfer area for the entrance fuel node ($ft^2$)

$A_{fcj}$ = heat transfer area between fuel and coolant (outside surface area of fuel cladding) for the $j^{th}$ axial node ($ft^2$)

AHX = auxiliary (NaK-NaK) heat exchanger

$\left(\frac{A}{L}\right)_{\ell g}$ = ratio of effective heat conduction area to effective heat conduction path length for lower grid plate (ft)

$\left(\frac{A}{L}\right)_{ug}$ = ratio of effective heat conduction area to effective heat conduction path length for upper grid plate (ft)

$A_t$ = flow area of mercury tube ($ft^2$)

$B_1$ = a correlation constant

$B_2$ = a correlation constant

$B_3$ = a correlation factor

$B_4$ = a correlation constant

$C_c$ = heat capacity of nuclear system coolant (Btu/lb-°F)

$C_f$ = heat capacity of fuel (Btu/lb-°F)

$C_i$ = concentration of delayed neutron precursors in the $i^{th}$ group

$C_{IHX}$ = heat capacity of metal and NaK in the intermediate heat exchanger (Btu/lb-°F)

$C_{\ell g}$ = heat capacity of lower grid plate (Btu/lb-°F)

$C_{ML}$ = heat capacity of mercury liquid at constant pressure (Btu/lb-°F)

$C_{ug}$ = heat capacity of upper grid plate (Btu/lb-°F)

$\frac{d}{dt}$ = derivative with respect to real time ($sec^{-1}$)

$\frac{d}{d\tau}$ = derivative with respect to analog time ($sec^{-1}$)

$D_i$ = internal diameter of mercury flow tubes (ft)

$D_p$ = diameter of plug in mercury flow tubes (ft)

f = indicates that one variable is a function, f, of another variable

$f_{MV}$ = friction factor for mercury vapor

g = acceleration due to gravity ($ft/sec^2$)

$G_e$ = heat generation rate in the entrance fuel node (Btu/sec)

$G_j$ = heat generation rate in the $j^{th}$ axial node (°F)

$h_c$ = convective heat transfer coefficient for NaK in the IHX (Btu/sec-$ft^2$-°F)

$h_{Mb}$ = convective heat transfer coefficient for mercury in the boiler section (Btu/sec-$ft^2$-°F)

$h_{MP}$ = convective heat transfer coefficient for mercury in the preheater section (Btu/sec-$ft^2$-°F)

$h_{Ms}$ = convective heat transfer coefficient for mercury in the superheater section (Btu/sec-$ft^2$-°F)

$H_M$ = heat of vaporization of mercury (Btu/lb)

IHX = intermediate (NaK-Hg) heat exchanger

$K_{fg}$ = thermal conductivity of the lower grid plate (Btu/sec-ft-°F)

$K_{ML}$ = thermal conductivity of liquid mercury (Btu/sec-ft-°F)

$K_{MV}$ = thermal conductivity of mercury vapor (Btu/sec-ft-°F)

$K_t$ = thermal conductivity of the mercury flow tubes (Btu/sec-ft-°F)

$K_{ug}$ = thermal conductivity of the upper grid plate (Btu/sec-ft-°F)

$\ell^*$ = effective prompt neutron lifetime (sec)

$L_b$ = length of the boiler section (ft)

$\ell n$ = natural (Napierian) logarithm

LDB = lower temperature control deadband setting (°F)

$L_{IHX}$ = length of the intermediate heat exchanger flow tubes (ft)

$(LMTD)_b$ = log mean temperature difference for the boiler section (°F)

$(LMTD)_p$ = log mean temperature difference in the preheater section (°F)

$L_p$ = length of the preheater section (ft)

$L_s$ = length of the superheater section (ft)

$M_{cj}$ = mass of coolant in the $j^{th}$ axial node (lb)

$M_{fe}$ = mass of fuel in the entrance fuel node (lb)

$M_{fj}$ = mass of fuel in the $j^{th}$ axial node (lb)

$M_{IHX}$ = mass of NaK and metal in the intermediate heat exchanger (lb)

$M_{\ell g}$ = mass of lower grid plate (lb)

$M_{ug}$ = mass of upper grid plate (lb)

n = neutron level

$O_{cjw}$ = a constant involving initial and reference NaK flow and initial and reference power (°F/sec)

PCS = power conversion system

PL = parasitic load

$P_{max}$ = maximum power (kwt)

$P_{Mbs}$ = mercury pressure at the interface between the boiler and superheater sections ($lb/ft^2$)

$P_{Mpb}$ = mercury saturation pressure at the interface between the boiler and preheater section ($lb/ft^2$)

$P_{Ms}$ = mercury pressure in the superheater section ($lb/ft^2$)

$P_{Msout}$ = mercury pressure at the mercury outlet of the superheater section ($lb/ft^2$)

$P_0$ = initial power (kwt)

$Q_s$ = heat absorbed by the mercury vapor in the superheater section (Btu/sec)

R = ideal gas constant (ft-lb/lb-°F)

$R^\$$ = reactivity (dollars)

$R^\$_d$ = reactivity inserted by the reactor control drums (dollars)

$t_c$ = time of increase of NaK flow (sec)

$t_t$ = thickness of mercury flow tubes (ft)

$t_{1M}$ = time of first increase in Hg flow (injection) (sec)

$t_{2M}$ = time of second increase in Hg flow (sec)

$T_{c1}$ = temperature of coolant in the first axial node (°F)

$T_{c5}$ = temperature of coolant in the fifth axial node (core outlet) (°F)

$T_{c5max}$ = maximum core outlet NaK temperature (°F)

$T_{c5mini}$ = minimum of core outlet NaK temperature before Hg flow reaches 100% (°F)

$T_{c5min2}$ = minimum of core outlet NaK temperature after Hg flow reaches 100% (°F)

$T_{ca}$ = temperature of the NaK coolant, actual level at the temperature sensor (°F)

$T_{cbs}$ = NaK coolant temperature at the interface between the boiler and superheater sections (°F)

$T_{cin}$ = core inlet coolant temperature (°F)

$T_{cj}$ = coolant temperature in the $j^{th}$ axial node (°F)

$T_{c,j-1}$ = temperature of the NaK coolant in the node previous to the $j^{th}$ node

$T_{cm}$ = temperature of the NaK coolant as measured by the temperature sensor (°F)

$T_{cpb}$ = NaK coolant temperature at the interface between preheater and boiler sections (°F)

$T_{cPLin}$ = coolant temperature at inlet to parasitic load (°F)

$T_{cPLout}$ = coolant temperature at outlet of parasitic load (°F)

$T_{cpout}$ = NaK coolant temperature at the NaK outlet of the preheater section (°F)

$T_{csin}$ = NaK coolant temperature at the NaK inlet to the superheater section (°F)

$\overline{T}_f$ = core average fuel temperature (°F)

$T_{fe}$ = fuel temperature in the entrance fuel node (°F)

$T_{fj}$ = fuel temperature in the $j^{th}$ axial node (°F)

$T_{\ell g}$ = temperature of the reactor lower grid plate (°F)

$T_{Mbs}$ = mercury temperature at the interface between the boiler and superheater sections (°F)

$T_{Mpb}$ = mercury temperature at the interface between preheater and boiler sections (°F)

$T_{Mpin}$ = mercury temperature at the mercury inlet to the preheater section (°F)

$T_{Ms}$ = mercury temperature in the superheater section (°F)

$T_{Msout}$ = mercury temperature at the mercury outlet of the superheater section (°F)

$T_{ug}$ = temperature of the reactor upper grid plate (°F)

$\dot{T}$ = time rate of change of temperature (°F/sec)

$|\dot{T}_{c5}|_{max}$ = maximum rate of change of core outlet NaK temperature (°F/min)

$|\dot{T}_{cin}|_{max}$ = maximum rate of change of core inlet NaK temperature (°F/min)

$\dot{T}_{cj}$ = time rate of change of coolant temperature in the $j^{th}$ axial node (°F/sec)

$|\dot{T}_f|_{max}$ = maximum rate of change of core average fuel temperature (°F/min)

$|\dot{T}_{f4}|_{max}$ = maximum rate of change of fuel temperature in the fourth axial node (°F/min)

$\dot{T}_{fj}$ = time rate of change of fuel temperature in the $j^{th}$ axial node (°F/sec)

$\dot{T}_{\ell g}$ = time rate of change of temperature of lower grid plate (°F/sec)

$\dot{T}_{ug}$ = time rate of change of temperature of upper grid plate (°F/sec)

$U_b$ = overall heat transfer coefficient for the boiler section (Btu/sec-$ft^2$-°F)

UDB = upper temperature control deadband setting (°F)

$U_{fc}$ = overall heat transfer coefficient from reactor fuel to coolant (Btu/sec-$ft^2$-°F)

$U_p$ = overall heat transfer coefficient for the preheater section (Btu/sec-$ft^2$-°F)

$U_s$ = overall heat transfer coefficient for the superheater section (Btu/sec-$ft^2$-°F)

$V_{MV}$ = volume of mercury vapor ($ft^3$)

$w_c$ = NaK coolant flow rate (lb/sec)

$w_M$ = mercury flow rate (lb/sec)

$w_{MI}$ = mercury flow rate at end of injection phase (lb/sec)

$w_{ML}$ = mercury liquid flow rate (lb/sec)

$w_{MV}$ = mercury vapor flow rate (lb/sec)

Z = number of mercury flow tubes

$\alpha_f$ = temperature coefficient of reactivity for the fuel (dollars/°F)

$\alpha_{fg}$ = temperature coefficient of reactivity for the reactor lower grid plate (dollars/°F)

$\alpha_{ug}$ = temperature coefficient of reactivity for the reactor upper grid plate (dollars/°F)

$\beta$ = effective fraction of delayed neutron precursors

$\beta_i$ = effective fraction of delayed neutron precursors in the $i^{th}$ group

$\epsilon_b$ = a small constant used for analog stability

$\epsilon_s$ = a small constant used for analog stability

$\theta_{AHX}$ = difference between auxiliary heat exchanger primary NaK inlet and outlet temperatures (°F)

$\theta_{core,0}$ = initial difference between core inlet and core outlet NaK temperature (°F)

$\lambda_i$ = decay constant for delayed neutrons in the $i^{th}$ group (1/sec)

$\mu_{MV}$ = absolute viscosity of mercury vapor (lb/ft-sec)

$\rho_{ML}$ = density of mercury liquid ($lb/ft^3$)

$\rho_{MV}$ = density of mercury vapor ($lb/ft^3$)

$\tau_c$ = delay before increase of NaK flow (sec)

$\tau_{IHX}$ = equivalent time constant for intermediate heat exchanger metal and mercury (°F)

$\tau_m$ = time constant of temperature sensor (sec)

$\tau_M$ = delay before increase of mercury flow from the injection level (sec)

$\tau_{RIR}$ = coolant transport delay time from reactor core outlet to IHX to reactor core inlet (sec)

$\tau_{Ta}$ = coolant transport delay time from core outlet to temperature sensor (sec)

$\tau_{TAP}$ = coolant transport delay time from AHX to parasitic load (sec)

$\tau_{TIA}$ = coolant transport delay time from IHX to AHX (sec)

$\tau_{TPR}$ = coolant transport delay time from parasitic load to reactor core inlet (sec)

$\tau_{TRI}$ = coolant transport delay time from reactor core outlet to IHX (sec)

$T_{\Delta R}$ = interval between successive control drum steps in the same direction (sec)

*The symbol $\Delta$ indicates change in the variable from its initial level. The subscript 0 indicates initial level of the variable and the subscript r indicates reference level.